DISSERTATION

BIOPHYSICAL, STRUCTURAL, AND FUNCTIONAL STUDIES OF HISTONE BINDING PROTEINS

Submitted by

Keely B. Sudhoff

Department of Biochemistry and Molecular Biology

In partial fulfillment of the requirements

For the Degree of Doctor of Philosophy

Colorado State University

Fort Collins, Colorado

Fall 2010

Doctoral Committee:

Department Chair: Pui Shing Ho

Advisor: Karolin Luger

Robert Woody
Chaoping Chen
Jeffrey Hansen
Charles Henry

ABSTRACT

BIOPHYSICAL, STRUCTURAL, AND FUNCTIONAL STUDIES OF HISTONE BINDING PROTEINS

Eukaryotic genomes are extensively compacted with an equal amount of histone proteins to form chromatin. A high level of control over chromatin structure is required to regulate critical cellular processes such as DNA replication, repair, and transcription. To achieve this feat, cells have developed a variety of means to locally or globally modulate chromatin structure. This can involve covalent modification of histones, the incorporation of histone variants, remodeling by ATP-dependent remodeling enzymes, histone chaperone-mediated assembly/disassembly, or any combination of the above activities. To understand how chromatin structure is affected by histones, it is essential to characterize the interactions between histones and their associated proteins.

In *Saccharomyces cerevisiae*, the multi-subunit SWR1 complex mediates histone variant H2A.Z incorporation. Swc2 (Swr1 complex 2) is a key member of the SWR1 complex and is essential for binding and transfer of H2A.Z. Chz1 (Chaperone for H2A.Z/H2B) can deliver H2A.Z/H2B heterodimers to the SWR1 complex *in vitro*. $Swc2_{1\text{-}179}$ (a domain of Swc2 that retains histone binding and the apparent preference for variant dimers) and Chz1 are intrinsically disordered, but become more ordered upon interaction with histones. Quantitative measurements done under physiological *in vitro* conditions demonstrate that Chz1 and $Swc2_{1\text{-}179}$ are not histone variant-specific. They

bind to histones with an affinity lower than that of previously described histone chaperones, and lack the ability to act on nucleosomes or other histone-DNA complexes. Small-angle X-ray scattering demonstrates that the intrinsic disorder of the proteins allows them to adopt a multitude of structural states, perhaps facilitating many different interactions and functions.

We show that $Swc2_{1\text{-}179}$, despite its overall acidic charge, can bind double stranded DNA, in particular, 3-way and 4-way junction DNA. These junctions are thought to mimic the central intermediates found in DNA damage repair. This characteristic is unique to $Swc2_{1\text{-}179.}$ Consistent with this unexpected activity, yeast phenotypic assays have revealed a role for *SWC2* in DNA damage repair, as indicated by sensitivity to DNA damaging agent methane methylsulfonate. Importantly, our data has exposed a novel role for Swc2 in DNA damage repair.

In an independent study, we investigated the histone chaperone Vps75, a Nap1 homolog. Rtt109 is a histone acetyltransferase that requires a histone chaperone for the acetylation of histone H3 at lysine 56 (H3K56). Rtt109 forms a complex with the chaperone Vps75 *in vivo* and is implicated in DNA replication and repair. We show that deletion of *VPS75* results in dramatic and diverse mutant phenotypes, in contrast to the lack of effects observed for the deletion of *NAP1*. The flexible C-terminal domain of Vps75 is important for the *in vivo* functions of Vps75 and modulates Rtt109 activity *in vitro*. Our data highlight the functional specificity of Vps75 in Rtt109 activation.

Keely Sudhoff
Department of Biochemistry and Molecular Biology
Colorado State University
Fort Collins, CO 80523
Fall 2010

ACKNOWLEDGEMENTS

The completion of this dissertation would not have been possible without the large, supporting group of people in and out of the laboratory who have encouraged and guided me. In looking back at the last five years, I'm amazed at the kindness I've been shown and I'm humbled.

Dr. Karolin Luger, my thesis advisor, has fostered my scientific development. She has encouraged my independence and greatly attuned my scientific methodology. I enjoyed watching Karolin in her element - writing or giving talks, from her I've learned the importance of scientific communication.

I would like to thank my committee members Dr. Jeffrey Hansen, Dr. Robert Woody, Dr. Chaoping Chen, and Dr. Charles Henry who provided great advice, encouragement, and criticism when needed. I always enjoyed my committee meetings and the exposure to new ideas and experiments. On a personal note, I've enjoyed interacting with them through the years. I've had many pleasant exchanges and conversations, be it scientific or otherwise. Dr. Laurie Stargell was very also very helpful with discussions and ideas about yeast genetics. Dr. Stargell provided me with one of my greatest graduate school experiences, that of a fifth-grade science teacher.

To all the wonderful people who I've worked with in the laboratory of the years, thank you. I always enjoyed our late night discussions, our weekend laughter and our spirited debates. Not only did you help me immensely with my science, you made the work environment enjoyable.

Brian, thanks for letting me turn our lives upside down (again). You have felt every high and low of graduate school with me. You've told me to work harder when I needed to hear it and you've also praised me when I had nothing left to give.

My parents are indescribable, they've let me live and make mistakes, but they've always been there to guide when needed. Thank you for giving me 28 wonderful people in my life who continue to inspire and teach me. From my siblings I have learned to achieve what I desire, to embrace life, to overcome obstacles, to live and laugh. It calms me to know your confidence in me far exceeds that of my own. This accomplishment is ours to share.

TABLE OF CONTENTS

CHAPTER I

Introduction

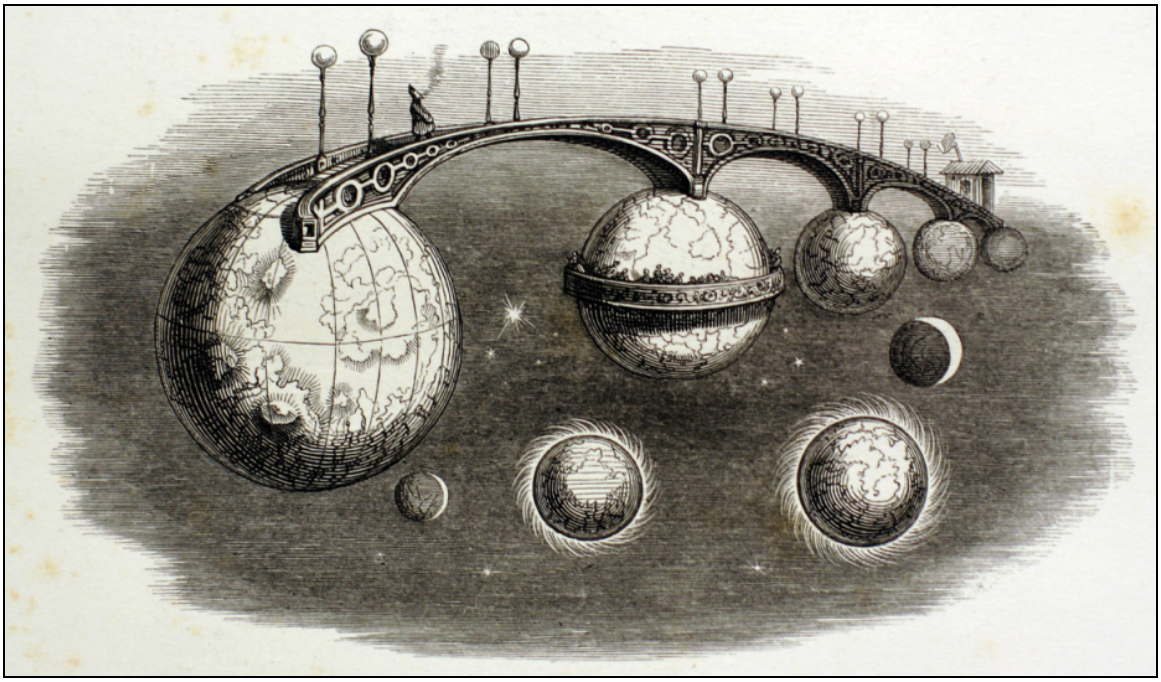

(J.J Grandville's Un Autre Monde 1844)

1.1 Introduction

Walther Flemming, a German biologist studying cell division, first published the term "chromatin" in 1881. He described it as a "substance in the cell nucleus which is readily stained" (Paweletz, 2001). During the late 1800's the study of chromatin began emerging, most notably in the laboratory of Felix Hoppe-Seyler. Two of his students, Johannes Miescher and Albrecht Kossel, made important discoveries pertinent to chromatin research, but the full significance would not be realized for some time. In the winter of 1869 Miescher developed methods for the isolation of a novel compound from nuclei of white blood cells which he called "nuclein" (Miescher, 1871), found to contain phosphorus and nitrogen (Dahm, 2008). Today nuclein is known as deoxyribonucleic acid (DNA), the building blocks of life. Following the direction of Miescher's work in nuclein and encouraged by Hoppe-Seyler, Albrecht Kossel went on to study the structure and chemical composition of nuclein. In addition to identifying the purine and pyrimidine bases found in nuclein, he discovered and first coined the term "histon" and his work earned him the Nobel Prize in 1910 (Kossel, 1910, 1911). It would not be known until 1944 (Avery et al., 1944) that DNA was the carrier of genetic information and the full significance of Mieschers research would be realized. Remarkably, the term chromatin still stands today and aptly describes how the genome of the eukaryotic cell is packaged into a macromolecular structure comprised of a roughly equal mass of histones and DNA (Kornberg and Lorch, 1999). Chromatin is a highly regulated protein-DNA complex that packages genetic material and is remodeled to permit cellular processes including: transcription, replication, differentiation, and DNA repair.

Eukaryotic chromatin is comprised of DNA, histones, and numerous other trans-acting chromatin-associated proteins. In non-dividing cells, the chromatin is dispersed throughout the nucleus, but prior to metaphase the chromatin is condensed into a tightly organized structure called the chromosome. Eukaryotic chromatin is folded in several ways, and the first order of folding produces a structure called the nucleosome. The nucleosome core particle (NCP) contains 146 base pairs of DNA wrapped around a core histone octamer, comprised of two each of histones H2A, H2B, H3 and H4 (Luger et al., 1997). Wrapping of DNA around the histones results in a tenfold reduction in the apparent length of the DNA and forms what we call the 10-nm fiber, otherwise known as 'beads on a string' (Hansen, 2002). Linker histone H1 binds to the nucleosomes and promotes further compaction to form the 30nm fiber. This fiber can undergo additional packaging to form a loop-like structure that is 100 nm - 300 nm in diameter (Horn and Peterson, 2002) (Figure 1.1).

1.2 Nucleosome Structure

The 2.8Å-resolution crystal structure of the nucleosome reveals 146bp palindromic DNA derived from the human α-satellite sequence wrapped in ~1.65 left-handed superhelical turns around a histone octamer composed of two (H2A/H2B) heterodimers and an $(H3/H4)_2$ tetramer (Luger et al., 1997) (Figure 1.1). The nucleosome structure was fundamental in understanding the nature of histone-DNA interactions and the DNA structure. Importantly it also confirmed details known about the histone octamer (Arents et al., 1991).

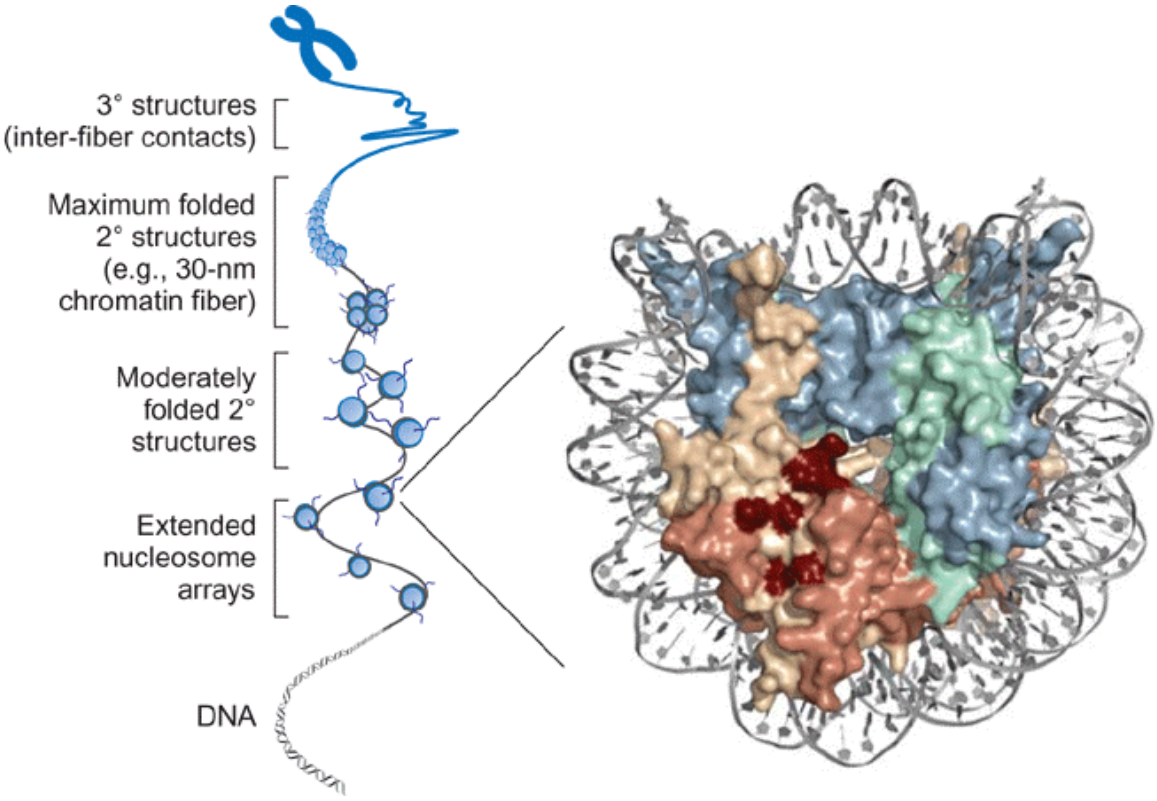

Figure 1.1: Nucleosome and chromatin compaction.
Left, a schematic of various levels of chromatin compaction. Right, nucleosome surface showing histones H2A (yellow), H2B (light red), H3 (blue) and H4 (green). Residues comprising the charged pocket are shown in dark red. Model courtesy of J. Chodaparambil. Adapted from Caterino & Hayes (2007), NSMB 4(11):1056-8.

Structurally, all of the histones contain the "histone fold" which consists of three alpha-helices (α1-3) linked by two loops (L1-L2) (Arents et al., 1991; Arents and Moudrianakis, 1995) (Figure 1.2). The histones dimerize in an anti-parallel manner along the α-2 helices forming an H2A/H2B and an H3/H4 heterodimer. The dimers are stabilized by hydrophobic interactions that span the histone fold portions of the monomers. The H3/H4 heterodimer further dimerizes to form the four-helix bundle that is stabilized by interactions between H3 C-terminal helices. The H2A/H2B dimer binds the H3/H4 tetramer and the interactions are stabilized by extensive hydrophobic contacts between H2B and H4 at the C-terminal helices. Two H2A/H2B dimers bind to opposite sides of the $(H3/H4)_2$ tetramer, forming the histone octamer.

The histones all contain unstructured extended N-terminal tails that make up roughly 28% of the mass of the core histones and are highly enriched in positively charged residues lysine and arginine. Histone H2A also has a short (>40 amino acid residue) C-terminal tail. The crystal structures of both the nucleosome and histone octamer lack fully resolved histone tails, presumably due to their intrinsic flexibility (Arents et al., 1991; Luger et al., 1997). However, it is possible that in the configuration of chromatin the core histone N-terminal tails assume structural motifs (Hansen et al., 1998). These tails are thought to facilitate interactions between the nucleosome and linker DNA or interactions between the octamers. Notably, the H4 tail is positioned to interact with the "face" of the nucleosome in the acidic region formed by H2A and H2B (Luger and Richmond, 1998b). The core histone N-terminal tails also interact with chromatin-associated proteins and are the sites of posttranslational modifications such as acetylation, methylation, and phosphorylation (Van Holde, 1988).

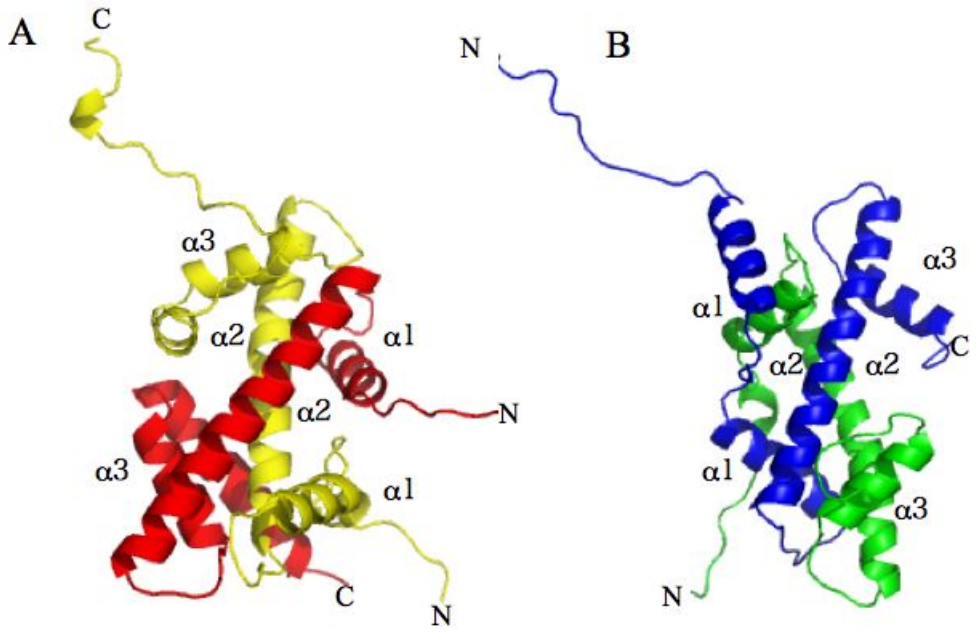

Figure 1.2: All core histones have a conserved histone fold.
(A) Histone H2A/H2B heterodimer with H2A (yellow) and H2B (red). The histone fold consists of three alpha-helices (α1-3) linked by two loops (L1-L2), marked on heterodimers. **(B)** Histone H3/H4 heterodimer with H3 (blue) and H4 (green).

The 1.9Å-resolution nucleosome structure offers an abundance of information regarding the structural characteristics of nucleosomal DNA (Davey et al., 2002). An extensive review of the DNA interactions in the structure of the NCP can be found in the following references (Davey et al., 2002; Richmond and Davey, 2003). A brief summary of the important features of the DNA in the NCP follows below. Notably, no interactions between the positively charged histones and the bases of the DNA were observed, lending credence to the role of histones as a sequence-independent organizer of chromatin. This helps facilitates a flexible and highly dynamic environment for chromatin. Over half of the protein-DNA interactions are formed by hydrogen bonds between the protein amide groups and the oxygen atoms of the phosphodiester backbone. Side-chain interactions with the minor groove occur each time the histone octamer faces the minor groove. The water-mediated interactions help stabilize the protein-DNA complex and facilitate H-bonds. The importance of these water-mediated interactions resides in their ability to accommodate structural changes in the DNA caused by sequence variation.

1.3 Higher Order Structures

The most extended unit of chromatin in the genome is the nucleosome array, thousands of nucleosomes organized on helical DNA in a linear fashion. These long arrays of nucleosomes can be further compacted to multiple higher-order levels of unknown architecture (Hansen, 2002) (Figure 1.1). Nucleosomes are connected, one to the next, by DNA that is referred to as linker DNA. A class of proteins, referred to as linker histone H1 or avian H5, bind to chromatin and affect chromatin dynamics (Ramakrishnan, 1997). The nucleosome, H1, and linker DNA comprise a structure

known as the chromatosome (Van Holde, 1988). H1 domain organization differs markedly from core histones; it is composed of a central globular domain flanked by a short N-terminal domain and a longer, basic C-terminal domain (Van Holde, 1988). Linker histones are slightly larger than core histones (>20kDa) and enriched in lysine residues. Although not required for folding, the linker histone leads to a more homogenous mixture of highly compacted chromatin fibers (Hansen, 2002).

The organization of the DNA that is achieved by the chromatosome cannot fully explain the packaging of DNA observed in the cell nucleus. Further compaction of chromatin is necessary, but the structural details of higher order structure are not well known. *In vitro*, nucleosomal arrays form an extended 10-nm fiber that condenses into compact 30-nm diameter fibers upon increasing the ionic strength (Hansen, 2002). Importantly, the histone tails are required for both intramolecular folding and for fiber-fiber interactions seen *in vitro* (Hansen, 2002). Beyond the 30-nm fiber, the structure of chromatin is poorly understood, but it is classically suggested that the 30-nm fibers are arranged into loops having a diameter or width between ~200-300nm.

Eukaryotic genomes are extensively compacted into chromatin, yet cells need to access and regulate specific local DNA structures independent of the lion's share of chromatin. A high level of control is required to regulate critical cellular processes such as DNA replication, repair, and transcription. To achieve this feat, cells have developed a variety of means to locally modulate chromatin structure. This can involve covalent modification of histones, the incorporation of histone variants, remodeling by ATP-dependent remodeling enzymes, or histone chaperone mediated assembly/disassembly.

1.4 Histone Variant H2A.Z

Substitution of one or more of the core histones with the corresponding histone variant has the potential to exert considerable influence on the structure and function of nucleosomes and chromatin (Jin et al., 2005). In contrast to canonical histones, variant histones are incorporated into chromatin independent of DNA replication. Distinct chromatin domains characterize the nucleus, and these specialized domains can be enriched in histone variants. Several histone variants for H2A, H3 and H1 have been determined and a few for histone H2B. (Bernstein and Hake, 2006). When not incorporated into chromatin, histones are found complexed with histone chaperones (Chang et al., 1997).

The histone H2A variant H2A.Z is found in all eukaryotes from *Saccharomyces cerevisiae* to humans (Redon et al., 2002). H2A.Z is essential for viability in many organisms including *Drosophila melanogaster, Tetrahymena thermophila, Xenopus laevis* and *Mus musculus* (Clarkson et al., 1999; Liu et al., 1996; Ridgway et al., 2004). H2A.Z is implicated in numerous biological functions such as gene activation, chromosome segregation, heterochromatin silencing, and progression through the cell cycle (Adam et al., 2001; Dhillon et al., 2006; Krogan et al., 2004). Yeast histone H2A.Z replaces the canonical H2A in about one in ten histones (Kobor et al., 2004). However, it was also reported that yeast H2A.Z is about 50-100 times less concentrated than its canonical counterpart H2A (Ghaemmaghami et al., 2003).

Substituting a canonical histone dimer with that of a histone variant is a fundamental means of altering the state of chromatin. The yeast *HTZ1* null mutant is

sensitive to DNA-damaging agents such as methyl methanesulfonate (MMS) and ultraviolet radiation (UV); additional phenotypes include sensitivity to caffeine, hydroxyurea (HU), 6-azauracil and mycophenolic acid (Desmoucelles et al., 2002; Mizuguchi et al., 2004). Sensitivity to 6-azauracil and mycophenolic acid, both of which deplete nucleotide pools in the cell, indicate a potential involvement in transcriptional elongation for H2A.Z.

A genome wide analysis of H2A.Z indicates it is found in promoter regions. In particular, H2A.Z has been found deposited next to nucleosome-free promoters throughout the yeast genome (Guillemette et al., 2005; Raisner et al., 2005; Zhang et al., 2005). In yeast, H2A.Z localizes to actively transcribed regions that are adjacent to heterochromatin such as telomeric DNA and mating-type loci, thereby buffering the spread of heterochromatin (Meneghini et al., 2003). The biological function of H2A.Z has been well studied in yeast, but in higher eukaryotes the function(s) is poorly defined.

The overall crystal structure of the nucleosome containing the histone variant H2A.Z is very similar to that of the nucleosome containing major histones. Main differences were found in the C-terminal docking domain of H2A.Z (Chakravarthy et al., 2004; Suto et al., 2000) where the amino acid changes result in an altered surface. This site mediates interactions between H2A and the $(H3/H4)_2$ tetramer. Structural studies have shown that this interface may be weakened by H2A.Z (Suto et al., 2000). The H2A.Z-containing nucleosomes have an interaction surface that binds a metal ion and bears a negatively charged region that extends to H2B (docking domain) (Figure 1.3).

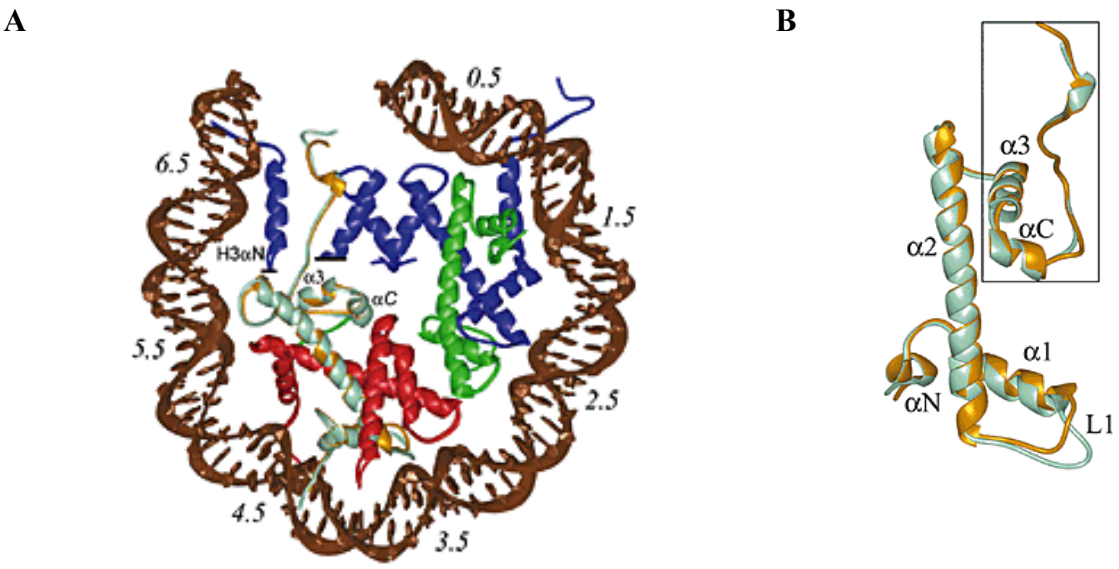

Figure 1.3: H2A.Z nucleosome closely resembles H2A nucleosome.
(A) Superposition of major-NCP and H2A.Z-NCP. Only 73 bp of the DNA and associated proteins are shown. Regions of protein−DNA interaction are numbered starting from the nucleosomal dyad. H3 is colored blue, H4 green, H2B red, H2A yellow, H2A.Z gray, and DNA brown. **(B)** Superposition of H2A and H2A.Z. The docking domain is boxed. Adapted from Suto et al. (2000), NSMB 7(12):1121-4.

This could be an important region for *trans*-acting factors to bind and modify chromatin structure. H2A.Z reconstituted nucleosomal arrays facilitate intra-fiber condensation, yet inhibit internucleosomal interactions (versus H2A arrays) with increasing ionic strength (Fan et al., 2002).

Histone H2A.Z clearly plays a very important role in chromatin architecture and function. However, the mechanism for histone variant H2A.Z incorporation into canonical nucleosomes remains elusive. Both ATP-dependent histone remodeling complexes (SWR1) and histone chaperone (Chz1) are implicated in key roles and found associated with H2A.Z. Thus, to fully understand the mechanism of H2A.Z incorporation, the interactions between the variant histone and its associated proteins must be characterized.

1.5 Histone Chaperones

Ron Laskey first coined the term "molecular chaperone" in 1978 to describe highly acidic proteins in extracts of *Xenopus laevis* which bound histones and transferred them to DNA (Laskey et al., 1978). Without the chaperones, nucleosomes would be incorrectly assembled and form a precipitate. The histone chaperone prevented incorrect interactions between positively charged histones and the negatively charged DNA (Laskey et al., 1978). It should be noted, that the chaperone does not become a component of the final product, the nucleosome; it simply assists in formation of the nucleosome. On the basis of Laskey's work with nucleosplasmin, a histone chaperone was defined as having histone-binding capabilities and nucleosome-assembly functions in an ATP-independent manner (Eitoku et al., 2008).

Histone chaperones play a role in many cellular processes including DNA replication, DNA damage repair, transcription, and histone-variant incorporation (H2A.Z or centromeric histone variants) (Park and Luger, 2008; Ransom et al., 2010). Chromatin assembly is a step-wise process initiated by the central ~80 bp of DNA organized by a heterotetramer of H3/H4. The additional 40bp of DNA on both sides are then bound by H2A/H2B dimers. During chromatin assembly the two H2A/H2B dimers are assembled after the association of H3/H4 tetramer with the DNA (Akey and Luger, 2003; Krude, 1999). Conversely, it's thought that during disassembly the H2A/H2B dimers are removed from the DNA prior to removal of the H3/H4 dimers. Currently, there is no unified theory on how histone chaperones mechanistically promote nucleosome assembly. However, recently published data shows that nucleosome assembly requires the elimination of competing (non-nucleosomal) histone-DNA interactions by Nap1 (Andrews et al., 2010).

Histone chaperones have been recognized as important players in regulating DNA accessibility and chromatin fluidity (reviewed by (De Koning et al., 2007; Eitoku et al., 2008)). Many histone chaperones are found in complex with histone modification enzymes or ATP-dependent chromatin-remodeling proteins. For example, human nucleosome assembly proteins 1 and 2 (Nap1 and Nap2) physically interact with p300 (Shikama et al., 2000); yeast Nap1 and other histone chaperones collaborate with the remodeling factor SWR1 in the replacement of histone H2A with the histone variant H2A.Z (Krogan et al., 2006), and the Nap1 family member Vps75 forms a complex with histone acetyltransferase (HAT) Rtt109 (Collins et al., 2007; Krogan et al., 2006).

1.5.1 Nap1 and Vps75

Nucleosome assembly protein 1 (Nap1) functions as a chromatin-assembly factor and a histone-storage protein. Functionally, Nap1 has been implicated in cell cycle regulation, transcription, exchange of histone variants, and nucleosome sliding (Mizuguchi et al., 2004; Park et al., 2005; Walter et al., 1995). Nap1 can also remove histone H2A/H2B dimers from assembled nucleosomes *in vitro* (Park et al., 2005). Importantly, nucleosome assembly requires the elimination of competing non-nucleosomal histone-DNA interactions by Nap1 (Andrews et al., 2010).

A novel Nap family member from yeast, called Vps75, was isolated and characterized (Han et al., 2007b; Selth and Svejstrup, 2007). Vps75 is a histone chaperone with a preference for H3/H4 tetramers and it may play a role in chromatin assembly (Selth and Svejstrup, 2007). Furthermore, Vps75 has been found in co-complex with yeast Rtt109, a HAT (histone acetyltransferase) that acetylates lysine 56 of H3 (H3K56), a modification that is likely to have a role in DNA replication and in maintaining genome stability in fungi (Driscoll et al., 2007; Han et al., 2007a; Jessulat et al., 2008; Schneider et al., 2006). Rtt109 is only the second known histone acetyltransferase (HAT) that seems to require a histone chaperone for its activity (Han et al., 2007b; Tsubota et al., 2007); the first documented case was the complex of Hat1 (the catalytic component) and Hat2 (the ortholog of the human histone-binding protein RBAP48 (Kelly et al., 2000)). *In vitro*, the reaction catalyzed by recombinant Rtt109 alone is slow and inefficient (Han et al., 2007a), and Vps75 serves to activate Rtt109's HAT activity (Tsubota et al., 2007). The precise role of Vps75 in the acetylation of K56 is unknown. Recent data shows that if the *VPS75* gene is deleted in yeast, there is no

effect on the acetylation of Lys-56, but both Rtt109 and Asf1 are required for H3K56 acetylation (Driscoll et al., 2007; Han et al., 2007a; Schneider et al., 2006; Tsubota et al., 2007). If Vps75 is always found in complex with the enzyme, why isn't it necessary for H3K56 acetylation?

Dr. Park in our laboratory has solved the structure of Vps75. Despite only 24% sequence identity between Vps75 and Nap1, the overall architecture of Vps75 is quite similar to that of Nap1. Vps75 is localized to the nucleus, whereas Nap1 shuttles between the cytoplasm and the nucleus. Vps75 is a bona fide histone chaperone on the basis of its ability to bind histones, to assemble chromatin *in vitro*, and to associate with chromatin *in vivo* (Selth and Svejstrup, 2007). We set out to discover and probe the mechanism by which Vps75 functions in Rtt109-mediated K56 acetylation. We hypothesized that the reason Vps75 was not required for H3K56 acetylation was because another histone chaperone was interacting with Rtt109 in the absence of Vps75. Additionally, we hypothesized that NAP1 was the putative protein. Asf1 may also be a good candidate for these redundant functions, because deletion of *ASF1* does lead to loss of H3K56ac (Adkins et al., 2007). Thus, the relationships between these chaperones and their roles in Rtt109 stimulation are unclear.

Chapter II of this thesis will discuss the crystal structure of *Saccharomyces cerevisiae* Vps75 and compare its structural and functional properties to those of *S. cerevisiae* Nap1. We found that both chaperones (the only two known Nap1 family members in yeast) bind histones with similarly high affinities, and both proteins stably interact with Rtt109; however, only Vps75 is capable of stimulating Rtt109 HAT activity.

Our data demonstrates a remarkable specialization of Vps75 for the interaction with and stimulation of Rtt109.

1.5.2 Chz1

Chz1 (Chaperone for H2A.Z/H2B) is characterized as a nuclear chaperone for H2A.Z/H2B. This discovery came about when Flag-H2A.Z/H2B was purified from whole cell extracts and found to associate with a previously uncharacterized protein, Chz1 (Luk et al., 2007). To confirm that Chz1 was H2A.Z/H2B specific, native Chz1 was immunoprecipitated from whole cell extracts and found to preferentially associate with H2A.Z/H2B versus H2A/H2B (Luk et al., 2007). *In vitro* His-tag pulldowns demonstrated that Chz1 was able to bind H2A.Z/H2B at higher ionic concentrations compared to canonical dimers (Luk et al., 2007). Although the data establishes that Chz1 is capable of binding H2A.Z, no evidence for chaperone activity (e.g. nucleosome assembly or disassembly) has been discovered.

Chz1 and H2A.Z have been shown to physically interact, but how Chz1 helps H2A.Z function *in vivo* has not been established. DNA microarrays were utilized to compare the mRNA expression levels (for a decrease or increase) in *chz1*Δ and *htz1*Δ strains. (Wan et al., 2009). Chz1 was found to regulate transcription in telomere-proximal genes, notably genes enriched in H2A.Z (Wan et al., 2009). The role of Chz1 in H2A.Z deposition was studied using chromatin immunoprecipitation assays (ChIP). Two different laboratories found that Chz1 was not required for the association or deposition of H2A.Z into chromatin. A *chz1Δ* strain had no effect on H2A.Z deposition into telomere-proximal regions on the right arm of Chromosome VI (Wan et al., 2009).

Furthermore, enrichment of H2A.Z at the promoter of *ADE17* and divergent promoters of *SOL2* and *SSK22*, remained unaffected by *chz1*Δ mutant (Luk et al., 2007). The lack of an *in vivo* effect on H2A.Z deposition could be explained by redundancy of function with other chaperones. If you delete *CHZ1*, then the pool of H2A.Z switches to almost exclusive binding to histone chaperone Nap1 (Luk et al., 2007). Additionally, the role of Chz1 could be to simply act as a binding protein for H2A.Z/H2B heterodimers that are unincorporated into nucleosomes.

Although redundancy between the two chaperones exists, Nap1 cannot complement all of the functions of Chz1. Chz1 and Nap1 display different phenotypes *in vivo.* If *CHZ1* is deleted the cells are sensitive to MMS, benomyl, and caffeine (Luk et al., 2007). Previous work has shown that the deletion of *NAP1* in yeast has no obvious phenotype under various conditions (Giaever et al., 2002; Park et al., 2008b). Nap1 and Chz1 differ significantly in other ways. Biophysical studies of Chz1 revealed a previously unidentified characteristic of a histone chaperone. Chz1 is intrinsically disordered, but upon binding histones, becomes more ordered (Luk et al., 2007). In sharp contrast, Nap1 has a well-folded structure in the absence of histones (Park and Luger, 2006b). The affinity of Chz1 for H2A.Z/H2B heterodimers was ascertained by isothermal titration calorimetry (ITC) and relaxation dispersion NMR spectroscopy (Hansen et al., 2009). The reported dissociation constant (Kd) for Chz1 binding to H2A.Z/H2B was ~0.2μM (Hansen et al., 2009). The affinity of Chz1 for other histones was not reported. Nap1 is also found in complex with H2A.Z/H2B *in vivo*, but a careful analysis of the binding affinities of Nap1 reveals that it binds histones H2A/H2B and H2A.Z/H2B with similar low nanomolar affinity (Andrews et al., 2008). The relative promiscuity of Nap1

for histones provides a rationale for further investigation into the putative histone specificity of Chz1. How does an intrinsically disordered chaperone specifically recognize and bind a histone variant that is structurally very similar to the canonical histone?

Structural information about the Chz1-H2A.Z/H2B interaction lacks evidence for H2A.Z/H2B specificity. The NMR structure of Chz1-H2A.Z/H2B was solved using truncated versions of a folded core including residues 71–132 of Chz1, residues 37–131 of H2B and residues 29–125 of H2A.Z (Zhou et al., 2008). As seen in Figure 1.4, the two histone chains were linked together to make a single chain of H2B (red) and H2A.Z (yellow). All of the unique residues of H2A.Z (yellow), defined as those that differ from H2A, are colored green in Figure 1.4. A careful analysis reveals that none of these residues are poised to interact with Chz1 (green).

In Chapter III of this thesis we studied Chz1, an intrinsically disordered protein (IDP) that binds histones H2A and H2A.Z. We confirmed previously published results that Chz1 is an intrinsically disordered protein that undergoes a conformational change upon binding H2A.Z/H2B. However, quantitative binding assays revealed that Chz1 is not histone variant-specific. Unlike the previously characterized histone chaperone Nap1, Chz1 did not affect the nucleosome structure under our conditions.

1.6 The SWR1 Complex

Three different labs discovered and purified the SWR1 complex that is required for the recruitment of H2A.Z into chromatin. The first lab utilized a genetic array screen to discover which of the 4700 deletion strains in yeast *Saccharomyces cerevisiae*

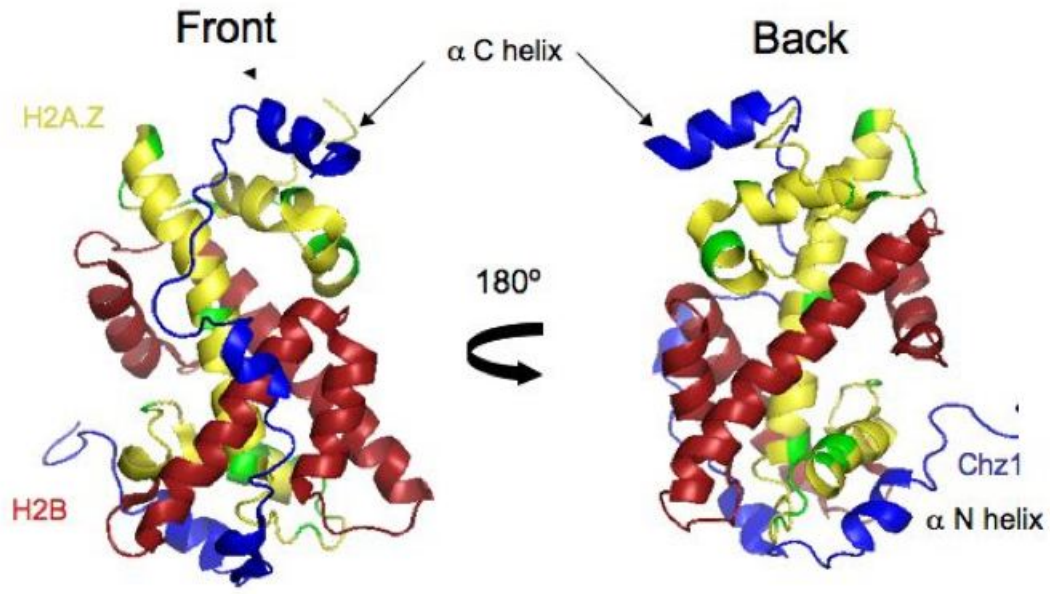

Figure 1.4: NMR structure of Chz1-H2A.Z/H2B.
The Chz1 core forms a long irregular chain capped by two short α-helices (blue) and makes broad contacts with H2A.Z (yellow) –H2B (red). Residues on H2A.Z that are unique from H2A are labeled in green. Described in Zhou et al. (2008), NSMB 15(8):868-9

produced synthetic growth events in conjunction with deletion of one of three yeast genes: *SET2*, *CDC73* or *DST1* (Krogan et al., 2003). Set2 physically interacts with RNAPII and is a histone methyltransferase (Hampsey and Reinberg, 2003). Cdc73 is a subunit of the PAF complex that is recruited to the coding regions of actively transcribed genes (Krogan et al., 2002). Dst1 or TFIIS, interacts with RNAPII and enables transcription through pause and arrest sites (Fish and Kane, 2002). Only five deletions genetically interacted with all three of the starting mutations: *HTZ1* which encodes the histone variant H2A.Z, three genes that encode members of the novel SWR1 complex, *SWC1*, *ARP6,* and *VPS71*; and an unrelated gene *SEC22* (Krogan et al., 2003). Vps71p was TAP-tagged and copurified from whole cell extracts with seven non-essential proteins and five essential proteins - the SWR1 complex (Krogan et al., 2003). Krogan had discovered 8 non-essential proteins (Swr1, Arp6, Yaf9, Swc2, Swc3, Swc5, Swc6, and Swc7) in addition to five essential proteins (Arp4, Act1, Swc4, Rvb1 and Rvb2) that comprised the SWR1 complex. Notably, all non-essential members of the SWR1 complex also co-purified with H2A.Z. Bdf1 copurified with some of the SWR1 components (Swr1, Swc5 and Swc6); perhaps this member of TFIID is loosely associated with the SWR1 complex (Krogan et al., 2003; Matangkasombut et al., 2000)**.**

The Wu laboratory identified the Swr1 complex through their interest in the *SWR1* gene, an uncharacterized member of the Swi2/Snf2 family of adenosine triphosphatases (ATPases). They too found Swr1 contained in a multi-component protein complex that catalyzed H2A.Z histone exchange. Experiments using flag-tagged Swr1 immunoprecipitations from yeast whole cell extracts revealed a 13-component complex associated with H2A.Z, the SWR1 complex (Mizuguchi et al., 2004). Only a small

fraction of the soluble H2A.Z was associated with the SWR1 complex, the rest was associated with yeast histone chaperone Nap1 or existed as free H2A.Z/H2B dimer (Mizuguchi et al., 2004). Later work by the Wu laboratory found that the H2A.Z/H2B dimer unincorporated in nucleosomes was always associated with a histone chaperone, either Chz1 or Nap1 (Luk et al., 2007). The difference is attributed to staining, as Chz1 can only be visualized by Coomassie blue and not silver staining.

The SWR1 complex was also discovered by a third group searching for proteins capable of selectively interacting with H2A.Z (Kobor et al., 2004). They identified 15 proteins associated with H2A.Z, 13 of which form the SWR1 complex. Notably, they found Bdf1 associated with TAP-tagged H2A.Z, hence they included Bdf1 as a SWR1 component. The SWR1 complex will henceforth known as a 14-subunit complex containing both Arp6 and Bdf1 (Figure 1.5).

Discovery of the SWR1 complex associated with H2A.Z led to a proposed ATP-dependent mechanism whereby the SWR1 complex can dissociate canonical nucleosomes and replace the major type histone H2A with H2A.Z (most likely as an H2A.Z/H2B dimer) (Mizuguchi et al., 2004). Using TAP-tagged purifications and immunoblots, the SWR1 complex was shown to selectively associate with H2A.Z versus H2A *in vivo* (Kobor et al., 2004). H2B is also found in conjunction with the SWR1 complex *in vivo*, which leads to the possibility that the substrate for H2A.Z exchange by the complex is H2A.Z/H2B (Kobor et al., 2004).

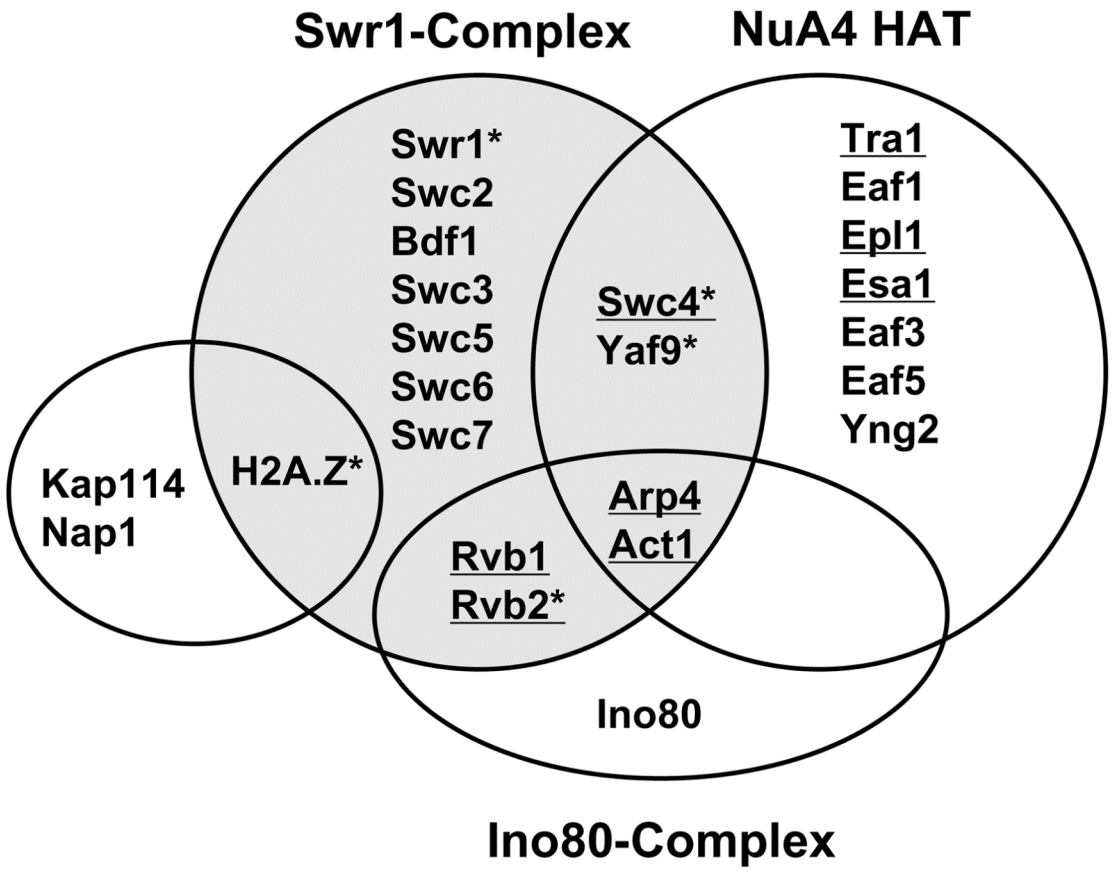

Figure 1.5: Components of the SWR1, INO80 and NuA4 complexes.
Shown is a Venn diagram of the proteins in the SWR1, INO80 and NuA4 HAT complexes. The proteins associated with H2A.Z can also be seen. Arp4 and Act1 are members of all 3 complexes. Swc4 and Yaf9 are members of the SWR1 and NuA4 complexes. INO80 and SWR1 share both the Arp4 and Act1 subunits. Adapted from Kobor et al. (2004), PLoS Biol. 2(5):131.

1.6.1 The SWR1 complex recruits H2A.Z *in vivo*.

If the SWR1 complex functions to deposit H2A.Z into chromatin *in vivo*, then mutations of the SWR1 components should result in a reduction of H2A.Z deposition. ChIP assays were used to monitor H2A.Z recruitment to chromatin. It was found that deletions of *SWC6, SWC2, ARP6, SWC3* and *SWR1* almost completely abolished H2A.Z binding (Krogan et al., 2003). This was not due to decreased synthesis of H2A.Z; western immunoblots revealed similar protein levels in both the wild type and mutant strains. The binding of H2A.Z was negatively affected at the promoter, coding region, and 3' untranslated regions of each gene tested in the various SWR1 complex mutant strains (Krogan et al., 2003). ChIP assays in the Wu laboratory also found that chromatin binding of H2A.Z *in vivo* required *SWR1*, but that H2A.Z protein levels were the same. H2A.Z binding was abolished at numerous chromosomal locations from ~3kb - ~416kb from the telomere in the *swr1Δ* strain compared to wild-type strain (Mizuguchi et al., 2004). Swr1 and other members of the SWR1 complex (e.g. Swc6, Arp6 and Swc2) clearly play an important role in H2A.Z deposition *in vivo*. However, deletion of either of the two chaperones known to associate with H2A.Z (*NAP1* or *CHZ1* see above) reveals that neither protein is necessary for the incorporation of H2A.Z as demonstrated by ChIP assays (Luk et al., 2007). Similarly a double knockout (*nap1*Δ*chz1*Δ) yeast strain is still capable of site-specific incorporation of H2A.Z (Luk et al., 2007). This further reinforces the role of the SWR1 complex as an ATP-dependent histone variant exchanger.

1.6.2 SWR1 complex replaces H2A with H2A.Z *in vitro*.

The SWR1 complex uses a novel mechanism for chromatin remodeling in that not only are protein-protein interactions disrupted, but also protein-DNA interactions. Transfer of H2A.Z/H2B appears to be nucleosome-dependent because no transfer occurs on naked DNA (Mizuguchi et al., 2004). An *in vitro* nucleosome exchange assay showed that the SWR1 complex, combined with ATP and H2A.Z/H2B dimers, is capable of exchanging H2A.Z for H2A in preformed, immobilized nucleosome arrays (Mizuguchi et al., 2004). The SWR1 complex was able to transfer 77% of the H2A.Z/H2B into preformed canonical nucleosomes, but showed a reduced transfer rate (of 11%) for H2A/H2B dimers in an identical reaction (Mizuguchi et al., 2004). Both Chz1-H2A.Z^{FLAG}-H2B and Nap1-H2A.Z^{FLAG}-H2B complexes can provide H2A.Z to the SWR1 complex in the in vitro replacement assay (Luk et al., 2007). The mammalian SRCAP complex (metazoan counterpart to Swr1) has also been found to catalyze *in vitro* H2A.Z exchange into preformed mononucleosomes containing H2A (Ruhl et al., 2006). This establishes the existence of ATP-dependent histone variant exchangers in higher eukaryotes.

1.6.3 Genetic analysis of *SWR1* reveals a role in DNA damage repair.

To further investigate genetic functions of the SWR1 complex, a mini array analysis was performed. The mini-array contained 384 deletion strains and each deletion is a protein known to function in some aspect of chromatin modification, remodeling or transcription (Krogan et al., 2003). Deletion strains of the seven non-essential subunits of the SWR1 complex were then crossed with the 384-deletion mini-array (Krogan et al., 2003). Genetic analysis of the SWR1 complex and its individual non-essential

components, including Swc2, were conducted. Components of the SWR1 complex were found to interact genetically with (partial list) elongation factors, Mediator, SAGA, H2B ubiquitination complex, deubiquitination enzymes, NuA4 histone acetylase, histone deacetylases, and other chromatin remodeling proteins such as Rsc1 and Isw1 (Krogan et al., 2003). These genetic interactions suggest that the SWR1 complex is involved in chromatin remodeling and modifications linked to transcription. Importantly, the large number and variety of genetic interactions indicates a direct or indirect role in many biological processes. It should be noted that this synthetic genetic array was specifically designed to look for genes clustered around functionality in chromatin elongation and chromatin remodeling, but other roles for the SWR1 complex may exist.

Phenotypic studies of the *htz1*Δ and *swr1*Δ mutants revealed a similar phenotypic sensitivity to DNA damaging UV radiation and methyl methanesulfonate (MMS), as well as genotoxic agent caffeine, indicating a role for the two proteins in DNA damage repair (Kobor et al., 2004; Mizuguchi et al., 2004). Of the phenotypes tested, a difference exists in that *htz1*Δ, unlike *swr1*Δ, exhibits sensitivity to hydroxyurea (HU). Genome-wide transcription profiles for the two mutants (*htz1*Δ and *swr1*Δ) were analyzed and it was found that 44% of genes activated by Swr1 are also activated by Htz1. Of the 77 genes repressed by Swr1, 38% are repressed by Htz1 (Mizuguchi et al., 2004). There exists some overlap, but functional independence between the two genes exists. Notably, Swr1p-dependent genes are over represented in regions proximal to the telomere, similar to Htz1p-dependent genes (Kobor et al., 2004). A microarray experiment was carried out with a SWR1 knockout strain and it was found that 112 genes had mRNA levels reduced by 1.7 fold (Krogan et al., 2003). Interestingly of these 112 genes, only 28% are

contained within Htz1 activated domains (Krogan et al., 2003). These findings suggest that the SWR1 complex serves a role independent of H2A.Z. Currently the ascribed function of the SWR1 complex is that of a histone variant exchanger, but the *in vivo* analysis alludes to an undefined role in DNA damage repair.

1.6.4 SWR1 is recruited to genomic regions after DNA damage.

Several subunits of the SWR1 complex are also members of the NuA4 histone acetylation complex and INO80 chromatin remodeling complex, supporting a functional link between the three complexes, a link that has been further verified by genetic studies (Kobor et al., 2004; Lu et al., 2009) (Figure 1.5). Both *INO80* and *SWR1* deletion strains result in a DNA damage phenotype, indicating that both may play a role in DNA damage repair (Kobor et al., 2004; Mizuguchi et al., 2004; Shen et al., 2000). The *in vivo* substrates of NuA4 HAT complex have also been shown to be important for DNA damage responses; strains lacking H2A and H4 tails are sensitive to MMS (Downs et al., 2004). It is highly likely that these complexes work together to facilitate DNA repair and although the function in repair is expected, the roles of each complex have not been elucidated.

Cells constantly battle harmful DNA lesions; some are potentially lethal. DNA DSBs are the most deleterious to cell viability. The inability to repair these lesions can result in mutations, cancer, cell death or chromosomal mutations (Finkel and Holbrook, 2000; Peltomaki, 2001). There are a variety of factors that are deployed once a cell detects DNA damage: some will engage in the physical repair of the damage, while others will trigger signaling pathways known as DNA damage checkpoints. Two

evolutionarily conserved pathways can repair DSB: homologous recombination (HR) or non-homologous end joining (NHEJ).

Yeast H2A (H2A.X in mammals) is phosphorylated on Serine 129 within ~50 kb of a single double strand break immediately by ATM and ATR checkpoint kinases (Tel1 and Mec1) (Burma et al., 2001; Downs et al., 2000; Redon et al., 2003). This phosphorylation event creates γ-H2AX in mammals (H2A-phospho in yeast), which is necessary for the recruitment of many DNA repair proteins (Paull et al., 2000). For the sake of clarity, I will use γ-H2AX when referring to phosphorylated H2A in yeast or phosphorylated H2A.X in mammals.

Pull-down assays revealed that natively purified SWR1 complex could bind γ-H2AX *in vitro* after treatment with MMS (Downs et al., 2004; Morrison et al., 2004). Using the *MAT* locus, it was shown that Swr1 ATPase is recruited to the DSB at the mating type locus *in vivo* (van Attikum et al., 2007). The presence of chromatin remodeler IN080 was established when ChIP assays revealed that Ino80 ATPase could bind near DSB sites up to 1.5kb away, but not at undamaged chromosomal loci (Downs et al., 2004; Morrison et al., 2004; van Attikum et al., 2004). If the H2A phospho-acceptor residue S129 was mutated, then the efficiency of recruitment was reduced by 75-80% for both Ino80 and Swr1 ATPases (van Attikum et al., 2007).

1.6.5 The SWR1 complex does not exchange or remove histones at DSBs.

Intriguingly, the SWR1 complex is recruited to DSBs, but the occupancy of H2A.Z surrounding an HO-endonuclease induced cut site decreases for up to four hours (van Attikum et al., 2007). Therefore, the SWR1 complex association at DSBs does not

function to exchange γ-H2AX for H2A.Z. Interestingly, the occupancy of H2A.Z did not decrease after HO-endonuclease cleavage in an *INO80* mutant strain (van Attikum et al., 2007). Therefore, the INO80 complex, not SWR1 is required for H2A.Z eviction (although no association between INO80 complex and H2A.Z has been previously described). Further analysis revealed that INO80, but not SWR1 recruitment, is needed to evict both core histones and histone variant γ-H2AX at *MAT* (van Attikum et al., 2007). Therefore, the role of the SWR1 complex at DSB is independent of histone exchange or removal. Interestingly, a *SWR1* gene deletion negatively affected the binding of yKu80 (van Attikum et al., 2007). The *Saccharomyces cerevisiae* Ku heterodimer comprising yku80 and yku70 binds DNA at DSBs and facilitates repair by the NHEJ pathway. The SWR1 complex therefore facilitates binding of yKu80 and plays a significant role in DSB repair.

1.7 Swc2, a histone-binding protein in the SWR1 complex.

Preliminary experiments performed on the non-essential subunits of the SWR1 complex established Swc2 as a binding module for H2A.Z (Wu et al., 2005) (Figure 1.6). Partial SWR1 complexes purified from *swc2*Δ, had severely reduced histone exchange activity *in vitro*, as indicated by little transfer of H2A.Z-Flag to immobilized nucleosomes (as did *arp6*Δ*, swc6*Δ, *swc5*Δ and *yaf9*Δ strains) (Wu et al., 2005). To determine if the lack of exchange was due to decreased H2A.Z binding, partial SWR1 strains were immunoprecipitated from whole cell extracts and H2A.Z (HA tagged) association was detected by western blot analysis. Strains lacking Swc2, Arp6, and Swc6 had decreased H2A.Z binding (Wu et al., 2005). Partial SWR1 complexes lacking Arp6

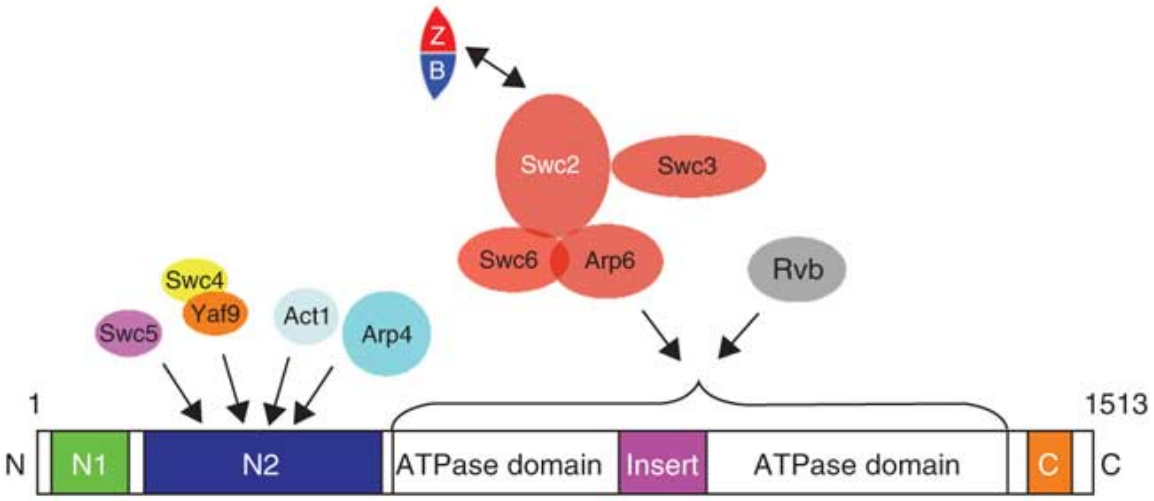

Figure 1.6: Model of the SWR1 complex.
The Swr1 ATPase is the architectural protein which organizes the complex. Swc2 is shown interacting with H2A.Z/H2B. Swc2, Swc6, Arp6 and Swc3 may form a smaller, functional complex. Adapted from Wu et al. (2005), NSMB 12(12):1064-71.

and Swc6 (and Swc2 to a lesser degree) also exhibited a decrease in immobilized nucleosome array binding compared to wild-type SWR1 complexes (Wu et al., 2005). As noted earlier, in an *arp6*Δ or *swc6*Δ strain, Swc2 does not associate with the SWR1 complex; it was therefore concluded that Swc2 is minimally necessary for H2A.Z association and nucleosome binding. Furthermore, in the absence of Swr1, Swc2 is still capable of binding H2A.Z *in vivo* (Wu et al., 2005). These studies implicate Swc2 as a protein with histone variant-specific binding activity capable of selectively interacting with H2A.Z/H2B. Further analysis of Swc2 revealed that the domain necessary for interacting and binding H2A.Z/H2B is contained within Swc2 N-terminal residues 1-281, as established using *in vitro* His-tag pulldowns (Wu et al., 2005).

Swc2 is a highly acidic protein and may interact with the positively charged histones to prevent improper interactions prior to assembly into chromatin. This could provide a reasonable explanation for why *swc2*Δ strain had reduced histone dimer exchange activity and reduced nucleosome binding. YL-1 is the metazoan counterpart of Swc2 and is a component of human SRCAP complex that remodels chromatin by incorporating H2A.Z (Cai et al., 2005; Ruhl et al., 2006). The amino acid sequence of Swc2 from yeast to humans exhibits a high degree of conservation, particularly residues 1-340. Notably, Swc2 and YL-1 are unusually enriched in charged residues. A yeast H2A.Z mutant in which the C-terminal region ('M6', (Clarkson et al., 1999)) was replaced with the corresponding region of H2A could not complement the *htz1Δ* (the gene for H2A.Z) when assayed for growth under restrictive conditions (Wu et al., 2005). Moreover, affinity purification of this mutant H2A.Z did not copurify with SWR1 components (Wu et al., 2005). This region is included within the "docking domain" that

mediates interactions between dimer and the $(H3:H4)_2$ tetramer within the histone octamer and may be important for interactions with the SWR1 complex.

In Chapter III and IV, our studies show that the N-terminal domain of Swc2 (1-179) is intrinsically unstructured *in vitro* and binds H2A.Z/H2B in a 1:1 ratio. Under our conditions, $Swc2_{1-179}$ is not histone variant-specific and binds H2A/H2B heterodimers with a similar affinity. Here we show that $Sw2_{1-179}$, despite its overall acidic charge, can bind dsDNA, in particular, 3-way and 4-way junction DNA.

1.8 Specific Aims

The primary objective of my thesis work was to study histone chaperones Vps75, Nap1, Chz1 and Swc2. Using yeast genetics, biophysics, structural and fluorescence studies we probed the structural and functional aspects of three yeast histone chaperones. Studies implicate Swc2 and Chz1 as proteins with histone-specific binding activity capable of interacting with H2A.Z/H2B dimers. However, the roles of Swc2 and Chz1 as independent histone chaperones have not been explored. The structures of a number of histone chaperones such as Nap1 (Park and Luger, 2006b), Vps75 (Park et al., 2008b), Asf1 (Daganzo et al., 2003) and Nucleoplasmin (Dutta et al., 2001) are known. These proteins have clearly defined tertiary structures (in addition to unstructured, acidic tails) even in the absence of histones and are only moderately specific for various histones (Andrews et al., 2008). In contrast, Swc2 (& Chz1) appear to be selective for histone dimers composed of the histone variant H2A.Z and H2B, as demonstrated by qualitative pulldown assays. However, no careful analysis of relative and absolute binding affinities has been described, nor has the affinity for other histones (e.g. H2A/H2B) been probed.

Unlike other histone chaperones, Swc2 and Chz1 are predicted to be intrinsically disordered proteins. Thus, the apparent specificity for H2A.Z/H2B is hard to reconcile with an intrinsically disordered protein and warrants further investigation.

We utilized biophysics and structural studies to determine that these proteins are intrinsically disordered, but become more ordered upon interaction with histones. Importantly, we discovered that Chz1 and $Swc2_{1-179}$ are not histone variant-specific; in fact, they bind histones with an affinity lower than that of previously described histone chaperones. We determined that due to their inability to affect nucleosome structure, these proteins aren't chaperones, but rather histone-binding proteins. Additionally, we identified an unexpected role of Swc2 in the recognition of unusual DNA structures. Yeast phenotypic analysis revealed that when *SWC2* is deleted, the mutant strain is sensitive to MMS, HU, and caffeine. This establishes a role for Swc2 in DNA damage repair that is likely related to its DNA binding. This could provide a clue as to why the SWR1 complex is found at sites of DSBs where it serves a function unrelated to H2A.Z incorporation.

The precise role of Vps75 in the acetylation of K56 is unknown. Recent data shows that if the *VPS75* gene is deleted in yeast, there is no effect on the acetylation of Lys-56, but both Rtt109 and Asf1 are required for H3K56 acetylation (Driscoll et al., 2007; Han et al., 2007a; Schneider et al., 2006; Tsubota et al., 2007). If Vps75 is always found in complex with the enzyme, why isn't it necessary for H3K56 acetylation? We set out to discover and probe the mechanism by which Vps75 functions in Rtt109-mediated K56 acetylation. We hypothesized that the reason Vps75 was not required for

H3K56 acetylation was because another histone chaperone was interacting with Rtt109 in the absence of Vps75. Additionally, we hypothesized that Nap1 was that putative protein.

Here we describe the crystal structure of *Saccharomyces cerevisiae* Vps75 and compare its structural and functional properties to those of *S. cerevisiae* Nap1. Both chaperones (the only two known Nap1 family members in yeast) bind histones with similarly high affinities, and both proteins stably interact with Rtt109; however, only Vps75 is capable of stimulating Rtt109 HAT activity. In addition, deletion of *VPS75* results in dramatic and diverse mutant phenotypes, in contrast to the lack of effects observed for the deletion of *NAP1*. The flexible C-terminal domain of Vps75 is important for the *in vivo* functions of Vps75 and modulates Rtt109 activity *in vitro*. Together, our data demonstrate a remarkable specialization of Vps75 for the interaction with and stimulation of Rtt109.

CHAPTER II

Histone Chaperone Specificity in Rtt109 Activation

Park YJ, Sudhoff KB, Andrews AJ, Stargell LA and Luger K

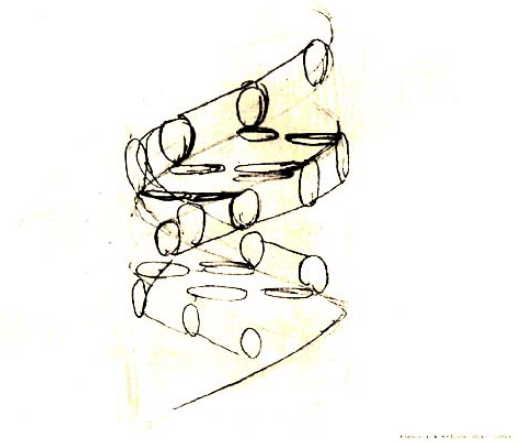

(Odile Crick, 1953)

This paper was published in the journal *Nature Structural and Molecular Biology*. Y.-.J.P. performed crystallography, gel shifts, enzymatic assays and initial yeast genetics studies; K.B.S. performed *in vivo* experiments; A.J.A. performed quantitative protein-protein interaction assays, MS and enzymatic assays; L.A.S. performed planning and advice for in vivo experiments; K.L. and Y.-J.P. planned and supervised the structural and biochemical experimental sections.

2.1 Abstract

Rtt109 is a histone acetyltransferase that requires a histone chaperone for the acetylation of histone 3 at lysine 56 (H3K56). Rtt109 forms a complex with the chaperone Vps75 *in vivo* and is implicated in DNA replication and repair. Here we show that both Rtt109 and Vps75 bind histones with high affinity, but only the complex is efficient for catalysis. The C-terminal acidic domain of Vps75 contributes to activation of Rtt109 and is necessary for in vivo functionality of Vps75, but it is not required for interaction with either Rtt109 or histones. We demonstrate that Vps75 is a structural homolog of yeast Nap1 by solving its crystal structure. Nap1 and Vps75 interact with histones and Rtt109 with comparable affinities. However, only Vps75 stimulates Rtt109 enzymatic activity. Our data highlight the functional specificity of Vps75 in Rtt109 activation.

2.2 Introduction

The packaging of DNA into chromatin has profound implications for all cellular processes that require access to the DNA substrate. Numerous activities have been identified that make compacted chromatin more amenable to the complex machinery responsible for transcription, replication and repair. These activities include histone chaperone–mediated nucleosome assembly and disassembly, post-translational modifications of histones, incorporation of histone variants and ATP-dependent chromatin remodeling. Evidence is emerging that all of these activities are tightly interwoven and cooperate in complex ways to achieve the delicate balance of chromatin compaction and decompaction.

Histone chaperones have been recognized as important players in regulating DNA accessibility and chromatin fluidity (reviewed by refs (De Koning et al., 2007; Eitoku et al., 2008)). Many histone chaperones are found in complex with histone modification enzymes or ATP-dependent chromatin-remodeling proteins. For example, human nucleosome assembly proteins 1 and 2 (NAP1 and NAP2) physically interact with p300 (Shikama et al., 2000); yeast Nap1 and other histone chaperones collaborate with the remodeling factor SWR1 in the replacement of histone H2A with the histone variant H2A.Z (Krogan et al., 2006), and the putative Nap1 family member Vps75 forms a complex with the newly discovered histone acetyltransferase (HAT) Rtt109 (Collins et al., 2007; Krogan et al., 2006; Tsubota et al., 2007).

Yeast Rtt109 acetylates H3K56, a modification that is likely to have a role in DNA replication and in maintaining genome stability in fungi (Driscoll et al., 2007; Han et al., 2007a; Jessulat et al., 2008; Schneider et al., 2006). Recent findings have demonstrated that Rtt109 also acetylates H3K9 (Fillingham et al., 2008). Rtt109 is only the second-known HAT that seems to require a histone chaperone for its activity (Han et al., 2007b; Tsubota et al., 2007); the first documented case was the complex of Hat1 (the catalytic component) and Hat2 (the ortholog of the human histone-binding protein RBAP48 (Kelly et al., 2000)). *In vitro*, the reaction catalyzed by recombinant Rtt109 alone is slow and inefficient (Han et al., 2007a), and Vps75 serves to activate Rtt109's HAT activity (Tsubota et al., 2007). Vps75 is a bona fide histone chaperone on the basis of its ability to bind histones and to assemble chromatin *in vitro* and to associate with chromatin *in vivo* (Selth and Svejstrup, 2007). Vps75 has approximately 24% sequence homology with yeast Nap1, a multifunctional histone chaperone with pleiotropic roles in

chromatin metabolism and cell-cycle regulation (reviewed by refs. (Park and Luger, 2006a; Zlatanova et al., 2007)). The unrelated histone chaperone Asf1 also stimulates Rtt109 activity *in vitro* (Driscoll et al., 2007; Tsubota et al., 2007). Notably, a deletion of *VPS75* has only minor effects on global H3K56 acetylation (H3K56ac) in yeast cells, also supporting redundant functions in vivo for the chaperones and Rtt109 stimulation (Han et al., 2007b; Selth and Svejstrup, 2007). Asf1 may be a good candidate for these redundant functions, because deletion of *ASF1* does lead to loss of H3K56ac, but it also leads to loss of H3K9ac, a modification that is performed by a different HAT, Gcn5 (Adkins et al., 2007). Moreover, Asf1 is not a member of the Nap1 family. Thus, the relationships between these chaperones and their roles in Rtt109 stimulation are unclear.

Here we describe the crystal structure of *Saccharomyces cerevisiae* Vps75 and compare its structural and functional properties to those of *S. cerevisiae* Nap1. Both chaperones (the only two known Nap1 family members in yeast) bind histones with similarly high affinities, and both proteins stably interact with Rtt109; however, only Vps75 is capable of stimulating Rtt109 HAT activity. In addition, deletion of *VPS75* results in dramatic and diverse mutant phenotypes, in contrast to the lack of effects observed for the deletion of *NAP1*. The flexible C-terminal domain of Vps75 is important for the *in vivo* functions of Vps75 and modulates Rtt109 activity *in vitro*. Together, our data demonstrate a remarkable specialization of Vps75 for the interaction with and stimulation of Rtt109.

2.3 Materials and Methods

2.3. 1 Expression and purification of recombinant proteins

Details are given in the Supplementary Methods (see below).

2.3.2 Structure determination

Recombinant Vps75 was crystallized by sitting-drop vapor diffusion at 16 °C from drops consisting of an equal mixture of protein (15 mg ml^{-1}) and reservoir solution (32% (v/v) PEG400, 50 mM NaCl and 25 mM HEPES, pH 7.5). Crystals (average size 0.05 × 0.30 × 0.03 mm) were obtained after 7 d. We flash-cooled crystals in liquid nitrogen directly from the well solution before data collection at beamline 4.2.2 at the Advanced Light Source (ALS). Data were processed and reduced with d*TREK (Pflugrath, 1999). We derived phases using MAD with data collected from SeMet mercury derivative crystals. The model was built with O (Jones et al., 1991), and refined with CNS (Brunger et al., 1997). The final model contains one dimer in the asymmetric unit. Diffraction data, refinement statistics and model parameters are given in Table 3. Structure superpositions were carried out using LSQMAN (Kleywegt, 1996).

2.3.3 Electrophoretic mobility shift assays

Protein complexes were analyzed by electrophoretic mobility shift assays (EMSAs) under native conditions. EMSAs were performed by incubating 10 μM Vps75 or Nap1 in a 10 μl reaction with the indicated concentrations of histones or Rtt109 at 4 °C for 16 h with 10 mM Tris, pH 7.5, 100 mM NaCl, 1 mM EDTA and 1 mM DTT. The samples were loaded onto a 5% acrylamide, 0.2× Tris-borate with EDTA (TBE) gel, electrophoresed for 50 min at 150 V and stained with Coomassie brilliant blue.

2.3.4 Binding-affinity measurements

Fluorescence titrations were used to determine the binding affinity of 0.2−0.4 nM Alexa-546 or Alexa-488 (H2A-H2B only)—labeled proteins (Vps75, H2A-H2B-T112C, or H3-H4(E63C)) to histone chaperones or Rtt109 in 300 mM NaCl, 0.5 mM EDTA, 1 mM DTT and 20 mM Tris-HCl, pH 7.5, using an AVIV model ATF105 spectrofluorometer. Labeled protein was added to both the sample and the reference cuvette, with nonlabeled protein added to the sample cuvette and buffer added to the reference. We normalized the ratio of the fluorescence signal from the sample cuvette to the reference cuvette using equation (1):

$$f.c._{obs} = \frac{R_{obs} - R_i}{R_{max} - R_i} \quad (1)$$

where $f.c._{obs}$ is equal to the fraction change for each concentration X added, R_{obs} is equal to the ratio at concentration X, the R_{max} is equal to the ratio at saturating protein, and R_i is the ratio where the protein concentration added is equal to zero. The binding affinity (K_d) of the various complexes was determined by fitting the $f.c._{obs}$ as a function of protein added (P_t) fit using equation (2) with the Kaleidagraph software:

$$f.c. = \frac{f.c._{max} * [P_t]}{[P_t] * K_d} \quad (2)$$

2.3.5 Stoichiometry

We determined stoichiometries by fluorescence titrations as above with the labeled protein concentration increased to more than ten-fold higher than the K_d. The fluorescence ratio was plotted as a function of the ratio of protein titrated to labeled protein. Under these conditions, the protein ratio at which the fluorescence ratio levels off is equal to the stoichiometry.

2.3.6 GST pull-down assay

0.5 nmoles of GST-tagged Rtt109 was immobilized on 50 μl of glutathione Sepharose 4B resin (GE Healthcare). The resin was then mixed with or without 1 nmol histone chaperone in the presence of various amount (5−500 pmol) of recombinant $(H3\text{-}H4)_2$ tetramer and incubated for 3 h. We removed unbound H3-H4 by washing three times with HEPES buffer (20 mM HEPES, 0.5 mM EDTA, 10% (v/v) glycerol, 0.05% (v/v) Nonidet p-40, 5 μM $ZnSO_4$ and 2.5 mM $MgCl_2$) at 450 mM KCl. To detect bound H3-H4, we used Alexa 488-labeled histone $(H3\text{-}H4)_2$ tetramer (labeled on H4-T71C). GST-tagged Rtt109 with Vps75 (full length), $Vps75_{1–223}$ or Nap1 (full length) interaction was tested separately in the same high-salt buffer condition. The results were analyzed by 15% SDS-PAGE and Storm (Amersham Biosciences). Minor nonspecific binding of H3-H4 was observed only at low-salt conditions (0−200 mM).

2.3.7 Yeast strains, plasmids and media

Yeast strain BY4741 (MATa his3Δ1 leu2Δ0 met15Δ0 ura3Δ0) was used for all investigations. We used yeast standard laboratory methods and techniques. Deletion mutants in the BY4741 background were purchased from Open Biosystems. BY4741

cells were grown for 48 h on rich media containing 2% (w/v) glucose. A shuttle vector encoding genomic *VPS75* was transformed into the *vps75*Δ mutant strain. The shuttle vector (pRS316) contained a full-length copy of the genomic DNA sequence for *VPS75* as well as a selectable marker URA3. The Vps75 shuttle vector was transformed into mutant *vps75*Δ cells and plated on selective media (CAA-U). Site-directed mutagenesis was used to generate pRS316 $Vps75_{1–223}$ and confirmed by sequencing before use. The shuttle vector pRS316 $Vps75_{1–223}$ was transformed into a *vps75*Δ mutant strain and grown on selective media (CAA-U). The final yeast strain containing pRS316-$Vps75_{1–223}$ was confirmed by PCR amplification of the *VPS75* locus and DNA sequencing. The ability of the truncated shuttle vector to recover phenotypes associated with the *vps75*Δ mutant strain was compared to that of the full-length *VPS75* shuttle vector. Cells were grown in media and then diluted to an absorbance at 600 nm (A_{600}) of 0.1. We made ten-fold serial dilutions of each culture and spotted them onto plates as indicated in Table 2.2. Cells were allowed to grow for 48−72 h at 30 °C or 38 °C. The MMS plate was made within 24 h of use. The yeasts were grown in liquid YPD medium (1% yeast extract, 1% bactopeptone and 2% glucose) at 30 °C. Plates for DNA damage assays contained YPD with or without 0.025% MMS or 0.2 M hydroxyurea and were photographed after 3 d of growth at 30 °C. For UV-sensitivity assays, cell cultures were diluted to an A_{600} of 0.2, along with ten-fold serial dilutions, and these were spotted on YPD plates. UV irradiation at 254 nm was performed with a Stratalinker 2400 (Stratagene) at 75 J m^{-2}. Duplicate sets of plated cells were exposed to UV irradiation and incubated at 30 °C for 3−4 d. All of our studies have been done in 8−16 replicate cultures.

2.3.8 Histone acetyltransferase assays

Reactions were performed in 50 mM Tris-HCl, pH 7.5, and 0.5 mM DTT, 100 mM NaCl using 1 mM acetyl CoA and analyzed by immunoblotting and acid urea gel. 10 µl reactions were incubated at 20 °C for 1 h, 2 h or 3 h and stopped by freezing in liquid nitrogen.

2.3.9 Western blot analysis

We resolved histone proteins by 15% SDS-PAGE for 30 min at 30 mA and transferred to nitrocellulose. Blots were probed with antibodies against H3K56ac (Upstate) or H3 (Abcam). Membranes were incubated at 4 °C for 10 h in TBST (5 mM Tris, pH 7.4, 27.4 mM NaCl, 0.5 mM KCl and 0.1% (v/v) Tween 20) with antibodies against either H3K56ac (1:6,000) or H3 (1:1,000). We diluted primary and secondary antibodies (a horseradish peroxidase—conjugated anti-rabbit IgG secondary antibody) in TBS containing 0.1% (v/v) Tween 20 and 5% (v/v) milk. Western blots were developed with an ECL detection kit (Amersham Biosciences). Secondary antibodies conjugated to horseradish peroxidase were detected using a Storm phosphorimager (Amersham Biosciences). To quantify modifications on histones, the intensity of the H3K56ac bands was analyzed by ImageQuant v5.1 (Amersham Biosciences). Data were reported as average values with s.d.; with a few exceptions, data points were derived from at least three independent gels. The gels were probed with antibodies against unmodified H3 to provide for a loading control. All data from the H3K56ac bands were normalized to unmodified H3.

2.3.10 Acid urea gel

We analyzed the total amount of H3 acetylation by acid urea gel electrophoresis. We used 15% polyacrylamide gels containing 5% (v/v) acetic acid and 6 M urea to separate modified from unmodified histones on the basis of differences in their charge (Shechter et al., 2007). Proteins were denatured in 6 M urea. Gels containing urea were prepared freshly to prevent nonspecific carbamylation of histone. The gel was run for 3 h at 150 V in 5% (v/v) acetic acid buffer and stained with Coomassie brilliant blue. Acetylated H3 was clearly separated from unmodified histones.

2.4 Results

2.4.1 Vps75 is a distinct member of the NAP1 family

The 24% sequence identity between yeast Nap1 and yeast Vps75 does not suggest a strong degree of structural homology between the two proteins (Fig. 2.1a). We determined the crystal structure of yeast Vps75 to a resolution of 1.85Å. Attempts to identify a molecular replacement solution with the previously published Nap1 structure as a search model (Park and Luger, 2006b) were unsuccessful, and we therefore used selenomethionine (SeMet) derivatives for MAD phasing. The electron density throughout almost the entire amino acid sequence was of excellent quality (Supplementary Fig. 2.1a).

Vps75 is a homodimer with two chains in the asymmetric unit. This is consistent with sedimentation velocity data that demonstrate the presence of a single species with an S(20,w) (the sedimentation coefficient corrected for water at 20 °C) of 3.8 (Supplementary Fig. 2.2a). To confirm unequivocally that Vps75 is a dimer in solution,

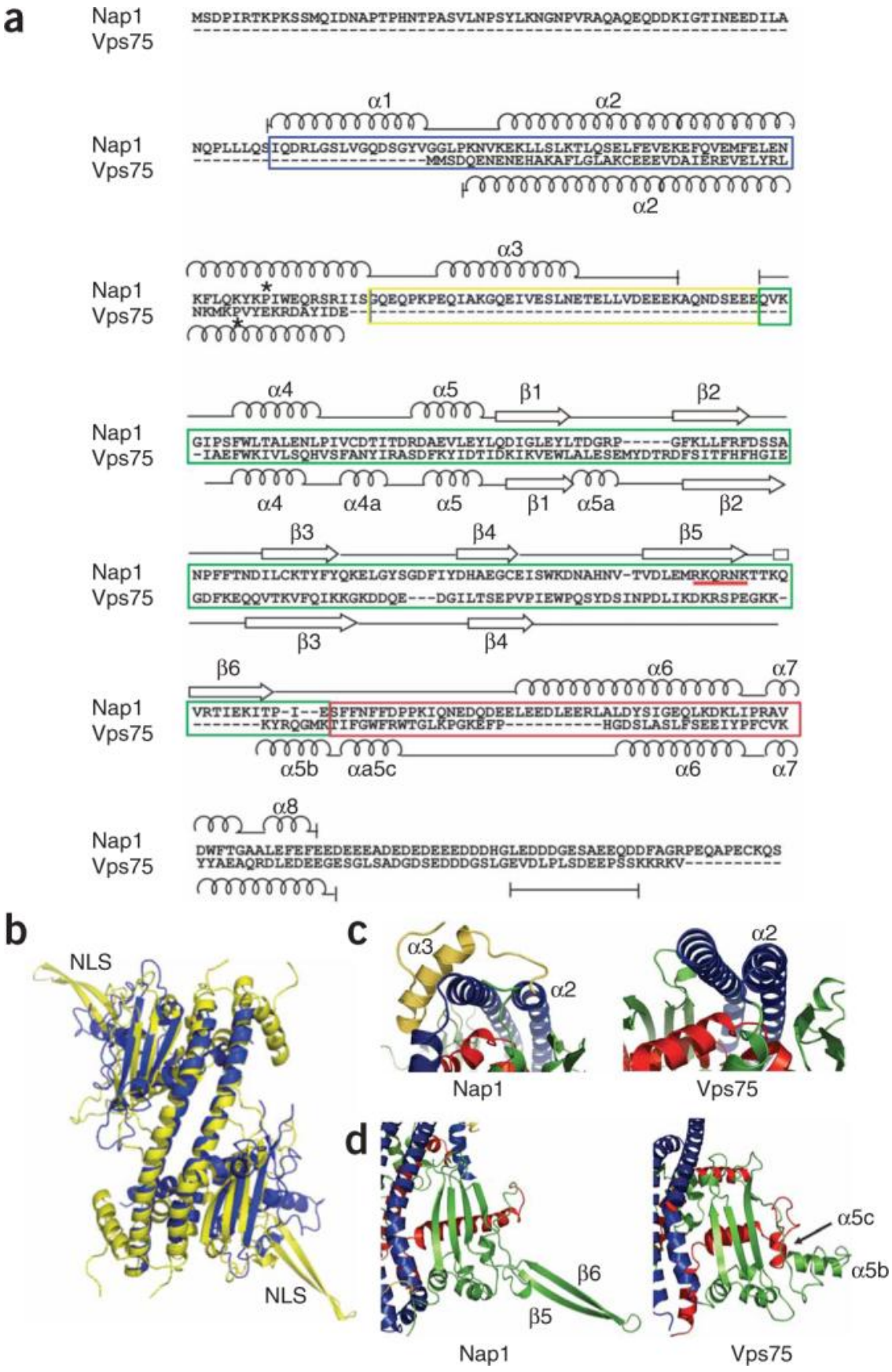
a
Nap1
Vps75
MSDPIRTKPKSSMQIDNAPTPHNTPASVLNPSYLKNGNPVRAQAQEQDDKIGTINEEDILA
α1
α2
NQPLLLQSIQDRLGSLVGQDSGYVGGLPKNVKEKLLSLKTLQSELFEVEKEFQVEMFELEN
MMSDQENENEHAKAFLGLAKCEEEVDAIEREVELYRL
α2
α3
KFLQKYKPIWEQRSRIISGQEQPKPEQIAKGQEIVESLNETELLVDEEEKAQNDSEEEQVK
NKMKPVYEKRDAYIDE
α4
α5
β1
β2
GIPSFWLTALENLPIVCDTITDRDAEVLEYLQDIGLEYLTDGRP-----GFKLLFRFDSSA
-IAEFWKIVLSQHVSFANYIRASDFKYIDTIDKIKVEWLALESEMYDTRDFSITFHFHGIE
α4
α4a
α5
β1
α5a
β2
β3
β4
β5
NPFFTNDILCKTYFYQKELGYSGDFIYDHAEGCEISWKDNAHNV-TVDLEMRKQRNKTTKQ
GDFKEQQVTKVFQIKKGKDDQE---DGILTSEPVPIEWPQSYDSINPDLIKDKRSPEGKK-
β3
β4
β6
α6
α7
VRTIEKITP-I--ESFFNFFDPPKIQNEDQDEELEEDLEERLALDYSIGEQLKDKLIPRAV
-------KYRQGMKTIFGWFRWTGLKPGKEFP----------HGDSLASLFSEEIYPFCVK
α5b
αa5c
α6
α7
α8
DWFTGAALEFEFEEDEEEADEDEDEEEDDDHGLEDDDGESAEEQDDFAGRPEQAPECKQS
YYAEAQRDLEDEEGESGLSADGDSEDDDGSLGEVDLPLSDEEPSSKKRKV
b
NLS
NLS
c
α3
α2
Nap1
α2
Vps75
d
β6
β5
Nap1
α5c
α5b
Vps75

Figure 2.1: Vps75 is a distinct member of the Nap1 family. (**a**) Structure-based amino acid sequence alignment of yeast Nap1 and Vps75. Blue, yellow, green and red boxes indicate subdomains A, B, C and D, respectively, as previously designated in the Nap1 structure. The alignment was generated using LSQMAN. Secondary-structural elements are shown above and below the corresponding sequences in both Nap1 and Vps75. Proline residues that induce helix curvature are indicated by asterisks. (**b**) Superposition of the Vps75 (blue) and Nap1 (yellow) structures. (**c,d**) Ribbon diagram of Nap1 and Vps75. Color coding is the same as in **a**. Secondary-structural elements are as defined in **a**. (c) A detailed comparison of the accessory domain in the same view as in Supplementary Fig. 2.1c. **(d)** Ribbon diagram of the region encompassing the nuclear localization signal (NLS) in Nap1 and the equivalent region in Vps75.

we performed sedimentation equilibrium of a version of Vps75 that lacks the C-terminal acidic domain (see below, $Vps75_{1–223}$, with a calculated molecular mass of 28,527 Da) under similar solution conditions and over a 16.2-fold range of concentrations. Details are given in Supplementary Figure 2.2b and Supplementary Methods online. $Vps75_{1–223}$ is best described as a homogenous population of Vps75 dimers under these conditions. Given the near-identical behavior of full-length and $Vps75_{1–223}$ in sedimentation velocity experiments, we conclude that full-length Vps75 is also a dimer in solution.

Vps75 shares several structural features with Nap1 (Fig. 2.1b). Both proteins are obligate homodimers that are held together through the antiparallel pairing of the long α2 helices of two monomers. The pronounced curvature of this helix, previously observed for Nap1, is maintained in Vps75 and is caused by the presence of a proline approximately two-thirds into the α2 helices (Fig. 2.1a, asterisk). Many hydrophobic residues are conserved between the two proteins. Like Nap1, Vps75 is an acidic protein with a pI of 4.64. The charge distribution for Vps75 is uneven, with a relatively random distribution of acidic, basic and neutral amino acids on the upper side of the dome-shaped dimer, whereas most of the acidic residues are clustered at the underside, especially in the cavity formed by the two β-fold domains (Supplementary Fig. 2.1b).

The Vps75 structure differs from that of Nap1 in several important aspects. First, Vps75 has neither an N-terminal tail nor the equivalent of the accessory domain previously defined in Nap1 (Park and Luger, 2006b) (Fig. 2.1a, yellow). Vps75 contains a C-terminal acidic domain (CTAD); however, this region has fewer negative charges (16 compared to 28) and a short stretch of hydrophobic amino acids that is not present in

Nap1 (Fig. 2.1a, underlined). This region of the CTAD is clearly visible in the Vps75 electron-density map (Supplementary Fig. 2.1c) because it is involved in crystal contacts with a neighboring Vps75 dimer. Second, the N-terminal end of the long α2 helix is almost completely covered by the accessory domain in Nap1, whereas it is solvent exposed in Vps75 (Fig. 2.1c). The accessory domain is absent in Vps75. Third, the region of Nap1 that contains the nuclear localization sequence (NLS) assumes different conformations in the two structures (Fig. 2.1b,d). In Nap1, the NLS is part of an extended β hairpin (β5-β6) that is responsible for oligomerization of Nap1 dimers (Park et al., 2008a). In Vps75, this region forms a helix-loop-helix conformation. As is the case with Nap1, this region in Vps75 harbors eight basic residues (Fig. 2.1a) and is the most positively charged region in the entire protein (Supplementary Fig. 2.1b). Fourth, the region equivalent to the Nap1 α1 helix is absent in Vps75 (Supplementary Fig. 2.1d). In Nap1, this helix forms an acute angle to α2 (Park et al., 2008a) and its presence restricts the orientation of the penultimate α7 and α8 helices. In Vps75, α7 and α8 form a single, uninterrupted helix, presumably allowing a wider range of motion for the C-terminal domain in solution.

Using gel-shift assays, we demonstrate that full-length Vps75 forms well-defined supershifts upon addition of increasing amounts of either H2A-H2B dimer or $(H3\text{-}H4)_2$ tetramer (Fig. 2.2a). H2A-H2B and H3-H4 do not enter the gel under these conditions because of their strong positive charge. We determined the binding affinities of the various Vps75-histone complexes by monitoring a change in fluorescence of a fluorophore attached to either H3 or Vps75 upon incubation with H2A-H2B dimer or (H3-H4)2 tetramer (Fig. 2.2b). Both histone complexes bind Vps75 with low nanomolar

affinity. This value is comparable to the affinity between Asf11−168 and H3-H4, which was measured under the same conditions (Table 2.1). The values were the same irrespective of the location of the fluorescent label (25 nM and 27 nM for labeled Vps75 or labeled H3-H4, respectively; Table 2.1). H3 binds Vps75 in the absence of H4, but with reduced affinity. As is the case for Nap1 (Park et al., 2005), the C-terminal domain of Vps75 does not contribute to histone binding (Fig. 2.2b,c, Table 2.1). The stoichiometry of a Vps75–H3-H4 complex was also determined using a fluorescence assay (Fig. 2.2d): one Vps75 dimer binds two molecules of H3-H4. At this stage, it is unknown whether Vps75 binds one $(H3\text{-}H4)_2$ tetramer or two half-tetramers (H3-H4). We believe that the presence of higher-order gel shifts (as seen in Fig. 2.2a,c) represent lower-affinity complexes of Vps75 and histones, possibly also multimers of histone-bound Vps75. Eventually, these higher-order (low-affinity) complexes become too large (or too positively charged) to enter the gel, a phenomenon that is commonly observed during native gel electrophoresis.

Nap1 can remove histone H2A-H2B dimers from assembled nucleosomes *in vitro* (Park et al., 2005*)* and we therefore tested whether Vps75 has this same ability. Nucleosomes were assembled with the fluorescently labeled mutant H2A-T112C and then incubated with equivalent amounts of Vps75 or Nap1 (Supplementary Fig. 2.3). Under conditions where the addition of Nap1 leads to the formation of a repositioned nucleosome species and H2A-H2B dimer—depleted nucleosomes, Vps75 had no discernible effect on nucleosome composition. These results suggest that the two chaperones are functionally distinct, despite their similar structure and histone binding properties.

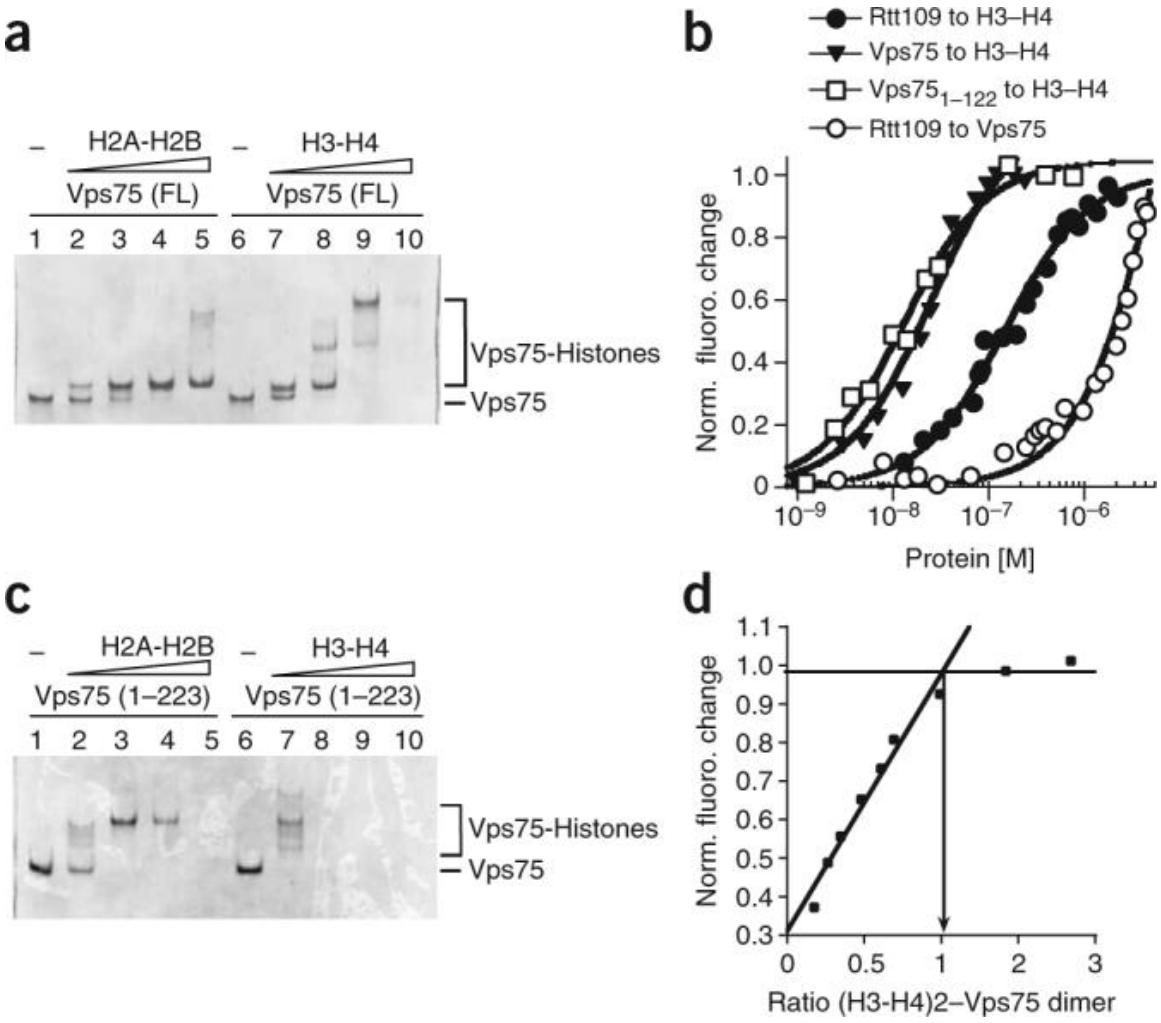

Figure 2.2: Vps75 binds histones with high affinity. (a) Vps75 dimer (5 μM) was incubated with recombinant yeast H2A-H2B dimer (lanes 1−5 show 0 μM, 1 μM, 2 μM, 3 μM and 4 μM, respectively) or recombinant yeast $(H3\text{-}H4)_2$ tetramer (lanes 6−10 show 0 μM, 1 μM, 2 μM, 3 μM and 4 μM, respectively) at 4 °C for 10 h. Complex formation was analyzed by 5% native PAGE and stained with Coomassie brilliant blue. The position of Vps75—histone dimer complexes is indicated. (b) Affinity measurement of the Vps75—H3-H4 interaction. The normalized fluorescence change (Norm. fluoro. change) upon binding of Rtt109 to H3-H4 and of Vps75 or $Vps75_{1—223}$ to Alexa-546-labeled H3-H4 measured by fluorescence titration. The binding curve for Vps75—Rtt109 is also shown. A standard binding isotherm (Methods) was fit to these data to determine the K_d for each interaction (see Table 2.1 for K_d values). (c) As in a, except that $Vps75_{1–223}$ was used instead of full-length Vps75. (d) Stoichiometry of H3-H4—Vps75 complexes. Normalized fluorescence change in labeled $(H3\text{-}H4)_2$ (where the labeled protein concentration is five times the K_d) as a function of ratio of $(H3\text{-}H4)_2$ to Vps75 dimer.

Table 2.1: Affinity measurements of protein-protein interactions

Interaction	Protein titrated	Protein labeled	K_d (M)
Vps75—H3-H4	Vps75	H3-H4	$2.5 \pm 0.3 \times 10^{-8}$
	H3-H4	Vps75	$2.7 \pm 0.1 \times 10^{-8}$
	$Vps75_{1-222}$	H3-H4	$1.3 \pm 0.1 \times 10^{-8}$
Vps75—H3	H3	Vps75	$1.2 \pm 0.1 \times 10^{-7}$
Vps75—H2A-H2B	Vps75	H2A-H2B	$4.5 \pm 0.3 \times 10^{-9}$
Vps75—Rtt109	Rtt109	Vps75	$>5 \times 10^{-6}$
Rtt109—H3-H4	Rtt109	H3-H4	$1.5 \pm 0.1 \times 10^{-7}$
Asf1—H3-H4	Asf1	H3-H4	$1.0 \pm 0.1 \times 10^{-8}$

All measurements were performed in 20 mM Tris-HCl, pH 7.5, 0.5 mM EDTA, 1 mM DTT, 0.1 mg ml^{-1} BSA and 300 mM NaCl. Labeled proteins were kept at 0.2−0.4 nM or <<five-fold the K_d. Standard errors from curve fitting are listed. See Methods for details.

2.4.2 The C-terminal acidic domain of Vps75 is required for *in vivo* function(s)

To further investigate the functional differences between Vps75 and Nap1, we compared the effects of gene disruptions *in vivo* (Fig. 2.3a and Table 2.2). Previous work has shown that the deletion of *NAP1* in yeast has no obvious phenotype under various conditions (Giaever et al., 2002), and this was confirmed in our analyses. In contrast, a strain in which *VPS75* was deleted showed sensitivity to UV radiation, hydroxyurea, methyl methanesulfonate (MMS) and methotrexate (Fig. 2.3a). All of these agents are known to induce DNA damage (Hampsey, 1997). The deletion of **VPS75** also resulted in temperature sensitivity (slow growth at 38 °C). We also observed slow growth on 1 M NaCl and in the absence of inositol (Table 2.2). The observed phenotypes are not reflective of overall growth defects, as the strain containing the deletion of **VPS75** grows normally on 1 M sorbitol (an inducer of osmotic stress) and H_2O_2 (an inducer of oxidative stress).

All of the phenotypes resulting from a deletion of *VPS75* were rescued with a shuttle vector encoding full-length Vps75 (Fig. 2.3b). However, a shuttle vector encoding a version of Vps75 that is missing the CTAD ($Vps75_{1–223}$) was, at most, partially able to revert any of the effects of *VPS75* deletion on growth under the conditions tested. Notably, under *in vitro* conditions, the CTAD did not contribute quantitatively to the interaction of Vps75 with histones (Table 2.1). Thus, the lack of phenotype rescue in the absence of the CTAD suggests previously unknown *in vivo* functional activities for this domain.

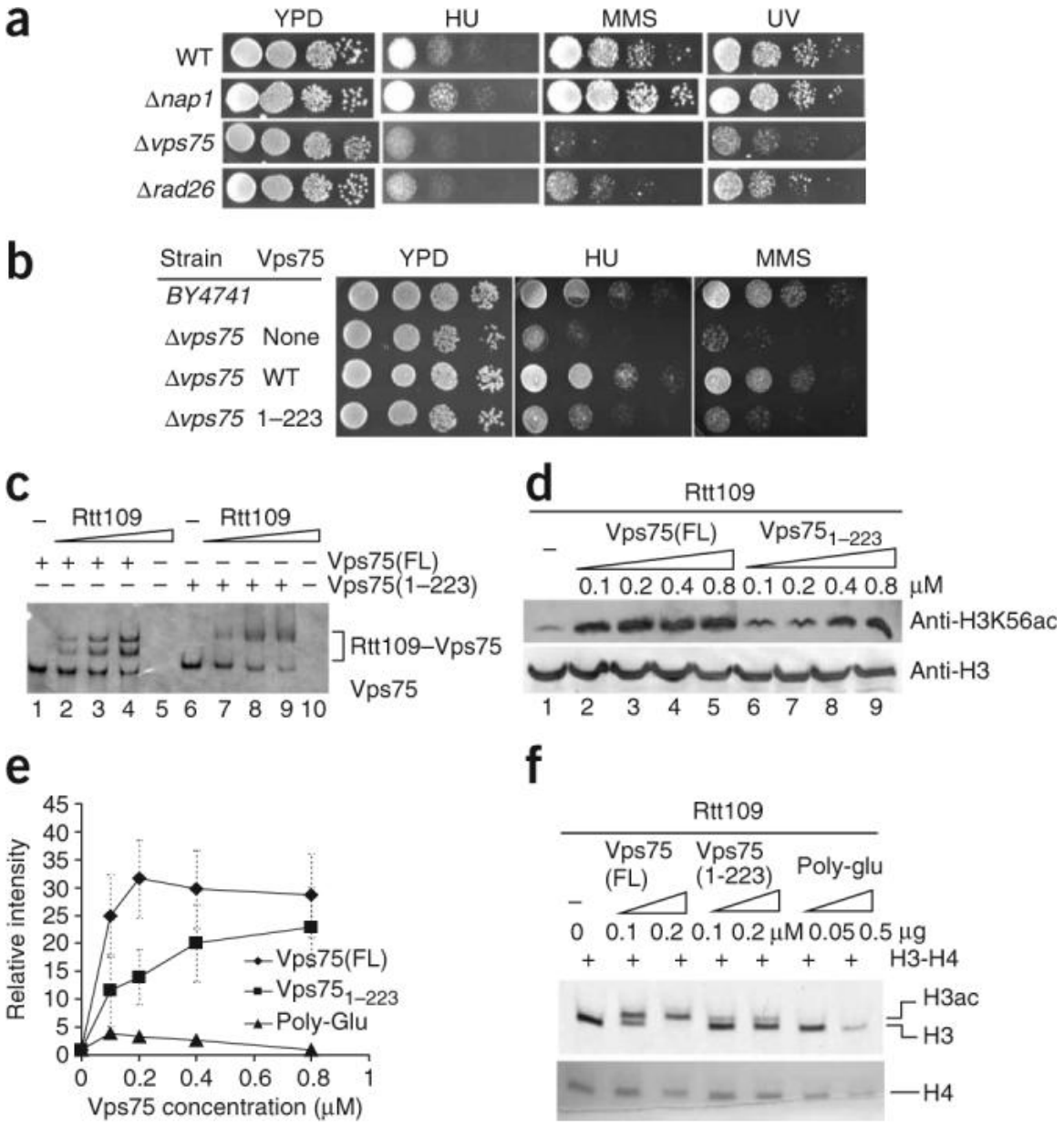
a
YPD
HU
MMS
UV
WT
Δnap1
Δvps75
Δrad26
b
Strain
Vps75
YPD
HU
MMS
BY4741
Δvps75 None
Δvps75 WT
Δvps75 1–223
c
– Rtt109
– Rtt109
Vps75(FL)
Vps75(1–223)
Rtt109–Vps75
Vps75
1 2 3 4 5 6 7 8 9 10
d
Rtt109
Vps75(FL)
Vps75 1–223
0.1 0.2 0.4 0.8 0.1 0.2 0.4 0.8 μM
Anti-H3K56ac
Anti-H3
1 2 3 4 5 6 7 8 9
e
Relative intensity
Vps75(FL)
Vps75 1–223
Poly-Glu
Vps75 concentration (μM)
f
Rtt109
Vps75 (FL)
Vps75 (1-223)
Poly-glu
0 0.1 0.2 0.1 0.2 μM 0.05 0.5 μg
H3-H4
H3ac
H3
H4

Figure 2.3: The C-terminal acidic domain of Vps75 contributes to *in vivo* and *in vitro* functions. (a) The *VPS75* deletion strain is sensitive to genotoxic agents, unlike a *NAP1* deletion strain. Ten-fold serial dilutions of wild-type (WT) and deletion strains were applied as spots to plates with rich media containing either glucose (YPD), hydroxyurea (HU 200 mM) or methane methylsulfonate (MMS 0.025%) and incubated at 30 °C. The deletion of *RAD26* (which is involved in transcription-coupled repair) is used as a control for the plates. **(b)** The C-terminal tail of Vps75 is required for restoring growth defects. Serial dilutions of the indicated strains were plated on YPD, HU (200 mM) and MMS (0.025%). **(c)** The ability of Vps75 to form a complex with Rtt109 was tested using gel shifts (5% polyacrylamide in 0.2× TBE). We combined 10 μl of 10 μM Vps75 dimer with increasing amounts of Rtt109 (lanes 1−4 or lanes 6−9: 0 μM, 1 μM, 2 μM and 3 μM, respectively; lanes 5 and 10 show a control of 3 μM Rtt109 which, owing to its strong positive charge, does not enter the gel). **(d)** Vps75 is required for the HAT activity of Rtt109. Purified Vps75 or $Vps75_{1–223}$ dimer (lanes 2−5 or lanes 6−9: 0.1 μM, 0.2 μM, 0.4 μM and 0.8 μM, respectively) and Rtt109 (0.5 μM) were incubated with 5 μM yeast $(H3\text{-}H4)_2$ tetramer in the presence of 1 mM acetyl-CoA for 3 h. The level of H3K56ac was detected by western blot analysis. Total protein H3 on the blot was detected by anti-H3 antibody. The activity of full-length (Vps75(FL), lanes 2−5) and C-terminal truncated $Vps75_{1–223}$ (above, lanes 6−9) were compared. $Vps75_{1–223}$ showed a reduction in H3K56ac compared to full-length Vps75. **(e)** Normalized HAT activity curves (obtained by monitoring changes in intensity of the western blot) are shown to the right. Error bars represent s.d. **(f)** The same reactions as in d were analyzed by acetic urea gel to identify other reaction products. Acetylation on H3 causes a reduction in gel mobility. Polyglutamate (Poly-glu) has no effect on acetylation.

Table 2.2: Phenotypic comparison of yeast deletion strains

	BY4741	Δ*nap1*	Δ*vps75*
30 °C	+ + +	+ + +	+ + +
38 °C	+ + +	+ + +	−
UV (75 J)	+ + +	+ + +	+
HU (200 mM)	+ + +	+ + +	−
MMS (0.025%)	+ + +	+ + +	−
MTX (50 μg ml^{-1})	+ + +	+ + +	+
NaCl (1 M)	+ + +	+ + +	+ +
Minus inositol	+ + +	+ + +	+ +
Sorbitol (1 M)	+ + +	+ + +	+ + +
H_2O_2	+ + +	+ + +	+ + +

Ten-fold serial dilutions of strains were applied as spots to the media indicated (see also Fig. 2.4). +++, robust growth, comparable to a wild-type strain; + to ++, intermediate values; −, no growth. HU, hydroxyurea; MMS, methyl methanesulfonate; MTX, methotrexate. Unless specified in Methods, the plates contained YPD medium.

2.4.3 The CTAD of Vps75 contributes to stimulation of Rtt109 HAT activity

In vivo, a substantial portion of Vps75 is found in complex with the HAT Rtt109 (Krogan et al., 2006). To test the possibility that the Vps75 CTAD functions through mediating the interaction with Rtt109, we compared the ability of full-length and truncated Vps75 to interact with recombinant, purified Rtt109 *in vitro*. Vps75 (either full-length or $Vps75_{1–223}$) was incubated with increasing amounts of Rtt109 (Fig. 2.3c). Rtt109 has a pI of 9.5 and does not enter the gel on its own (lanes 5 and 10). In contrast, both versions of Vps75 form clearly defined bands (lanes 1 and 6). Upon addition of Rtt109, supershifts of Vps75 were observed at comparable concentrations, demonstrating that the Vps75 CTAD is not required for the interaction with Rtt109.

To further verify the composition of the complexes in the shifted bands, we took two approaches. First, we excised the bands from the native gel and analyzed them by SDS-PAGE (Supplementary Fig. 2.4). Both Vps75 and Rtt109 were present in all excised bands we analyzed. Furthermore, the two proteins were present at apparently equal stoichiometries (Supplementary Fig. 2.4, lanes 4−6 and 8−10). To further investigate the homogeneity of the Vps75—Rtt109 complexes, we compared the solution state of a Vps75—Rtt109 complex at a 1:1 molar ratio to that of Vps75 (full-length and $Vps75_{1–223}$) and Rtt109 alone. Under our experimental conditions, Vps75 and Rtt109 are both monodisperse, and they sediment with an *S*-value of 3.1 and 3.8, respectively. A 1:1 complex of Vps75 (or $Vps75_{1–223}$) and Rtt109 sediments with an *S*-value of 6.1, with a portion of the material still in the unassociated form (Supplementary Fig. 2.2a). Given the relatively low K_d of the complex (Table 2.1), it is to be expected that some of the protein remains unassociated under the experimental conditions of 8 μM. Under our experimental

conditions, we observed no higher-order complexes. Together, these data indicate that both full-length and truncated Vps75 form defined and uniform complexes with Rtt109.

It may be that the CTAD of Vps75 acts to modulate the HAT activity of Rtt109. We incubated recombinant yeast $(H3\text{-}H4)_2$ tetramer with preformed Rtt109—Vps75 or Rtt109—$Vps75_{1–223}$ complexes and probed for H3K56ac (Fig. 2.3d). The ability of Rtt109 to acetylate H3K56 was increased about 30-fold upon the addition of full-length Vps75 (Fig. 2.3e). Comparatively, $Vps75_{1–223}$ was clearly not as efficient in promoting Rtt109-mediated H3K56 acetylation, especially under conditions where Vps75 is limiting (substoichiometric amounts of Vps75 to Rtt109). The addition of polyglutamate (40−100 kDa (Park et al., 2005)) had no effect on Rtt109 HAT activity, indicating that the function of the Vps75 CTAD goes beyond merely adding negative charge. The most straightforward explanation for our results (quantified in Fig. 2.3e) is that the CTAD of Vps75 contributes to the stability of the interaction between Vps75 and Rtt109 (Table 2.1), because acetylation levels reach near wild-type levels at higher concentrations of $Vps75_{1–223}$.

We next tested whether the CTAD of Vps75 contributes to the specificity of Rtt109-mediated acetylation. We analyzed the end products of the HAT reaction by acid-urea gels (Fig. 2.3f). This method allows for the separation of H3 molecules with one or more acetyl groups. This confirmed that in the absence of Vps75, no acetyl group is added to either H3 or H4, and that the stimulatory effect of $Vps75_{1–223}$ is much weaker than that of full-length Vps75 (Fig. 2.3f, above and below, respectively). No additional bands of acetylated histones were detected in the presence of $Vps75_{1–223}$.

To determine the affinity of Rtt109 for histones, we used fluorescently labeled $(H3\text{-}H4)_2$ tetramer and measured the changes in fluorescence upon Rtt109 addition. Rtt109 binds H3-H4 with an affinity of 150 nM (Table 2.1). In contrast, the interaction between Rtt109 and Vps75 (in the absence of histones) is much lower (~5 μM; Table 2.1). Both values argue against a simple role of a histone chaperone in increasing the affinity of Rtt109 for its histone substrate.

2.4.4 Nap1 binds Rtt109 but does not stimulate its enzymatic activity

As a deletion of *VPS75* has no effect on overall levels of H3K56ac *in vivo*, we asked whether Nap1 could functionally replace Vps75 in Rtt109 activation. We used gel-shift assays to demonstrate that Nap1 interacts robustly with Rtt109 (Fig. 2.4a). The presence of defined and similar supershifts obtained upon addition of increasing amounts of Rtt109 to either Vps75 or Nap1 indicates that Rtt109 forms equivalent complexes with either chaperone. The interaction between Nap1 and Rtt109 was also demonstrated through co-immunoprecipitation assays *in vivo* in a strain carrying a deletion of *VPS75* (Supplementary Fig. 2.5a). This interaction persists through extensive washing steps at 500 mM NaCl.

The addition of Nap1 to Rtt109 does not result in a detectable stimulation of H3K56 acetylation, as tested by western blot analysis (Fig. 2.4b,c). Only minor levels of acetylation were observed by urea acid gels on H3 in the presence of the Rtt109—Nap1 complex, even when a large excess of Nap1 over Rtt109 was used (Fig. 2.4d). Whereas Vps75 stimulated efficient Rtt109-mediated acetylation of H3 (in the absence of H4), Nap1 showed no such effect on Rtt109 (Supplementary Fig. 2.5b).

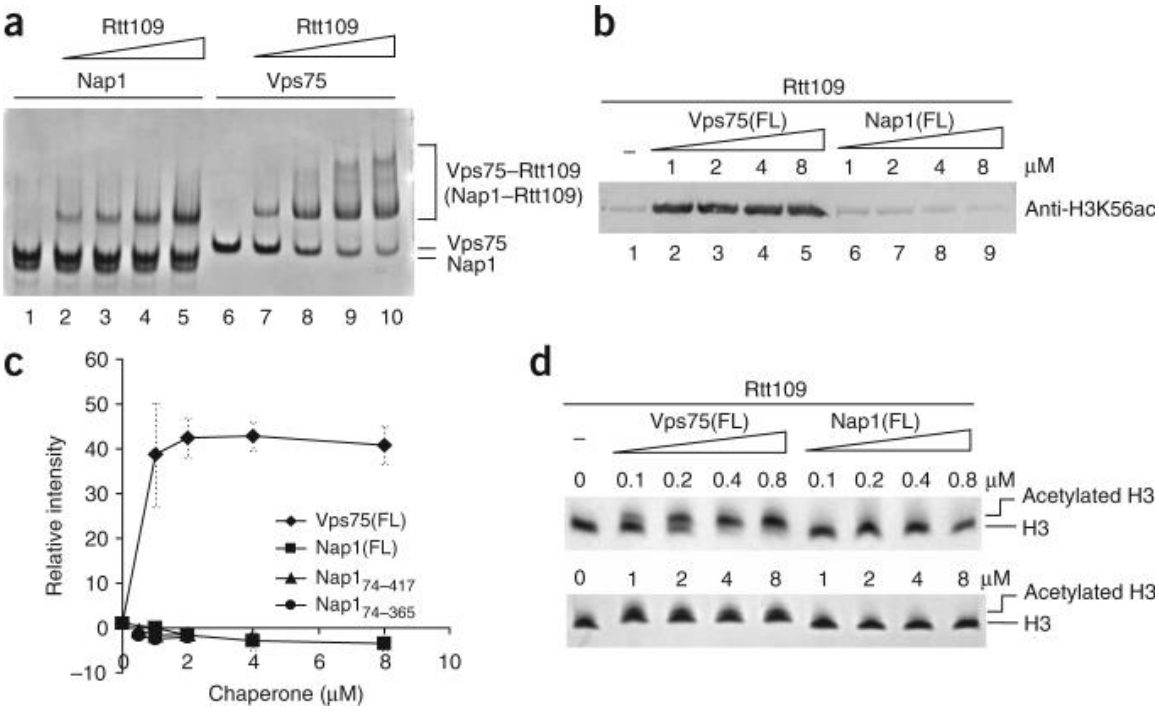

Figure 2.4: Nap1 does not stimulate Rtt109 HAT activity. (a) The ability of Nap1 to form a complex with Rtt109 was tested by gel-shift analysis. 10 μM Nap1 or $Vps75_{1–223}$ was incubated with Rtt109 (lanes 1−5 or lanes 6−10: 0 μM, 1 μM, 2 μM, 3 μM and 4 μM, respectively) at 4 °C for 10 h, and complex formation was analyzed by 5% native PAGE. **(b,c)** Nap1 does not enhance Rtt109-dependent H3 acetylation. The HAT activity of Rtt109 in the presence of Vps75 (lanes 2−5) or Nap1 (lanes 6−9) was tested using western blotting (b,c). 0.5 μM Rtt109 and 5 μM yeast $(H3\text{-}H4)_2$ tetramer were incubated in the presence of 1 mM acetyl-CoA and histone chaperone for 2 h (b). The amount of histone chaperones (0−8 μM) is indicated. The gels were probed with an anti-H3K56ac antibody, and the normalized densitometer scans of three independent experiments (obtained by monitoring changes in intensity of western blot) are shown in c. Note different scale of *x* axis compared to figure 2.3e. **(d)** The same samples as in b were analyzed on an acid urea gel to detect modifications on residues other than H3K56.

2.5 Discussion

Numerous homologs of Nap1 have been identified in metazoans, many with ill-defined functions in transcription regulation and other cellular functions (reviewed by refs. (Eitoku et al., 2008; Park and Luger, 2006a; Zlatanova et al., 2007)). In contrast, only two Nap1 family members exist in yeast: Nap1 and Vps75. The structural homology between Vps75 and Nap1 is immediately apparent from our studies, despite the low degree of sequence conservation. Vps75 also shares several structural characteristics with the Nap1 family member SET, a human oncoprotein with pleiotropic nuclear functions (Eitoku et al., 2008). Both proteins lack the extended N-terminal tail as well as the accessory domain previously identified in Nap1, and both proteins lack the nuclear export sequence and are thus predominantly nuclear in location. On the basis of this observation, it can be argued that Vps75 is a structural homolog of SET in yeast. SET is involved in histone and nucleosome metabolism, interacts with various transcription factors and has been found as a part of a complex that inhibits the acetyltransferase activity of p300/CBP and PCAF (Seo et al., 2001). Thus, like Vps75, it seems to have specialized in noncanonical histone-chaperone functions.

2.5.1 Vps75 binds histones with high affinity, but does not dissociate nucleosomes

Vps75 binds histones with high affinity *in vitro*. Low nanomolar affinities for various histone complexes seem to be a hallmark of the histone chaperones tested to date—Vps75, Asf1 and Nap1 from various species (this study, and A.J.A. and K.L., unpublished observations). Previously published studies (including ours) have used glutathione *S*-transferase (GST) pull-down assays to establish a preference of the three chaperones for H3-H4 (Lee et al., 2007; Muto et al., 2007; Zlatanova et al., 2007). Our

quantitative binding studies presented here suggest that H2A-H2B binds Vps75 with higher affinity than H3-H4. Thus, under the conditions tested, Vps75 is not an exclusive H3-H4 histone chaperone but is capable of binding both types of histone complexes with high affinity. One dimer of Vps75 binds two molecules of H3 and H4, either in the form of a $(H3\text{-}H4)_2$ tetramer or as two half- tetramers. The CTAD of Vps75 does not contribute to binding affinity. As is always the case with *in vitro* studies, we cannot exclude the possibility that the proteins may interact differently *in vivo*.

As Vps75 and Nap1 bind histones with similar affinities, the inability of Vps75 to disassemble nucleosomes under conditions where Nap1 disrupts them was unexpected. We have previously shown that the Nap1 CTAD is required for efficient nucleosome disruption *in vitro* (Park et al., 2005*)*, whereas the Vps75 CTAD (which differs in amino acid composition compared to Nap1) seems to contribute to Rtt109 stimulation.

2.5.2 *VPS75* and *NAP1* deletions cause different phenotypes in yeast

Further indications for nonoverlapping functions of Vps75 and Nap1 and for the importance of the CTAD of Vps75 *in vivo* come from gene-knockout studies. Whereas no growth defects were observed for the *NAP1* deletion, our results suggest a role for Vps75 in DNA damage repair (see also (Jessulat et al., 2008)). Published work (as well as our own unpublished data) on the deletion of *RTT109* demonstrates similar hydroxyurea and MMS mutant phenotypes (Jessulat et al., 2008), confirming the functional link between Vps75 and Rtt109. There is controversy in the field about the mutant phenotypes of a *VPS75* deletion strain (Driscoll et al., 2007; Jessulat et al., 2008; Selth and Svejstrup, 2007). We have found that the *VPS75* deletion strain is extremely vulnerable to

spontaneous suppression of growth phenotypes. Whether this, strain background or the actual experimental growth conditions are involved in these discrepancies is unclear at this time.

If H3K56ac levels remain unchanged in a *VPS75* deletion strain (Driscoll et al., 2007; Selth and Svejstrup, 2007), why then does this strain have phenotypes that are consistent with a role of Vps75 in DNA repair? Vps75 may have other roles in DNA damage repair that may result in the Rtt109-dependent acetylation of targets other than histones, or that are unrelated to Rtt109 activity. Of note, a global protein-expression profiling study in yeast showed that Vps75 was one of 157 proteins whose level increased by more than three-fold upon treatment with MMS(Lee et al., 2007). Notably, Rtt109 was not listed in this group of proteins. It is possible that Vps75 is functionally redundant with another protein, such as Asf1, with respect to Rtt109 activity. We have demonstrated that another logical candidate, Nap1, is capable of interaction with Rtt109 both *in vivo* and *in vitro*, but fails to stimulate acetylation.

It is surprising that two structurally unrelated histone chaperones (Vps75 and Asf1) with seemingly different histone binding properties (but similar affinities for histones) are capable of stimulating the enzymatic activity of Rtt109 to a similar extent *in vitro* (Tsubota et al., 2007). It has been argued that Vps75 either increases the binding affinity of Rtt109 for H3-H4 or that it helps provide specificity for H3K56 (Han et al., 2007b). However, the affinity of Rtt109 for H3-H4 in the absence of chaperone is certainly tighter than most reported K_m's of other HATs. *In vitro* data support the hypothesis that Asf1 functions to present H3-H4 to an Rtt109—Vps75 complex,

especially at limiting concentrations of Rtt109—Vps75 (Han et al., 2007b). Consistent with this interpretation, we observe a saturation of HAT activity at roughly equimolar concentrations of Rtt109 and Vps75, making it unlikely that Vps75 acts as part of the substrate. Rather, Vps75 could function through (i) a direct stimulation of the enzymatic activity, (ii) modulating the affinity of Rtt109 for either the Asf1—H3-H4 substrate or for the product of the enzymatic reaction, or (iii) through correctly positioning H3K56 in the active site. Any of these functional models requires the CTAD of Vps75.

Structural information for the chaperone–histone interaction is available for only Asf1 (English et al., 2005). Given that there are no structural or sequence similarities between Vps75 and Asf1, it is unlikely that the two proteins bind histones and Rtt109 in a similar manner; however, both can stimulate HAT activity to similar extents *in vitro*. Notably, Nap1, a structural homolog of Vps75 with similar histone-binding properties and the demonstrated ability to form a complex with Rtt109, does not stimulate HAT activity. The differences in sequence composition of the Nap1 and Vps75 CTAD may explain why Nap1 has no effect on Rtt109 activity. Together, these results suggest that Vps75 and Nap1 have distinct functions although they retain structural homology and a high affinity for histone complexes.

2.6 Supplementary methods

2.6.1 Expression and purification of recombinant proteins

We generated recombinant yeast Vps75 and yeast Rtt109 by cloning the open reading frames into pET28a or pGEX6P2, respectively. Rtt109 and Vps75 ORFs were PCR-amplified from yeast genomic DNA. We expressed Vps75 in *Escherichia coli* BL21

cells and purified it over a nickel affinity resin using standard techniques. After cleaving the his-tag with thrombin, we purified the protein by MonoQ chromatography. To express GST-Rtt109, we grew transformed E. coli Rosetta (Novagen) cells to an OD600 of 0.8, and induced protein expression with 0.1mM isopropyl β-d-thiogalactoside at 18°C for 16 hours. We purified GST-Rtt109 using glutathione sepharose beads. The GST-tag was cleaved off with precession protease (GE). We expressed and purified full-length and truncated versions of Nap1 (NAP-1ΔN and NAP-1ΔNC) of yeast NAP-1 as described (McBryant et al., 2003)**.** Recombinant histones (yeast and *Xenopus*) were generated in bacteria as described (Dyer et al., 2004; Luger et al., 1999). Recombinant histones were refolded to histone H2A/H2B dimer, H3/H4 tetramer or octamer. We tested the purity of individual proteins on 15% SDS-PAGE and stained with coomassie brilliant blue. Proteins thus prepared are fully functional because the histones we make are capable of forming nucleosomes (thus protein-protein interactions and DNA-protein interactions are fully functional); Vps75 was analyzed in solution, binds histones with high affinity, and stimulates Rtt109 activity, in addition to forming highly diffracting crystals; and Rtt109 is an active acetyl transferase in the presence of Vps75 or Asf1.

2.6.2 Analytical Ultracentrifugation

Sedimentation velocity experiments were performed with either a Beckman XL-I or XL-A analytical ultracentrifuge using the absorbance optical system. Sedimentation velocity was performed using two-sector charcoal-filled Epon centerpieces. Samples were spun at 50,000 rpm (201,600 x g), and the absorbance was monitored at 230 nm (individual proteins) or 280 nm (complexes). Samples were centrifuged until a thermodynamic equilibrium (as judged by overlaying scans collected 4 hours apart) was

reached. The boundaries were analyzed using the method of Demeler and van Holde (Demeler and van Holde, 2004) using Ultrascan (version 7.3). This analysis yields an integral distribution of sedimentation coefficients, G(s). Sedimentation coefficients (*s*) were corrected to that in water at 20° (*s*20,w). The solvent densities (ρ) and partial specific volume (v-bar) of proteins were calculated from the primary amino acid sequence within Ultrascan. Modeling of hydrodynamic parameters was performed within Ultrascan. Vps75, Vps751-223, and Rtt109 were dialyzed separately against 20mM Tris pH 7.5, 1mM TCEP, 200mM NaCl and 1mM EDTA, and mixed as indicated in the figure legends.

Runs from four rotor speeds resulting in a total of 22 data sets (Supplementary Figure 2.2B, upper panel) were globally fit to a variety of models within Ultrascan. The best fit, as judged by the residuals (see lower panel) and variance was to a single, ideal species model, with a resulting molecular mass of 55,330 Da. This value is within 3% of the calculated mass of a VPS75 1-223 dimer (557,054 Da) and resulted in non-systematic residuals.

Sedimentation equilibrium analytical ultracentrifugation of Vps751-223: Following extensive dialysis, the protein was diluted to 1.12, 3.6 and to 18.15 μM in dialysis buffer (10mM Tris pH 7.5, 250mM NaCl, 0.1mM TCEP). Samples were sedimented at 18, 26, 32 and 36k RPM (26 -105k x G, respectively). Scans were collected at 229nm (1.12 and 3.6 μM) and 280nm (18.15 μM). 22 of the resulting 24 scans (two were discarded due to anomalous baselines) were globally fit to a single, ideal species model in Ultrascan. The raw data is shown as black spheres, while the fits to the data are shown as solid lines. The

residuals to the fit are shown in the lower panel, and the variance for the fit to this model was 2.9e-4.

2.6.3 Histone H2A-H2B dimer dissociation assay

We reconstituted nucleosomes by dialysis of recombinant yeast histone octamer and 5S DNA against decreasing salt concentration (Dyer et al., 2004), and heat-shifted them for 60 minutes at 37°C to obtain a unique species of nucleosomes. 3.5 µM nucleosomes, reconstituted with CPM-labeled H2A- H2B dimer (labeled on H2BT112C) were incubated with increasing molar ratios of Vps75 or Nap1, and incubated at 4° C for 10 hours. H2A-H2B dimer dissociation was analyzed by native PAGE on 5% polyacrylamide gels (acrylamide : bis-acrylamide 59:1) in 0.2 X TBE as previously described (Park et al., 2004). The nucleosome-like species are indicated with N1 and S1, and Nap1 - H2A/H2B complex is indicated with S2, respectively based on published results (Park et al., 2004).

2.6.4 Co-immunoprecipitation assays

Yeast cells (a *VPS75* deletion strain expressing either Myc-tagged Rtt109 or untagged Rtt109; (Longtine et al., 1998)) were grown overnight to late logarithmic phase (*A*600 = 1.0) in 100 ml of the appropriate media. The cells were harvested by centrifugation, washed in 50 ml of TBS, and resuspended in 500 µl of Co- IP buffer (50mM HEPES pH 7.5, 1mM EDTA, 1% Triton X-100, 0.1% Na-deoxycholate, 150mM NaCl, 5µg ml-1 leupeptin, chymostatin, pepstatin A, aprotinin and 0.5µM PMSF). 0.5g acid washed glass beads were added and cells were vortexed for 15 minutes at 4°C. The lysate was clarified by centrifugation at 13,000 x *g* for 15 min at 4°C and protein

concentration was measured with Sigma Bradford reagent. 1-2 mg of protein lysate were used for IP and incubated with 5µl of anti-Myc antibody at 4 °C for 1–2 h with mild shaking. 80 µl of 50% Protein A-Sepharose slurry (GE Healthcare) were added to each sample and incubation was continued at 4 °C with mild shaking overnight. The samples were washed 1 time with Co-IP buffer and three times with Co-IP buffer in 500mM NaCl. The pellet was resuspended in 50 µl of 1x Laemmli sample buffer, boiled for 10 min, and electrophoresed on a 12% polyacrylamide SDS gel (PAGE) with protein size standards. The gel was transferred to nitrocellulose membrane and probed with anti-Nap1 antibodies.

2.7 Acknowledgements

We thank S. McBryant for help with analytical ultracentrifugation, N.J. Krogan, D.A. Goldstrohm and C.A. Radebaugh for discussion, and K. Brown for critical reading of the manuscript. We also thank J. Nix at MBC 4.2.2., Advanced Light Source, for data collection. This work was funded by the US National Institutes of Health (NIH) grant GM067777 to K.L. and by NIH grant GM056884 to L.A.S. Y.-J.P., A.J.A. and K.L. are supported by the Howard Hughes Medical Institute.

Supplementary Figures

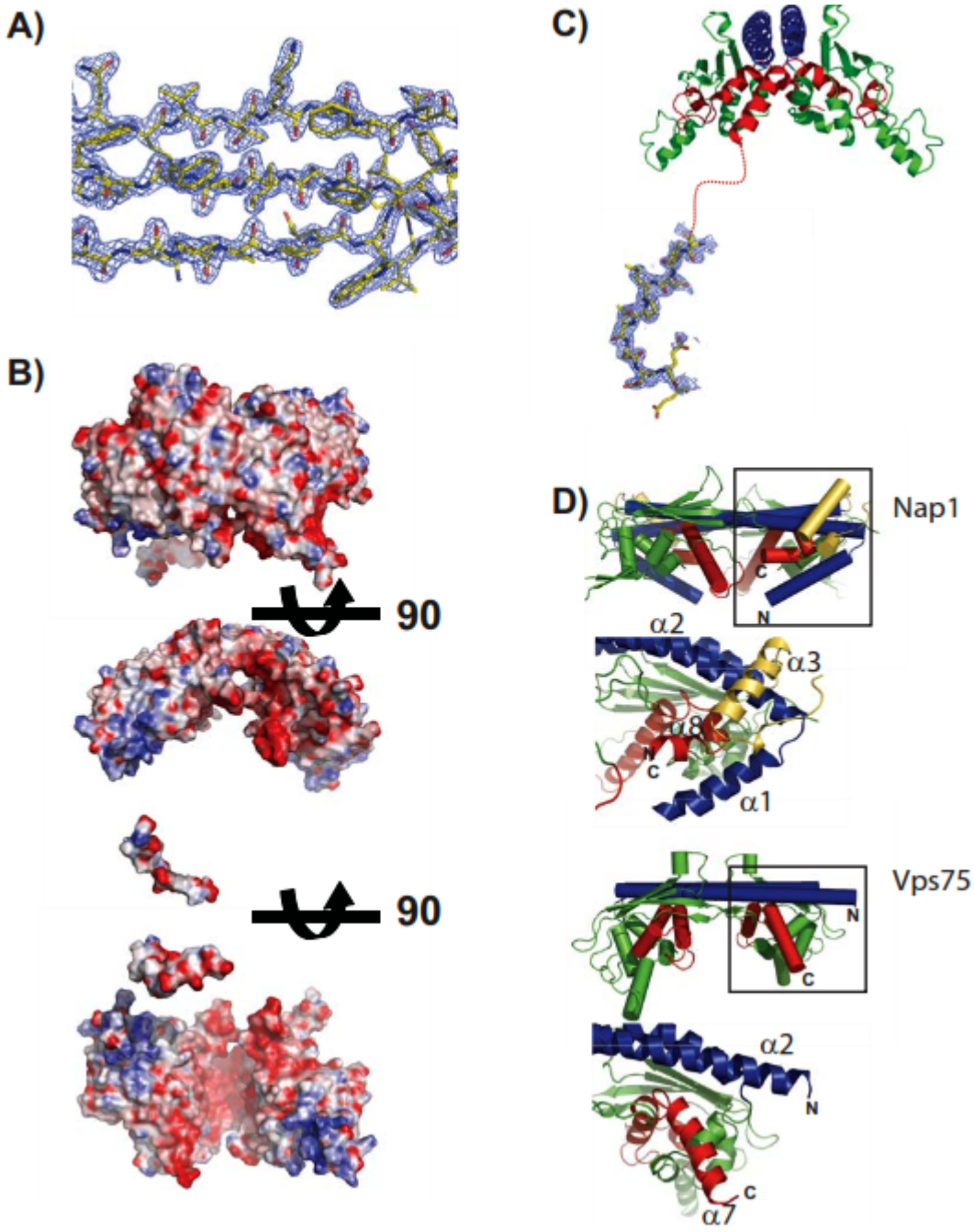

Supplementary Figure 2.1: Vps75 is a structurally distinct member of the Nap1 family. **(A)** A section of the final 1.85 Å resolution 2Fo-Fc electron density map for Vps75, contoured at 2.5 σ. Shown is the section of the map β1-β3. **(B)** Electrostatic potential of the Vps75 surface, shown in three orthogonal views. The surface structure was colored based on electrostatic potential, calculated with PYMOL-APBS. Blue - red represents the spectrum between + and - 20kT/e. **(C)** A side view of the Vps75 dimer is shown as a ribbon diagram, using the same color scheme as in Figure 2.1a. Parts of the C-terminal domain of Vps75 were clearly visible in the electron density map, and this is shown together with the 2Fo-Fc electron density map (contoured at 2 σ) for residues 247-259. **(D)** Schematic diagram showing the topology of Nap1 and Vps75 at the N-terminal end of α2. α helices in the insets are shown as blue, yellow, green, and red cylinders for clarity. The connecting loops and beta sheets are shown as ribbons. C and N termini are indicated.

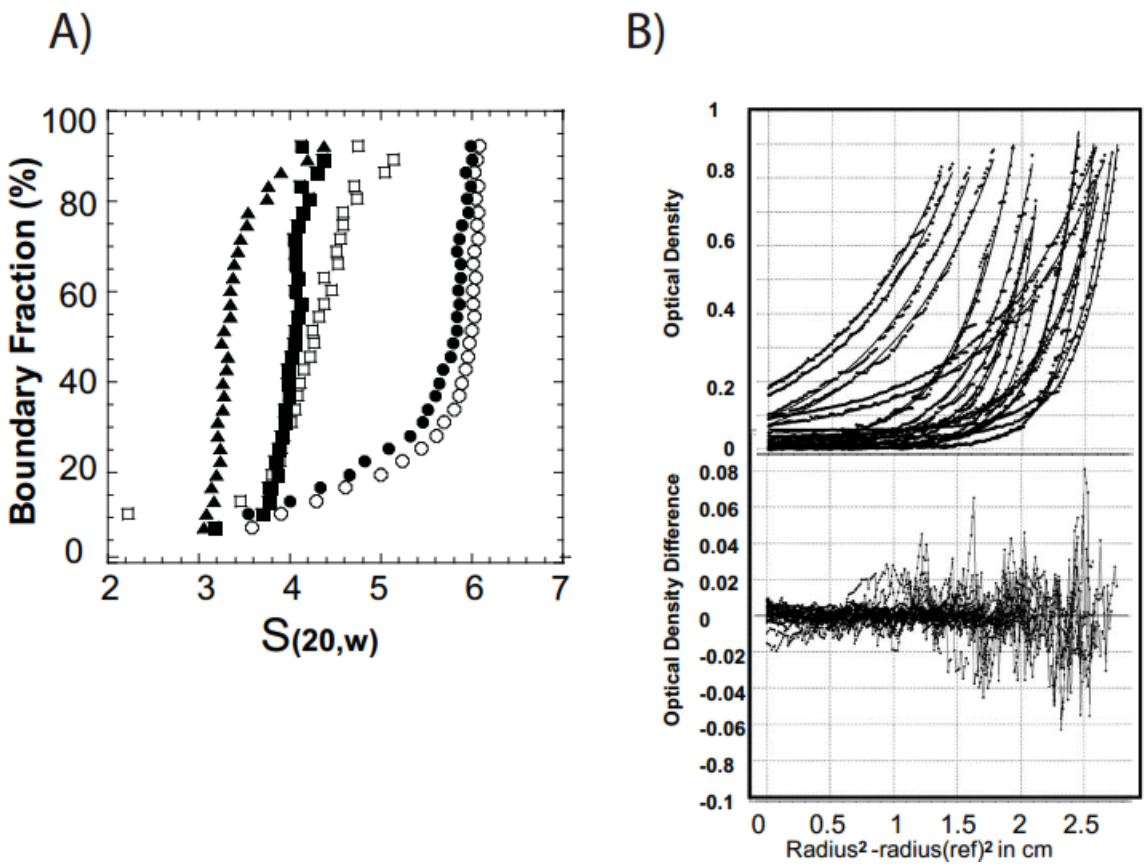

Supplementary Figure 2.2: Solution state of Vps75, Rtt109, and the Vps75 – Rtt109 complex. (A) Sedimentation velocity analysis of Rtt109 (■; 1.2 μM), Vps75 (□; 4.7 μM), and $Vps75_{1-223}$ (■; 4.7 μM). Vps75 and Rtt109 (1:1 mixture, 8 μM each; ○), and $Vps75_{1-223}$ and Rtt109 (1:1 mixture, 8 μM; ●) were detected at 280 nm wavelength. All samples were spun at 201,600 x g in buffer containing 200 mM NaCl, with the exception of Rtt109 (250 mM NaCl). Single proteins were detected at 230 nm, complexes at 280 nm. Data was analyzed by the method of Demeler and van Holde (Demeler and van Holde, 2004). The diffusion corrected integral distribution of S over the boundary is shown; corrected for water at 20 °C ($S_{20,W}$). **(B)** Sedimentation equilibrium runs were performed as follows: Vps75 (1.12-18.15 μM protein) in 250mM NaCl was spun at 18, 26, 32, and 36 kRPM. 22 of the resulting 24 scans (two were discarded due to anomalous baselines) were globally fit to a single, ideal species model (Demeler and van Holde, 2004). The raw data is shown as black spheres; the fit to the data is shown as solid lines. The residuals to the fit are shown in the lower panel, and the variance for the fit to a single ideal species model with a Mw of 55,300 was $2.9e^{-4}$.

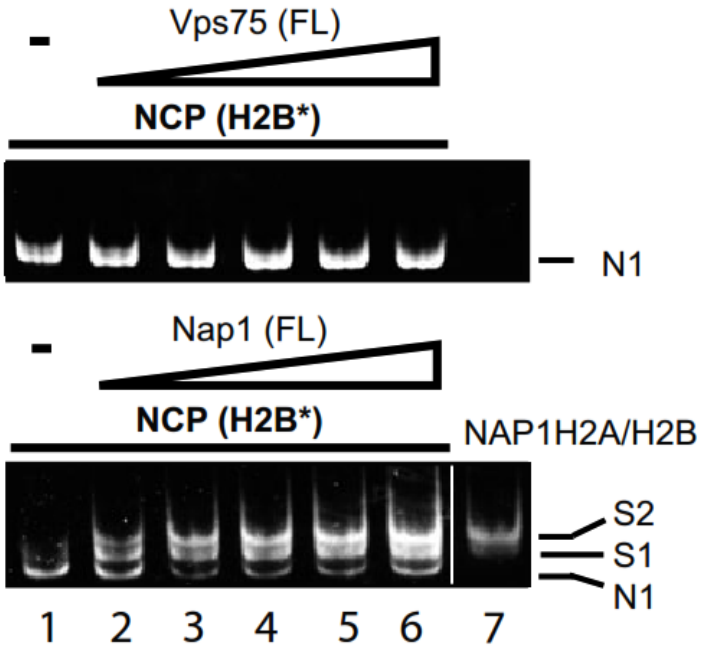

Supplementary Figure 2.3: Nap1, but not Vps75, affects nucleosome structure and composition. Histone chaperone-dependent H2A/H2B dimer dissociation: 3.5 μM nucleosome containing CPM-labeled H2A-H2B dimer (labeled on H2B T112C) was incubated with increasing molar ratios of Vps75 or yNap1. Lane 1: no Histone chaperone, lanes 2-6: 0.5, 1, 2, 3, 4, fold molar ratio of histone chaperone dimer over nucleosome, Lane 7: yNap1 - CPM-labeled H2A/H2B dimer complex. Nucleosomes were analyzed by 5% native PAGE. The gel was photographed without staining to view fluorescence. The position of a yNap1 H2A/H2B complex (S2) is shown as a control (lane 7). Nucleosome (N1), shifted nucleosome (S1), and the yNap1 W H2A/H2B complex (S2) are indicated based on previous studies (Park et al., 2005).

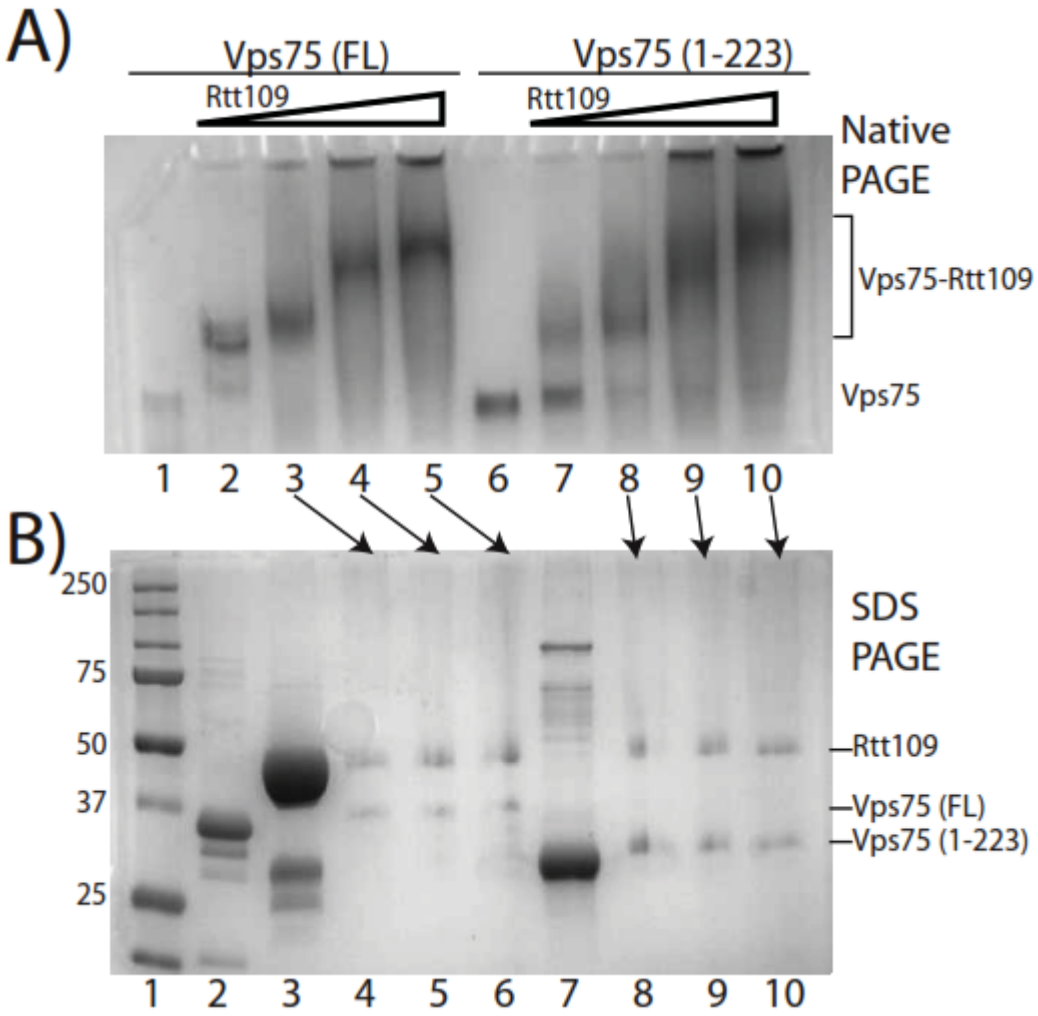

Supplementary Figure 2.4: Full-length and truncated Vps75 bind Rtt109 at similar stoichiometries. (A) The ability of Vps75 to form a complex with Rtt109 was tested using gel shifts (5% polyacrylamide in 0.2X TBE). 10µl of 10µM Vps75 monomer was titrated with increasing amounts of Rtt109 (lanes 1-5 and lanes 6-10: 0, 2, 5, 10 and 20 µM respectively). **(B)** Bands were excised from the gel shown in (A) and ran on a 12% SDS gel Lane 1: Size marker; lanes 2 and 3: full length Vps75 and Rtt109 respectively. Lanes 4-6 correspond to shifted bands from lanes 3, 4 and 5 in (A). Lane 7 shows $Vps75_{(1-223)}$. Lanes 8-10 correspond to complex bands in lanes 8, 9 and 10 in (A).

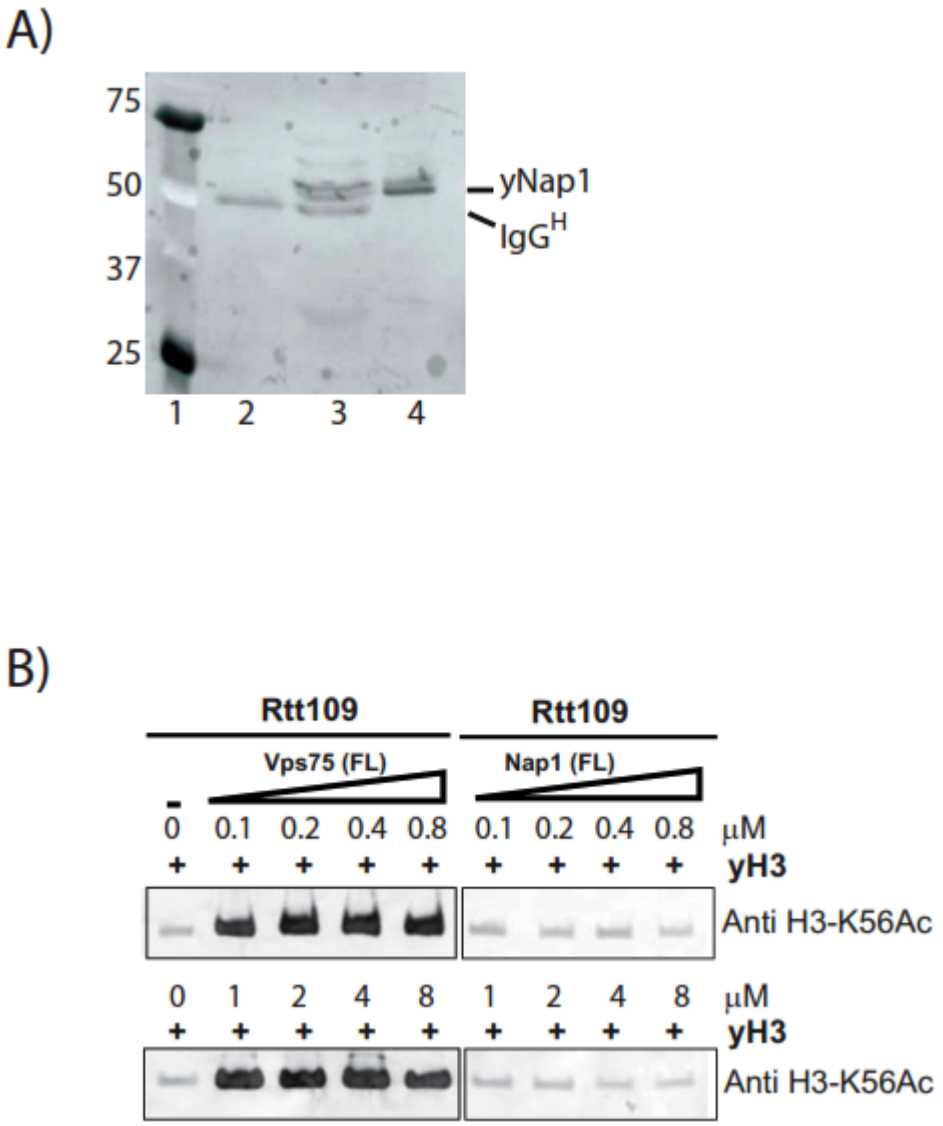

Supplementary Figure 2.5: Rtt109 and yNAP1 form a complex in a VPS75 deletion strain, but Nap1 is unable to stimulate histone acetylation. (A) The Co-IP was carried out using anti-Myc antibodies on extracts prepared from the VPS75 deletion strain with untagged (lane 2) or Myc-tagged Rtt109 (lane 3). The beads were washed three times with 500 mM NaCl to eliminate weak interactions. Lane 4 shows protein extract prepared from the VPS75 deletion strain to ensure that Nap1 was present (input). The samples were analyzed by 12 % SDS-PAGE followed by Western blotting using anti-Nap1 antibodies. **(B)** Vps75, but not Nap1, stimulates efficient acetylation of H3K56 in the absence of H4, as demonstrated by urea-acid gel.

CHAPTER III

Biophysical Characterization of Intrinsically Disordered Histone-Binding Proteins Chz1 and $Swc2_{1-179}$

Sudhoff KB, Croke C, Sakurai T and Luger K

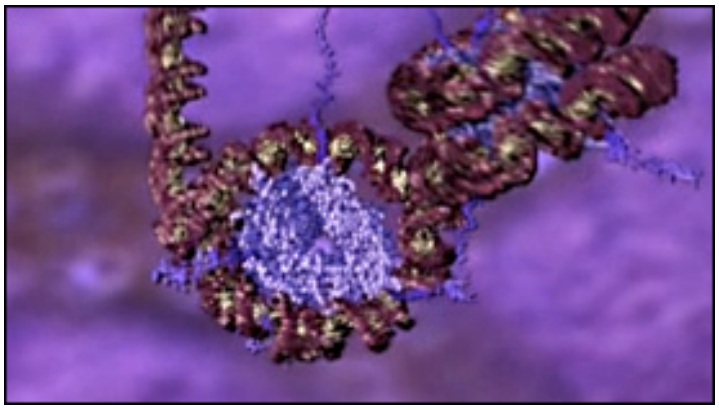

(Image by Drew Barry)

K.B.S. performed the biophysical, SAXS and gel-shift binding assays; T.S. performed the initial quantitative protein-protein interactions; C.C. obtained the AUC and ITC data for Chz1; K.L. and K.B.S. planned and supervised the structural and biochemical experimental sections.

3.1 Abstract

In *Saccharomyces cerevisiae*, histone-variant H2A.Z incorporation is mediated by the multi-subunit SWR1 complex which catalyzes exchange of H2A for H2A.Z. Swc2 (Swr1 complex 2) is a key member of the SWR1 complex and previous studies have shown that Swc2 is essential for binding and transfer of H2A.Z. Chz1 (Chaperone for H2A.Z/H2B) can deliver H2A.Z/H2B heterodimers to the SWR1 complex *in vitro*. Unlike other histone chaperones, $Swc2_{1-179}$ (a domain of Swc2 that retains histone binding and the apparent preference for variant dimers) and Chz1 are predicted to be intrinsically disordered proteins. Thus, the apparent specificity for H2A.Z/H2B is hard to reconcile with an intrinsically disordered protein and warrants further investigation. We utilized biophysical and structural studies to determine that these proteins are intrinsically disordered, but become more ordered upon interaction with histones. Importantly, under physiological *in vitro* conditions, Chz1 and $Swc2_{1-179}$ are not histone-variant specific; in fact, they bind histones with an affinity lower than that of previously described histone chaperones. We used small-angle x-ray scattering to examine the structure of the N-terminal domain of Swc2 and Swc2 in complex with H2A.Z/H2B in solution. From the SAXS data, we were able to ascertain structural parameters of an intrinsically disordered protein complexed with a variant histone dimer.

3.2 Introduction

The nucleosome is the basic repeating unit of chromatin and consists of 146 base pairs of DNA wrapped in 1.65 superhelical turns around a histone octamer of two (H2A/H2B) heterodimers and an $(H3\text{-}H4)_2$ tetramer (Luger et al., 1997). Chromatin assembly is a stepwise process that begins when one tetramer of $(H3\text{-}H4)_2$ binds the

central ~70 base pairs of DNA, followed by binding of two (H2A/H2B) dimers, each organizing approximately 40 base pairs of peripheral DNA (Akey and Luger, 2003). Despite its apparent stability and the high degree of chromatin compaction in the nucleus, chromatin is surprisingly dynamic (Luger, 2006). The histone-DNA interactions inside the nucleus are altered in response to protein complexes that regulate gene expression, DNA replication, recombination, and repair (Akey and Luger, 2003).

Substitution of one or more of the core histones with the corresponding histone variant has the potential to exert considerable influence on the structure and function of nucleosomes and chromatin (Jin et al., 2005). In contrast to canonical histones, variant histones are incorporated into chromatin independent of DNA replication. Distinct chromatin domains characterize the nucleus and these specialized domains can be enriched in histone variants. To date, histone variants for H2A, H3 and H1 have been characterized, and to a lesser extent, H2B variants (Bernstein and Hake, 2006).

The histone H2A variant H2A.Z is found in all eukaryotes from *Saccharomyces cerevisiae* to humans (Redon et al., 2002). H2A.Z is essential for viability in many organisms including *Drosophila melanogaster, Tetrahymena thermophila, Xenopus laevis*, and *Mus musculus* (Clarkson et al., 1999; Liu et al., 1996; Ridgway et al., 2004). H2A.Z is implicated in the activities of numerous biological functions such as gene activation, chromosome segregation, heterochromatin silencing, and progression through the cell cycle (Adam et al., 2001; Dhillon et al., 2006; Krogan et al., 2004). In yeast, H2A.Z localizes to actively transcribed regions that are adjacent to heterochromatin such as telomeric DNA and mating-type loci, thereby buffering the spread of heterochromatin

(Meneghini et al., 2003). To date, mechanistic and structural insight into how these variants are incorporated into nucleosomes in a replication-independent manner is virtually non-existent.

A protein complex has been identified which can specifically exchange H2A with H2A.Z in yeast chromatin in a replication-independent manner (Kobor et al., 2004; Krogan et al., 2003; Mizuguchi et al., 2004). Previous experiments performed on the non-essential subunits of the SWR1 complex established Swc2 as a binding module for H2A.Z (Wu et al., 2005). Partial SWR1 complexes purified from *swc2*Δ strains had severely reduced histone exchange activity, as indicated by little transfer of H2A.Z-Flag to immobilized nucleosomes, and showed an approximately two-fold decrease in nucleosome binding compared to wild-type SWR1 complexes (Wu et al., 2005). The SWR1(*swc2*Δ*)* complex also had decreased levels of H2A.Z association compared to the wild-type SWR1 complex (Wu et al., 2005). The previously defined domain necessary for interacting and binding H2A.Z/H2B is contained within Swc2 N-terminal residues 1-281, as established using *in vitro* His-tag pulldowns (Wu et al., 2005). These studies implicate Swc2 as a protein with an N-terminal histone-specific binding activity capable of interacting with H2A.Z/H2B dimers.

The incorporation of H2A.Z *in vivo* is dependent upon the SWR1 complex, but unincorporated histones are complexed with histone chaperones (Chang et al., 1997; De Koning et al., 2007). In cell extracts H2A.Z/H2B is found in complex with histone chaperone Nap1 and Chz1 (Luk et al., 2007). Chz1 preferentially associates with H2A.Z/H2B versus H2A/H2B in cell extracts (Luk et al., 2007). *In vitro*, both Nap1 and

Chz1 can deliver H2A.Z/H2B heterodimers to the SWR1 complex for incorporation into nucleosomes (Luk et al., 2007). Chz1 is unusual amongst histone chaperones in that it lacks a defined folded structure in the absence of H2A.Z/H2B (Luk et al., 2007). A recently published NMR structure of Chz1-H2A.Z/H2B depicts a long chain capped by two short α–helices. The interactions between histones and Chz1 were mainly electrostatic (Zhou et al., 2008). A careful analysis reveals that there are no unique residues of H2A.Z (those that differ from H2A) at the interaction interface with Chz1, raising questions about the molecular basis for the apparent preference for variant dimers. Nap1 is also found in complex with H2A.Z/H2B *in vivo*, but published binding affinities reveal no preference for heterodimers composed of either H2A/H2B or H2A.Z/H2B (Andrews et al., 2008).

Swc2, part of the SWR1 complex, is implicated as the protein which specifically binds H2A.Z for incorporation into nucleosomes. Chz1 has been characterized as a histone variant-specific chaperone for H2A.Z/H2B. The structures of a number of histone chaperones such as Nap1 (Park and Luger, 2006b), Vps75 (Park et al., 2008b), Asf1 (Daganzo et al., 2003) and Nucleoplasmin (Dutta et al., 2001) are known. These proteins have clearly defined tertiary structures (in addition to largely unstructured, mostly acidic tails) even in the absence of histones and are only moderately specific for various histones (Andrews et al., 2008). In contrast, Swc2 and Chz1 are intrinsically unstructured proteins that appear to be selective for heterodimers of H2A.Z/H2B as demonstrated by qualitative pulldown assays (Luk et al., 2007; Wu et al., 2005). However, no careful analysis of relative and absolute binding affinities for H2A.Z/H2B

and H2A/H2B has been described, nor has the affinity for other histones (e.g. H2A/H2B) been studied.

We utilized biophysical and structural studies to determine that these proteins are intrinsically disordered, but become more ordered upon binding H2A.Z/H2B heterodimers. Importantly, we discovered that Chz1 and $Swc2_{1-179}$ are not histone variant specific; in fact, they bind histones with an affinity lower than that of previously described histone chaperones. We determined that due to their inability to affect nucleosome structure, these proteins aren't chaperones, but rather histone-binding proteins. We used small-angle x-ray scattering (SAXS) to examine the structure of the N-terminus of $Swc2_{1-179}$ and $Swc2_{1-179}$ -H2A.Z/H2B in solution. Our SAXS data reveals the N-terminus of $Swc2_{1-179}$ is intrinsically disordered with an extended and flexible conformation. The $Swc2_{1-179}$-H2A.Z/H2B complex has a significantly smaller maximum dimension and radius of gyration when compared to $Swc2_{1-179}$ alone.

3.3 Materials and Methods

3.3.1 Expression and Purification

All constructs of Swc2 and Chz1 are in pET28a vectors. The plasmids were transformed into Bl21 (43) cells by electroporation or heat shock. The cells are then grown in 2XYT media and induced at an OD_{600} of 0.6 with 0.7mM IPTG for 5 hours. Lysates were purified using batch Ni resins, gel-filtration chromatography Superdex S200 16/60, and ion exchange MonoQ HR5/5. Recombinant histones (yeast and *Xenopus*) were generated in bacteria as described (Dyer et al., 2004). Recombinant histones were refolded to H2A/H2B or H2A.Z/H2B dimer, H3/H4 tetramer or octamer.

We tested the purity of individual proteins on 15% SDS-PAGE and stained with Coomassie brilliant blue.

3.3.2 Bioinformatics

CLC Sequence Viewer 6 by CLC Bio was used for generating the sequence alignment of $Swc2_{1-179}$ and Chz1. Disorder in $Swc2_{1-179}$ and Chz1 was assessed using Foldindex (Prilusky et al., 2005) and the VL-XT algorithm in PONDR (Li et al., 1999; Romero et al., 2001) .

3.3.3 Proteinase K Assay

Proteinase K digestion was carried out in 20µl of digestion buffer (10mM Tris ph7.5, 100mM NaCl, and 1mM EDTA), at a proteinase K concentration of 500ng/ml at 37°C, as described by Fontana et al., (2004). The reaction was stopped by the addition of Laemmli protein gel-loading buffer with 5mM PMSF and incubated at 95°C for 5 minutes. The ratio of enzyme to substrate was approximately 1:1500 (w:w). The samples were run on a 12% SDS polyacrylamide gel after proteolysis and stained with Coomassie brilliant blue.

3.3.4 Circular Dichroism

CD spectra were obtained on a JASCO J720 circular dichroism (CD) spectrometer. The sample buffer contained 10mM NaH_2PO_4 pH 7.0 and 100mM NaCl. A 0.01cm cell pathlength was used for each sample. The concentration were as follows; $Swc2_{1-179}$ (40µM), Chz1 (40µM), H2A.Z/H2B (40µM), $Swc2_{1-179}$-H2A.Z/H2B (1:1 20µM) and Chz1-H2A.Z/H2B (1:1 20µM). The protein concentrations were determined

using a Bradford assay. Each trace displayed has been corrected for the contribution of the buffer.

3.3.5 Isothermal Titration Calorimetry

A MicroCal ITC was utilized for this experiment and data was analyzed using Origin 7 software. $Swc2_{1-179}$, Chz1 and H2A.Z/H2B were repeatedly dialyzed in 20mM HEPES pH7.5, 100mM NaCl, and 0.2mM TCEP to ensure all samples were in the same buffer conditions. ITC was performed by titrating excess Chz1 or $Swc2_{1-179}$ into a cell containing H2A.Z/H2B. The heat of dilution (acquired by titrating Chz1 or Swc2 into buffer) was subtracted from the titrations of chaperone into H2A.Z/H2B. The concentration of H2A.Z/H2B in the reference cell was 10μM and the concentration of Chz1 (or $Swc2_{1-179}$) titrated in was 100-150μM. The experiment was performed at 25°C. 30 injections of 7μl $Swc2_{1-179}$ were added to the reference cells with 240 seconds between injections. The reference power was 12.1 and the stirring speed was 460 rpm.

3.3.6 Analytical Ultracentrifugation

Samples for AUC were prepared by repeat dialysis in a buffer containing 10 mM Tris pH7.5, 100mM NaCl, and 1mM TCEP. All experiments were performed in Beckman XL-I using the absorbance optical system and a four-hole AN60-Ti rotor. A ~1:1.5 ratio ($Swc2_{1-179}$ or Chz1 to H2A.Z/H2B) was incubated at 4°C overnight, then purified over an S200 size exclusion column. The free dimer eluted separately from the co-complex. The sedimentation velocity samples had an A_{230} absorbance reading between 0.4 – 0.7 (5-20μM). For SV experiments 400μl samples were sedimented at

~50,000 rpm for 5 h at 22°C. For SE experiments 100µl samples at three different concentrations of each sample were spun to equilibrate.

3.3.7 Fluorescence

Affinity measurements were carried out on the Perkin-Elmer Victor 3V plate reader. The microplate wells contain 40nM labeled histone (H2BT112C) at a final buffer concentration of 300mM NaCl, 10mM Tris pH7.5, 0.25mM EDTA, and 0.1% BSA. The histones were Alexa-488-labeled H2A/H2B* and Alexa-488-labeled H2A.Z/H2B* (as described in (Dyer et al., 2004)). The titration of $Swc2_{1\text{-}179}$ (or Chz1) spanned between 100 nM and 7.5 mM. The labeled dimer was excited at 496 nm and emission observed at 515 nm. Three scans of the plate were taken, the signal in each well was averaged, and a standard error of the mean was calculated. The data was plotted and the binding fitted using Graphpad Prism using equation (1), where R_{max} is the maximum change in fluorescence, $[L]_t$ is the total ligand concentration, K_d is the binding affinity and n is the Hill coefficient.

$$Ratio = R_{max} \frac{[L]_t^{\,n}}{\left([L]_t^{\,n} + K_d^{\,n}\right)} \qquad (1)$$

3.3.8 Multi-Angle Light Scattering

Samples of $Swc2_{1\text{-}179}$ (2mg/ml), H2A.Z/H2B (3mg/ml), or $Swc2_{1\text{-}179}$-H2A.Z/H2B (3mg/ml) in 20mM Tris pH7.5, 300mM NaCl, and 5% glycerol were loaded onto an AKTA purified HPLC system. Samples were run over a SHODEX-803 size-exclusion column at 0.3ml/min prior to flowing into a Wyatt Dawn Heleos II multi-angle light scattering instrument, followed by a rEX refractive index detector (Wyatt Technologies).

To determine the concentrations of the proteins we used a differential index of diffraction (dn/dc) of 0.185.

3.3.9 Small Angle X-ray Scattering

Data was collected on the SIBYLS beamline (Beamline 12.3.1) at the Advanced Light Source at the Lawrence Berkeley National Laboratory in Berkeley, California USA using a Mar CCD area detector. The proteins were dialysed into 20mM Tris pH7.5, 300mM NaCl, and 5% glycerol. Intensity curves for $Swc2_{1\text{-}179}$ were measured at 7, 3.5 and 1.75 mg/ml. For H2A.Z/H2B, intensity curves were measured at 4, 2 and 1 mg/ml and for the $Swc2_{1\text{-}179}$-H2A.Z/H2B complex at 5, 2.5 and 1.25 mg/ml. The scattering patterns were measured with a short, long, and short exposure time (2, 5 and 2 sec) for multiple concentrations ranging from 7mg/ml to 1mg/ml. The data was processed using standard procedures and the PRIMUS program package (Svergun, 2003a). The radius of gyration for each particle was approximated using PRIMUS to approximate the Guinier and using GNOM to evaluate the P(r) function (Svergun, 1992, 2003a).

Ensemble optimization method (EOM) software package was utilized to characterize $Swc2_{1\text{-}179}$ (Bernado et al., 2007). RanCh (Ran*dom* Ch*ain*) creates the random models of intrinsically unfolded proteins. It does so by building a polypeptide chain where the amino acid conformations are randomly selected from a library of coil conformations found in high-resolution X-ray structures (Lovell et al., 2003). RanCh generated 10,000 conformers for $Swc2_{1\text{-}179}$. The scattering profiles for the 10,000 conformers are then generated using a program called CRYSOL (Svergun, 1995). The program GAJOE (G*enetic* A*lgorithm* J*udging* O*ptimization of* E*nsembles*) from the EOM

suite is the ensemble selection program. GAJOE randomly selects 50 ensembles comprised of 20 scattering profiles (and subsequently 3 dimensional models) and subjects them to genetic algorithms, therefore exploring a large variety of combinations. For each ensemble generated, an average of the individual SAXS profiles is compared with the experimental SAXS profile giving a fitness functions ($\chi 2$). GAJOE then selects the best ensemble (based on lowest $\chi 2$) and creates several PDB's of the curves represented in that ensemble.

Ab initio particle reconstructions for H2A.Z/H2B and $Swc2_{1\text{-}179}$-H2A.Z/H2B were built by the program GASBOR (Svergun et al., 2001). The protein structure is represented by an ensemble of dummy residues placed anywhere in continuous space. The centers of these residues approximate the positions of the C-α atoms in the protein structure (Svergun et al., 2001). For each final model, 15 independent reconstructions were aligned and averaged using programs DAMAVER and SUPCOMB (Svergun, 2003b). When comparing the structures from reconstructions (EOM or GASBOR) the normalized spatial discrepancy (NSD) was calculated with the program SUPCOMB. The most typical averaged model was filtered to an appropriate volume with program DAMFILT (Svergun, 2003b).

Lastly, *Situs* BioMachina software was utilized to convert the *ab initio* SAXS bead models into 3D volumes (Wriggers, 2010). This allows for better visualization when docking a crystal structures into the outer contoured surface of the bead model. Furthermore, it allows for additional manipulations such as flexible docking and volumetric difference maps (Wriggers et al., 1999).

3.3.10 Electrophoretic Mobility Shift Assay

Approximately 5μM 146 5S nucleosomes (prepared as described in (Dyer et al., 2004)) were incubated overnight with increasing molar ratios of $Swc2_{1-179}$ or Chz1 (0.2 - 10 fold molar excess). The binding buffer for the reaction was 20mM Tris pH7.5, 100mM NaCl, 1mm EDTA and 1mM DTT. The samples were run on a 5% native gel at 150V for 60 minutes. The gel was ethidium bromide-stained, followed by staining with Coomassie brilliant blue.

3.4 Results

3.4.1 $Swc2_{1-179}$ and Chz1 bind H2A.Z/H2B and H2A/H2B heterodimers.

The amino acid sequence of Swc2 from yeast to humans exhibits a high degree of conservation, particularly residues 1-340. The N-terminus of Swc2 (residues 1-281) contains the histone-binding domain capable of interacting with H2A.Z/H2B, whereas residues 345-795 showed little association with histones (Wu et al., 2005). The 795 amino acid residues of Swc2 can be divided into three charged domains: the first 1-179 is very acidic (pI 4.5), followed by a basic tract of residues 181-360; pI 9.92). The C-terminal half of the protein (amino acids 361-795) is again highly acidic (pI 4.61) (Figure 3.1A). The N-terminal region of Swc2 (1-281) has been established as the H2A.Z/H2B binding domain (Wu et al., 2005). However, repeated attempts at purifying $Swc2_{1-281}$ revealed quick degradation of the protein and instability. Based on a prominent degradation band, sequence alignments, and secondary structure predictions, new constructs of Swc2 (1-179 and 1-189) were designed. The first construct designed

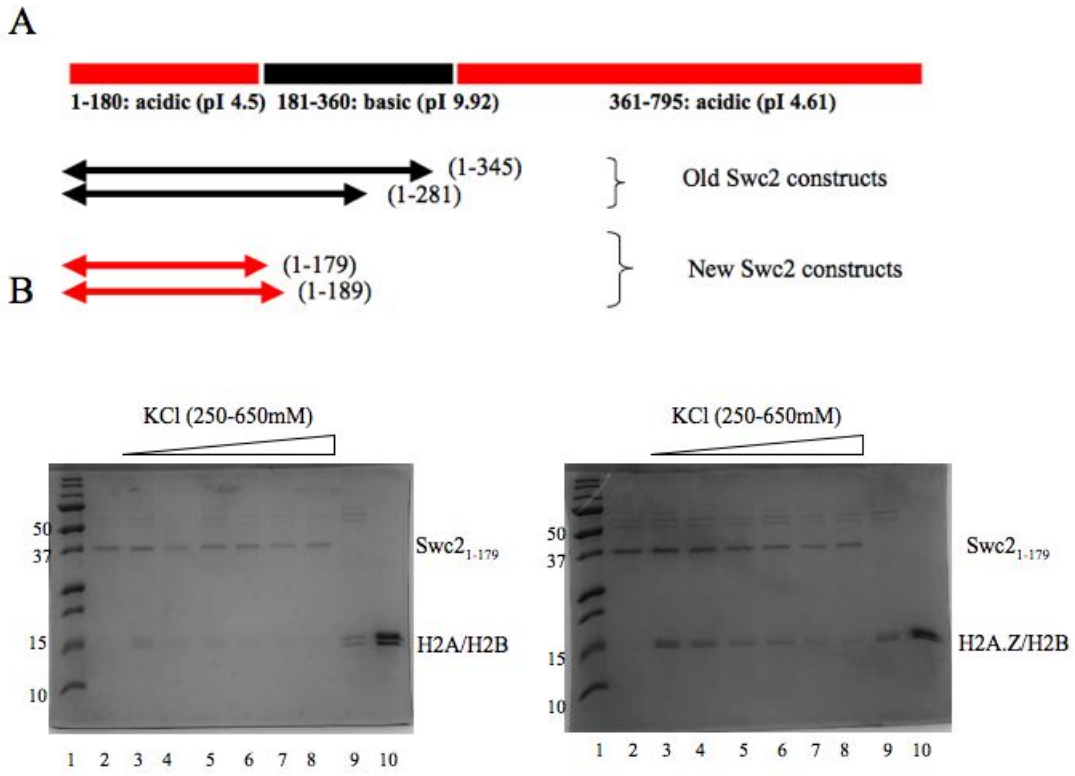

Figure 3.1: $Swc2_{1-179}$ binds H2A.Z/H2B and H2A/H2B heterodimers.
(A) Schematic of full length Swc2 where the acidic domains are shown in red and the basic domain is in black. New constructs were designed to encompass the N-terminal acidic region and are indicated in the figure. **(B)** Ni-resin beads (50ul) were saturated with 0.5 nmol of the His-tagged $Swc2_{1-179}$. After rotating at 4°C, the resin was washed with HPD-25 buffer (20mM HEPES, 10% Glycerol, 0.01 % Nonidet p-40, 25mM KCl) and then 100 pmoles of H2A/H2B dimer or H2A.Z/H2B dimer were added. After rotating the resins for an additional 12 hours at 4°C, the resins were washed with increasing concentrations of HPD-KCl from 250-650mM. Lastly the Ni-resin beads were boiled for five minutes at 95°C. The beads were spun and the remaining supernatants were analyze by 15% SDS-PAGE. *Lane* 1 is the marker and *Lane* 2 is $Swc2_{1-179}$ binding to the Ni-resin. *Lanes* 3-8; $Swc2_{1-179}$ saturated resin incubated with heterodimers of H2A/H2B (left) or H2A.Z/H2B (right) and washed with increasing concentrations (250, 350, 450, 500, 550, and 650mM) of KCl. *Lane* 9 is a control showing that histone dimers can associate with unbound Ni resin washed at 250mM KCl. *Lane* 10 is the amount of H2A/H2B (left) or H2A.Z/H2B (right) used in the reactions.

contains Swc2 residues 1-179 and encompasses the highly acidic, conserved N-terminal region. The majority of the experiments in this paper utilize $Swc2_{1-179}$. The second construct designed contains residues 1-189, which includes the acidic region and a linker region that separates the acidic and basic tracts (Figure 3.1A).

With the use of an *in vitro* binding assay, we found that the newly designed constructs were capable of binding histones H2A.Z/H2B and H2A/H2B (Figure 3.1B). Figure 3.1 illustrates that the acidic region (1-179) binds to both histone dimers, but only retains association with the H2A.Z/H2B heterodimer at higher salt concentrations. The variant dimer retained its association with $Swc2_{1-179}$ at the highest salt concentration tested (650mM). However, the canonical dimer exhibits significantly decreased binding at every salt concentration tested. Preliminary results for both constructs of Swc2 (1-179 and 1-189) indicate a preference for the histone variant dimer versus that of the canonical H2A/H2B dimer under conditions of increasingly stringent ionic strength. An *in vitro* His-tag pull-down binding assay revealed that Chz1 associated with H2A.Z/H2B at higher salt concentrations (0.5M) versus H2A/H2B heterodimers (Luk et al., 2007).

3.4.2 $Swc2_{1-179}$ and Chz1 are intrinsically disordered proteins.

$Swc2_{1-179}$ contains ~45% charged residues, less than 3% aromatic amino acids (Phe, Trp and Tyr) and has a low content of hydrophobic amino acids (17%.) Chz1 has a relatively low degree of sequence homology to $Swc2_{1-179}$, but the amino acid composition is strikingly similar (Figure 3.2A). The primary structures of both $Swc2_{1-179}$ and Chz1 have a high content of disorder-promoting amino acids (A, G, R, Q, S, P, E, K) and a lower content of order-promoting amino acids (W, C, F, I, Y, V, L) (Dunker et al., 2001).

Bioinformatics analysis programs such as PONDR and FoldIndex predict that $Swc2_{1-179}$ and Chz1 contain substantial stretches of disordered regions (Li et al., 1999; Prilusky et al., 2005; Romero et al., 2001). The FoldIndex plots for $Swc2_{1-179}$ and Chz1 (Figure 3.2B) have negative values for each residue and this indicates that both proteins are intrinsically disordered (Li et al., 1999). Ordered or classically structured regions would have FoldIndex values that are positive. Neither Chz1 nor $Swc2_{1-179}$ have residues with positive values. The PONDR VL-XT plot for $Swc2_{1-179}$ has a positive score of 1 for most of the sequence, indicative of disorder. There is a small portion of the sequence (amino acids 15-25) for which some degree of order is predicted (Figure 3.2C). The Chz1 PONDR VL-XT plot predicts large regions of disorder (+1) and a few small regions of order (Figure 3.2C).

Limited proteolysis was employed to probe the tertiary structure of $Swc2_{1-179}$. Intrinsically disordered proteins are more susceptible to protease digestion than globular proteins (Fontana et al., 2004). $Swc2_{1-179}$ proteinase K digestion was compared to that of lysozyme, a globular protein resistant to proteases. $Swc2_{1-179}$ was more sensitive to proteinase K digestion than lysozyme (Figure 3.2D).

Circular dichroism (CD) in the far UV range was used to assess the secondary structure of the N-terminus of Swc2, the histone heterodimer (H2A.Z/H2B) and the co-complex ($Swc2_{1-189}$-yH2A.Z/H2B). $Swc2_{1-189}$ has a CD spectrum characteristic of that of

A

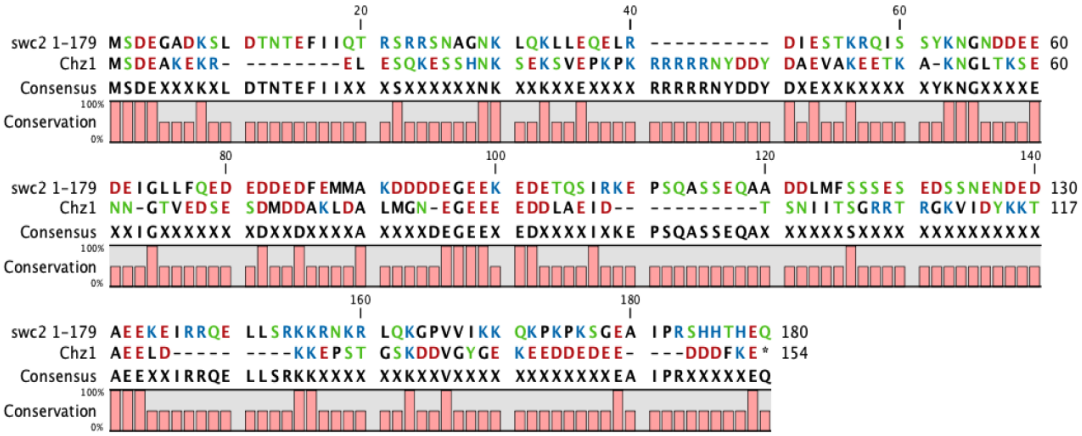
swc2 1-179 MSDEGADKSL DTNTEFIIQT RSRRSNAGNK LQKLLEQELR ---------- DIESTKRQIS SYKNGNDDEE 60
Chz1 MSDEAKEKR- --------EL ESQKESSHNK SEKSVEPKPK RRRRRNYDDY DAEVAKEETK A-KNGLTKSE 60
Consensus MSDEXXXKXL DTNTEFIIXX XSXXXXXXNK XXKXXEXXXX RRRRRNYDDY DXEXXKXXXX XYKNGXXXXE
Conservation
swc2 1-179 DEIGLLFQED EDDEDFEMMA KDDDDEGEEK EDETQSIRKE PSQASSEQAA DDLMFSSSES EDSSNENDED 130
Chz1 NN-GTVEDSE SDMDDAKLDA LMGN-EGEEE EDDLAEID-- ----------T SNIITSGRRT RGKVIDYKKT 117
Consensus XXIGXXXXXX XDXXDXXXXA XXXXDEGEEX EDXXXXIXKE PSQASSEQAX XXXXXSXXXX XXXXXXXXXX
Conservation
swc2 1-179 AEEKEIRRQE LLSRKKRNKR LQKGPVVIKK QKPKPKSGEA IPRSHHTHEQ 180
Chz1 AEELD----- ----KKEPST GSKDDVGYGE KEEDDEDEE- ---DDDFKE* 154
Consensus AEEXXIRRQE LLSRKKXXXX XXKXXVXXXX XXXXXXXXEA IPRXXXXEQ
Conservation

B

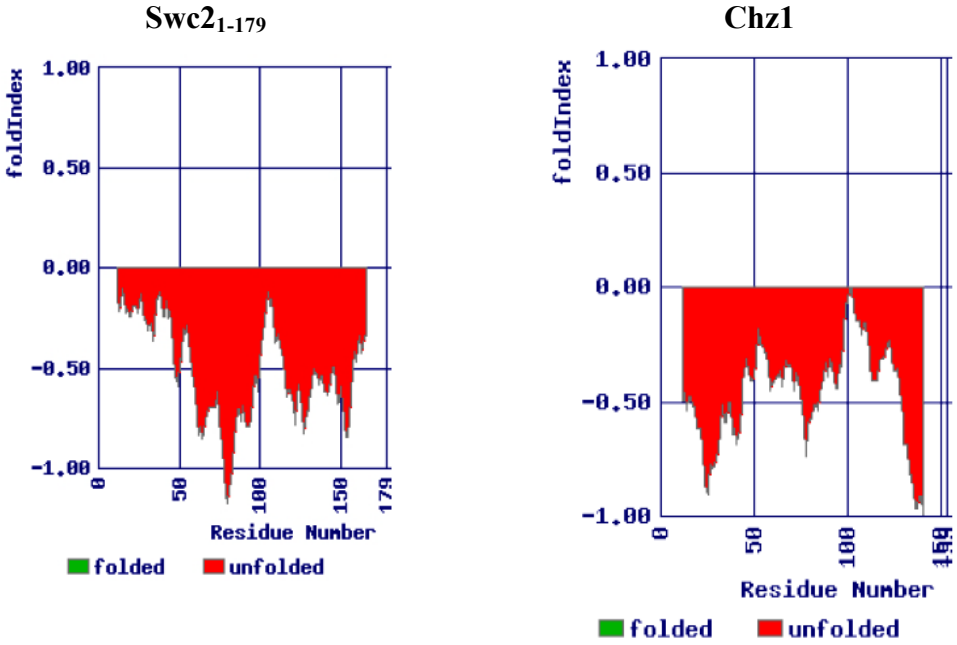
Swc2 1-179
Chz1
foldIndex
1.00
0.50
0.00
-0.50
-1.00
0
50
100
150
179
Residue Number
folded
unfolded

C

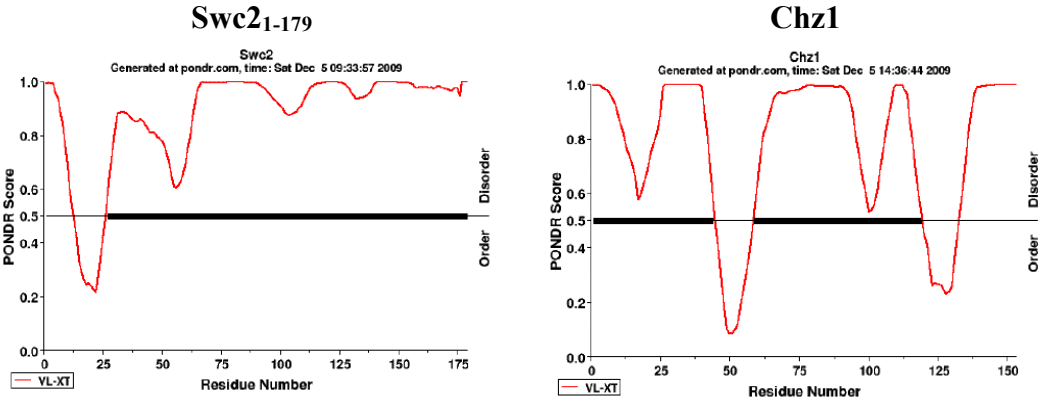
Swc2 1-179
Chz1
Swc2
Generated at pondr.com, time: Sat Dec 5 09:33:57 2009
Chz1
Generated at pondr.com, time: Sat Dec 5 14:36:44 2009
PONDR Score
Disorder
Order
VL-XT
Residue Number

D

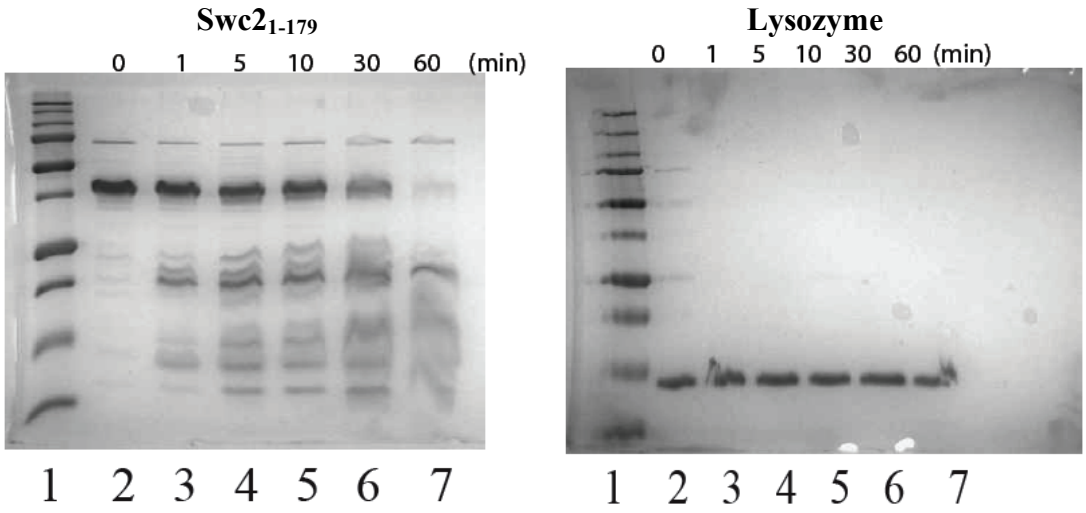
Swc2$_{1-179}$
0 1 5 10 30 60 (min)
1 2 3 4 5 6 7
Lysozyme
0 1 5 10 30 60 (min)
1 2 3 4 5 6 7

E

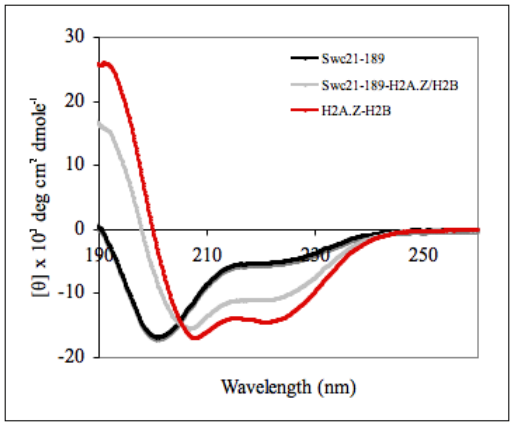
Swc21-189
Swc21-189-H2A.Z/H2B
H2A.Z-H2B
[θ] x 10³ deg cm² dmole⁻¹
Wavelength (nm)

F

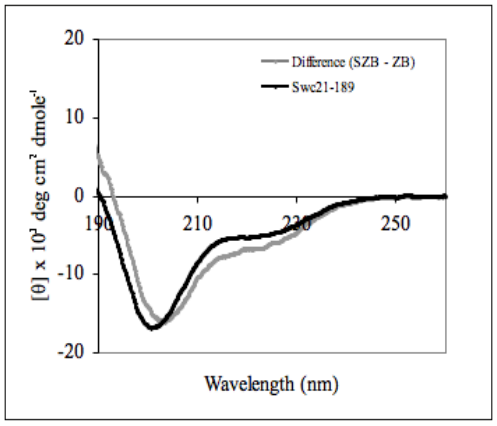
Difference (SZB - ZB)
Swc21-189
[θ] x 10³ deg cm² dmole⁻¹
Wavelength (nm)

G

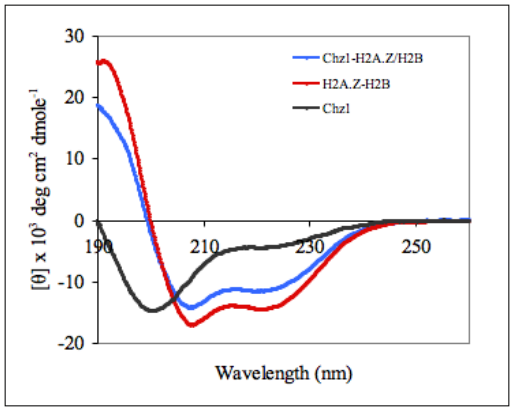
Chz1-H2A.Z/H2B
H2A.Z-H2B
Chz1
[θ] x 10³ deg cm² dmole⁻¹
Wavelength (nm)

Figure 3.2: $Swc2_{1-179}$ and Chz1 are intrinsically disordered proteins.
(A) Sequence comparisons of *S. cerevisiae* $Swc2_{1-179}$ and Chz1 aligned using CLC Sequence Viewer 6. $Swc2_{1-179}$ and Chz1 have approximately 20% sequence alignment. Acidic residues (D, E) are highlighted in red and basic residues (H, K, R) in blue. Polar residues (S, T, Q, N, Y) are highlighted in green. **(B)** The Fold Index prediction of yeast $Swc2_{1-179}$ (Left Panel) and Chz1 (Right Panel). Red indicates sequences that are predicted to be unfolded or intrinsically disordered. Green regions are sequences predicted to have secondary structures such as α-helices or β-sheets. The window size is 25 amino acids. **(C)** PONDR (Predictor of Natural Disordered Regions) predictions for $Swc2_{1-179}$ (Left Panel) and Chz1 (Right Panel). VL-XT output is between 1 (ideal prediction of disorder) and 0 (ideal prediction of order). $Swc2_{1-179}$ output for the majority of residues is greater than 0.5 and often near 1, indicating disorder. The PONDR output scores for Chz1 predict predominant disorder. **(D)** Digestion of $Swc2_{1-179}$ by proteinase K. *Lane* 2 is $Swc2_{1-179}$ prior to the addition of proteinase K. *Lanes* 3-7 correspond to $Swc2_{1-179}$ incubated with proteinase K for increasing periods of time (1, 5, 10, 30 and 60 minutes). Digestion of lysozyme by proteinase K. *Lane* 2 is lysozyme prior to the addition of proteinase K. *Lanes* 3-7 correspond to lysozyme incubated with proteinase K for increasing periods of time (1, 5, 10, 30 and 60 minutes). **(E)** CD Analysis of $Swc2_{1-189}$, H2A.Z/H2B and $Swc2_{1-189}$-H2A.Z/H2B. The CD spectra of the co-complex (gray) and H2A.Z/H2B (red) are α-helical in nature (characteristic double minima at 205nm and 220nm). $Swc2_{1-189}$ can be seen in black and the spectrum is characteristic of an unordered secondary structure. The data is plotted in mean residue ellipticity or [θ] (10^3 deg cm^2 $dmole^{-1}$) versus wavelength (nm). **(F)** The difference spectrum ($Swc2_{1-189}$-H2A.Z/H2B – H2A.Z/H2B) is in gray and a change in the secondary structure of $Swc2_{1-189}$ (when compared to Swc2 before binding in black) can be seen. The data is plotted in mean residue ellipticity or [θ] (10^3deg cm^2 $dmole^{-1}$) versus wavelength (nm). **(G)** The CD spectra of Chz1-H2A.Z/H2B (blue) and H2A.Z/H2B (red) are α-helical in nature (characteristic double minima at 205nm and 220nm). Chz1 can be seen in black and the spectrum is characteristic of an unordered secondary structure. The data is plotted in mean residue ellipticity or [θ] (10^3deg cm^2 $dmole^{-1}$) versus wavelength (nm).

an unfolded polypeptide with a pronounced negative band around 200nm (Figure 3.2E black). Both $Swc2_{1-189}$-H2A.Z/H2B and the histone dimer spectra exhibit characteristic alpha-helical negative maxima around 207 and 222nm (Figure 3.2E red and gray).

The $Swc2_{1-189}$-H2A.Z/H2B CD spectrum is significantly different than the Swc2 spectrum (Figure 3.2E). To determine if $Swc2_{1-189}$ underwent a change in structure upon binding H2A.Z/H2B, we compared the spectra of $Swc2_{1-189}$ before and after binding H2A.Z/H2B. In order to obtain the $Swc2_{1-189}$ difference spectrum, the H2A.Z/H2B molar ellipticity was subtracted from the $Swc2_{1-189}$-H2A.Z/H2B complex molar ellipticity. The data was then normalized per residue. Figure 3.2E is the CD spectrum of $Swc2_{1-189}$ before (black) and after binding H2A.Z/H2B (gray). A slight, but significant change in the CD spectrum of $Swc2_{1-179}$ can be seen. The CD spectrum of Chz1 (Figure 3.2G) closely resembles that of $Swc2_{1-189}$ and the Chz1-H2A.Z/H2B spectrum is similar to the $Swc2_{1-189}$-H2A.Z/H2B spectrum (Figure 3.2G). Our results confirm previously published data, which shows that Chz1 is intrinsically disordered, but becomes more ordered upon binding H2A.Z/H2B (Luk et al., 2007).

3.4.4 $Swc2_{1-179}$ and Chz1 bind H2A.Z/H2B heterodimers in a 1:1:1 ratio.

Analytical ultracentrifugation was used to further characterize $Swc2_{1-179}$, Chz1 and their complexes with H2A.Z/H2B dimers by sedimentation velocity and sedimentation equilibrium. Experiments were performed and the boundaries were analyzed using the boundary analysis method of van Holde and Weischet to obtain

diffusion-corrected sedimentation coefficient distribution (Demeler and van Holde, 2004).

The results of the sedimentation velocity experiments revealed that $Swc2_{1-179}$, Chz1, Swc_{1-179}-H2A.Z/H2B and Chz1-H2A.Z/H2B are homogenous (Figure 3.3A). Moreover, the higher molecular weight co-complexes ($Swc2_{1-179}$-H2A.Z/H2B and Chz1-H2A.Z/H2B) have sedimentation coefficients larger than of the individual components ($Swc2_{1-179}$, Chz1, or H2A.Z/H2B). The frictional coefficient ratio (f/fo) for Chz1 and $Swc2_{1-179}$ are 2.0 and 1.7 respectively, indicating that they are non-spherical. The frictional coefficient ratio (f/fo) for Chz1-H2A.Z/H2B and $Swc2_{1-179}$-H2A.Z/H2B are 1.7 and 1.6 respectively.

Sedimentation equilibrium (SE) results comparing the calculated molecular weight (MW) with those expected for single interacting species are summarized in Table 3.1. For both $Swc2_{1-179}$ and Chz1 the theoretical molecular weight of a monomer closely matches the experimental molecular weight (Table 3.1). The sedimentation equilibrium data for $Swc2_{1-179}$-H2A.Z/H2B and Chz1-H2A.Z/H2B complexes indicate a 1:1:1 binding ratio. Thus, AUC data reveals that $Swc2_{1-179}$ and Chz1 are monomers that bind one dimer of H2A.Z/H2B.

Isothermal titration calorimetry (ITC) can be used to determine stoichiometry (n), heat of binding, and binding constant (Kb) or dissociation constant Kd = 1/Kb (Freyer and Lewis, 2008). In Figure 3.3B, the raw ITC data can be seen (change in heat over

A

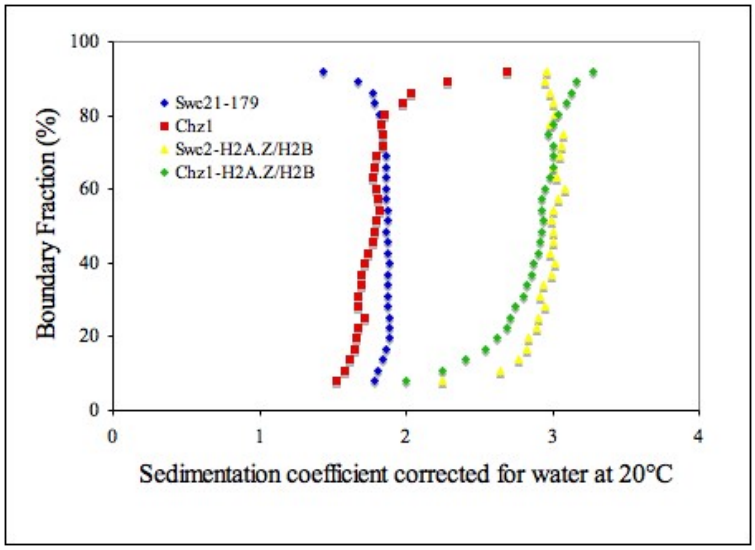
Boundary Fraction (%)
Sedimentation coefficient corrected for water at 20°C
Swc21-179
Chz1
Swc2-H2A.Z/H2B
Chz1-H2A.Z/H2B

B

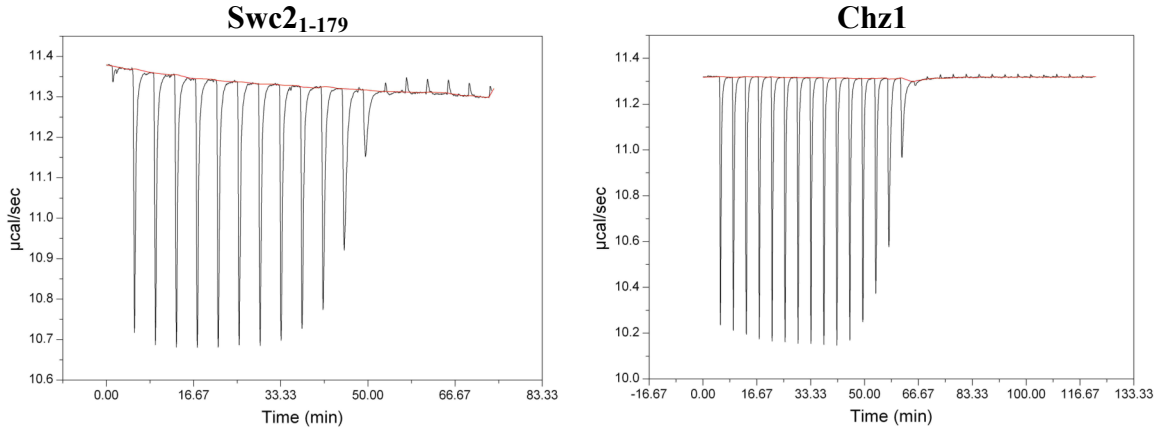
Swc2 1-179
Chz1
µcal/sec
Time (min)

C

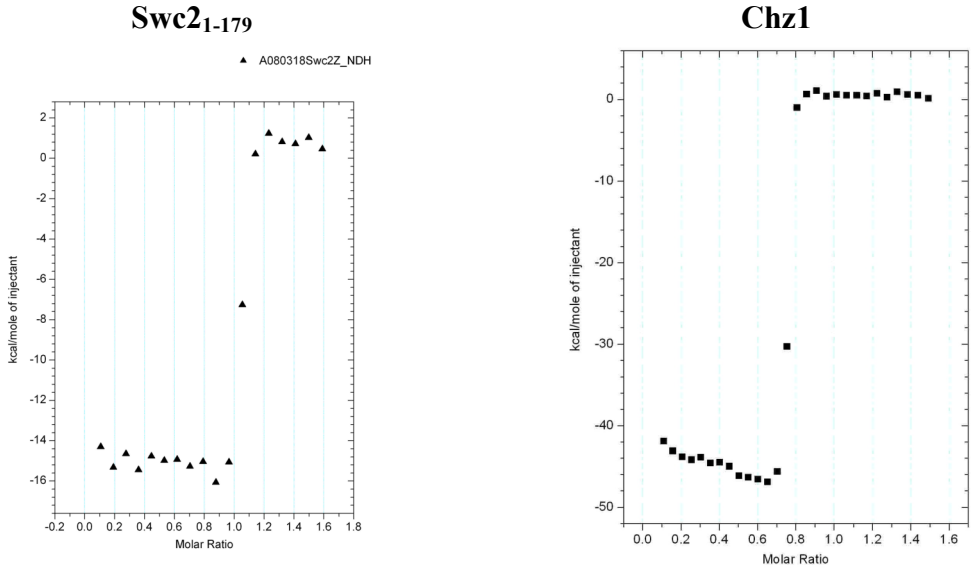
Swc2 1-179
Chz1
A080318Swc2Z_NDH
kcal/mole of injectant
Molar Ratio

Figure 3.3: $Swc2_{1-179}$ and Chz1 bind histones at a 1:1 ratio.
(A) Sedimentation velocity analysis of $Swc2_{1-179}$ (blue 20μM, Chz1 (dark red 20μM) Chz1-H2A.Z/H2B (dark green 7μM) and $Swc2_{1-179}$-H2A.Z/H2B (yellow 5μM) were detected at 229nm wavelength. Boundaries were analyzed using the van Holde-Weischet method and the resulting distributions of S (20,w) corrected for water are shown (Demeler and van Holde, 2004)**. (B)** Isothermal titration calorimetry was performed by titrating 150μM $Swc2_{1-179}$ (or 100μM Chz1) into 10μM H2A.Z/H2B. The change in heat (μcal/sec) versus time (min) for $Swc2_{1-179}$ (left) or Chz1 (right) titration into H2A.Z/H2B. **(C)** The ΔH plot of heat (kcal/mol of $Swc2_{1-179}$ injected) versus the molar ratio of $Swc2_{1-179}$-H2A.Z/H2B is on the left. The ΔH plot of heat (kcal/mol of Chz1 injected) versus the molar ratio of Chz1-H2A.Z/H2B is on the right.

Table 3.1: Sedimentation equilibrium results

Sample	Theoretical MW (Da)	Single Interacting Species MW (Da)
Swc2 $_{1\text{-}179}$	23,096	23,870
Chz1	19,423	20,010
Swc2$_{1\text{-}179}$-Z/B	51,766	50,250
Chz1-Z/B	47,080	42,370

Sedimentation equilibrium results for the indicated samples. The theoretical molecular weight (MW) was calculated using ExPASY proteomic server (http://expasy.org/tools/protparam.html).

exothermic, and saturation (heat no longer released) occurs. The raw data was fit to a ΔH plot (Figure 3.3C) from which the stoichiometry and association constant can be calculated. The ITC analysis indicates that $Swc2_{1-179}$ binds H2A.Z/H2B in a 1:1 ratio and Chz1 binds H2A.Z/H2B in a 0.8:1 ratio (Figure 3.3).

A careful analysis of figures 3.3C and 3.3D shows that early in the experiment the binding isotherm has a very small negative slope corresponding to a small increase in heat change per injection. This could be due to either a weak binding event or a small artifact of the data collection (bubble or faulty plunger tip). Additionally, there is only one point on the slope of the binding isotherm. The transition is too sharp and there are too few points collected near equivalence. We therefore could only ascertain the stoichiometry of binding and we were unable to fit the data to obtain the Kb.

3.4.5 $Swc2_{1-179}$ and Chz1 bind H2A/H2B and H2A.Z/H2B with similar affinities

Pulldown assays revealed that $Swc2_{1-179}$ binds H2A.Z/H2B at higher salt concentrations than H2A/H2B (Figure 3.1B). However, a more careful analysis of the binding affinity of $Swc2_{1-179}$ and Chz1 to histone dimers under more physiological conditions was desired. A fluorescence assay monitors the change in fluorescence as increasing amounts of $Swc2_{1-179}$ or Chz1 are added to fluorescently labeled histone dimers (Figure 3.4). The results in Table 3.2 indicate that $Swc2_{1-179}$ does not have a preference for H2A.Z/H2B and it binds with low μM affinity to both wild-type and variant histone dimers. Chz1 has a similar low micromolar binding affinity for H2A.Z/H2B and H2A/H2B (Table 3.2). These results indicate that Swc21-179 and Chz1 (at the salt concentration tested) are not histone variant-specific.

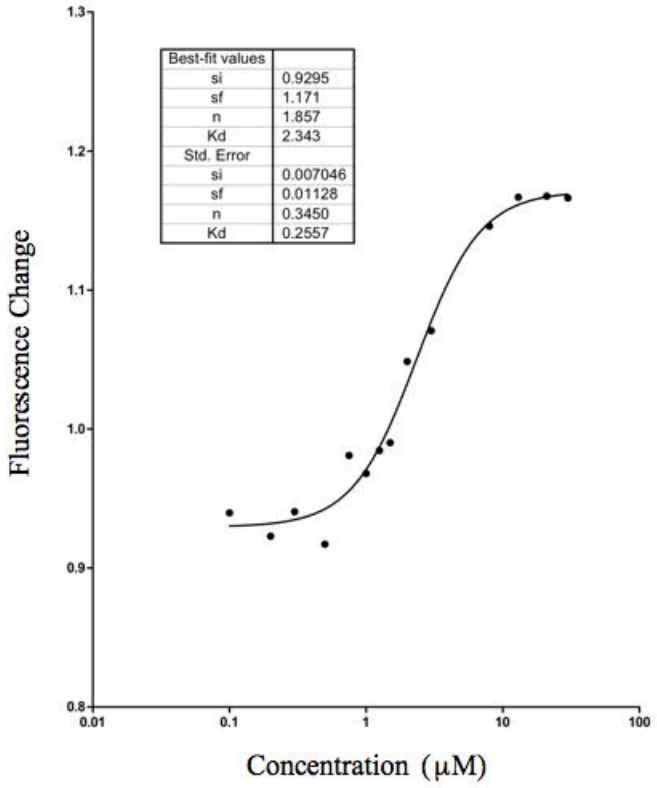

Figure 3.4: $Swc2_{1-179}$ and Chz1 bind H2A/H2B and H2A.Z/H2B heterodimers with similar affinities. The normalized fluorescence change upon $Swc2_{1-179}$ binding to Alexa 488 labeled histone H2A/H2B as measured by fluorescence titration. A standard binding isotherm was fit to the data (Methods) to determine the Kd for the interaction. See Table 3.2 for complete list of Kd values for Chz1 and $Swc2_{1-179}$.

Table 3.2: Affinity measurements of protein-protein interactions

Interaction	Protein Titrated	Protein Labeled	Kd (μM)
$Swc2_{1-179}$-H2A/H2B	$Swc2_{1-179}$	H2B	2.3 ± 0.2
$Swc2_{1-179}$-H2A.Z/H2B	$Swc2_{1-179}$	H2B	3.2 ± 0.8
Chz1-H2A/H2B	Chz1	H2B	1.9 ± 0.1
Chz1-H2A.Z/H2B	Chz1	H2B	1.7 ± 0.5

All measurements were performed in 10 mM Tris-HCl, pH 7.5, 0.25 mM EDTA, 0.1 % BSA and 300 mM NaCl. Labeled proteins were kept at 40 nM. See Methods for details.

3.4.6 SAXS data evaluation

Size-exclusion chromatography in conjunction with multi-angle light scattering (SEC-MALS) was used as a direct measurement of the molecular masses of the samples that were ultimately analyzed by SAXS. Figure 3.5A depicts a graph of the molecular mass (g/mol) versus elution time (min) for the SAXS samples. $Swc2_{1-179}$-H2A.Z/H2B (in blue) elutes slightly earlier than $Swc2_{1-179}$ (red), followed by the histone variant dimer (green). Table 3.3 shows the molecular masses determined from SEC-MALS. Based on the molecular mass, $Swc2_{1-179}$ forms a heterotrimer complex with H2A.Z/H2B under the conditions utilized for SAXS. Importantly, the samples used for SAXS were homogenous.

SAXS can provide important structural parameters like the overall size, shape and volume of a macromolecule in solution (Mertens and Svergun, 2010). However, prior to starting data analysis, it is important to ensure that SAXS samples are free of aggregation and radiation damage. Samples were collected at various concentrations and the scattering curves were overlaid to determine any concentration-dependent effects. The Guinier plot (ln (I(q)) vs. q^2) was used to analyze the SAXS scattering curve at very small scattering angles or low resolution (Putnam et al., 2007). If the plot is linear at low q-ranges where the Guinier approximation is valid (R_g*q<1.3), the samples aren't aggregated. Moreover, from the Guinier plot, the radius-of-gyration, R_g can be determined using the equation $I(s) = I(0) \exp[-(sR_g)^2/3]$ (reviewed by (Putnam et al., 2007)). $Swc2_{1-179}$, H2A.Z/H2B, and the $Swc2_{1-179}$-H2A.Z/H2B complex were not aggregated (Figure 3.5B-D). Their respective R_g values are listed in Table 3.4.

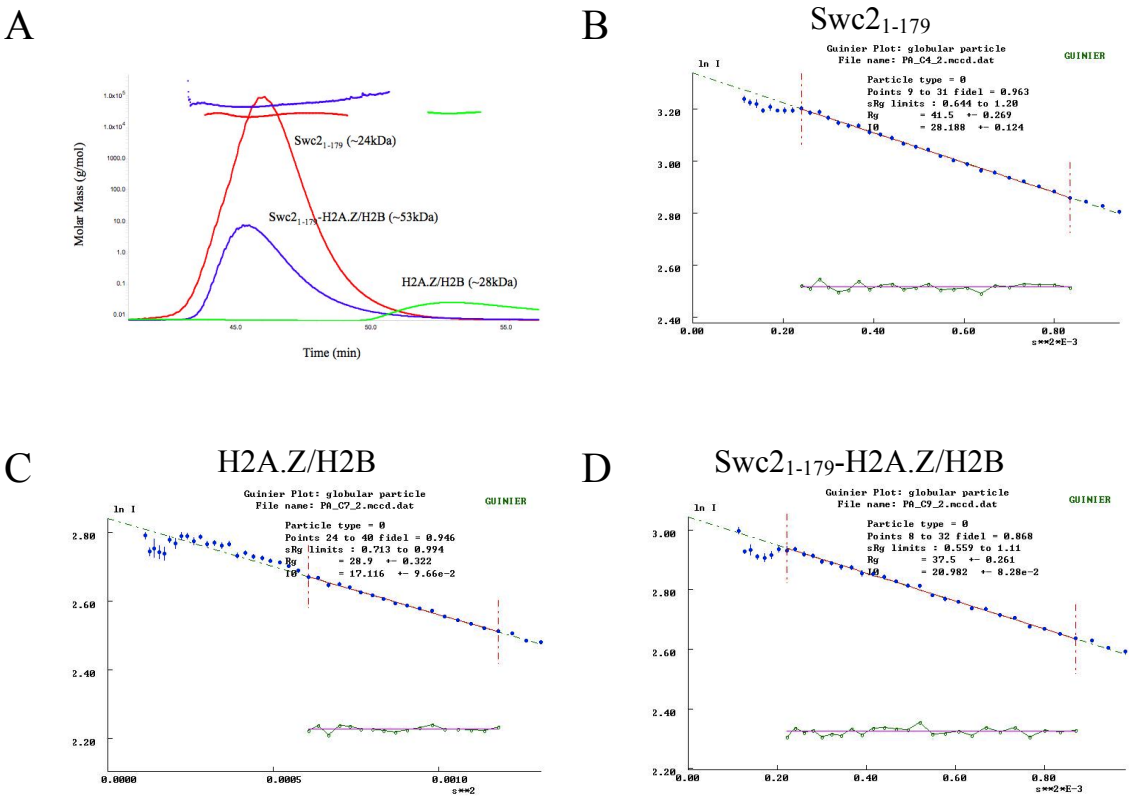

Figure 3.5: SAXS samples are homogenous.
(A) Size-exclusion chromatography and inline static light scattering of $Swc2_{1-179}$ (red), H2A.Z/H2B (green) and $Swc2_{1-179}$-H2A.Z/H2B (blue). Each sample elutes in a single peak from a size-exclusion column. The static light-scattering average molecular mass for each peak is illustrated by a line above or within the peak and denoted on the figure. The molecular masses are listed in Table 3.3. **(B)** Guinier plot (ln (I(q)) vs. q^2) of $Swc2_{1-179}$ (3.5 mg/ml), defined using points 9-21 with a fidel score of 0.96* (Svergun, 1992). The continuous line indicates regions used in the Guinier analysis. The bottom of the plot displays deviations from the fit of the line. The R_g from the Guinier plot is 41.2Å. **(C)** Guinier plot of H2A.Z/H2B (2 mg/ml), defined using points 24-40 with a fidel score of 0.95* (Svergun, 1992). The R_g from the Guinier plot is 28.9Å. **(D)** Guinier plot of $Swc2_{1-179}$-H2A.Z/H2B (2.5 mg/ml), defined using points 8-32 with a fidel score of 0.87*. The R_g from the Guinier plot is 37.5Å.

*The fidel score measures the quality of the fit and should be close to 1.

Table 3.3: Molecular masses from multi-angle light scattering

Sample	Theoretical (Da)	Experimental (Da)	Polydispersity
Swc2 $_{1\text{-}179}$	23,096	24,280 (7%)[a]	1.012
H2A.Z/H2B	28,389	28,230 (18%) [a]	1.001
Swc2$_{1\text{-}179}$-Z/B	51, 766	52,570 (6%) [a]	1.042

[a] = error associated with the experimental data
All measurements were performed in 20 mM Tris-HCl, pH 7.5, 300mM NaCl and 5% glycerol. Sample concentrations were between 2 – 3mg/ml. Described in methods.

Table 3.4: Structural parameters obtained from SAXS

Sample	Swc2$_{1\text{-}179}$	H2A.Z/H2B	Swc2$_{1\text{-}179}$-H2A.Z/H2B
R_g (Å), Guinier	41.2	28.9	37.5
R_g (Å), P(r) analysis	41.5	29.1	37.2
D_{max} (Å), P(r) analysis	141	100	129

All measurements were performed in 20 mM Tris-HCl, pH 7.5, 300mM NaCl and 5% glycerol. The data was processed using standard procedures and the GNOM and PRIMUS software program packages (Svergun, 1992, 2003a).

From the preliminary data evaluation, we deemed the samples to be of sufficient quality for further processing.

3.4.7 Solution structure of $Swc2_{1-179}$

SAXS is an excellent technique for the study of flexible proteins in solution; it has been used extensively to characterize intrinsically disordered proteins (Paz et al., 2008; Rajasekar et al., 2010; Tsutakawa et al., 2007). The observed scattering curve for $Swc2_{1-179}$ is shown in Figure 3.6A (gray) (obtained as described in materials and methods). The Krakty plot ($q^2(I(q))$ vs. q) is commonly used in SAXS analysis to distinguish between a compact or an extended conformation (Putnam et al., 2007). The $Swc2_{1-179}$ Kratky plot (Figure 3.6B gray) plateaus at higher q-values and is linear with respect to q in the large q-region. This is typical of proteins with flexible chains and a less compact core. The scattering data was then analyzed by GNOM to derive the pair distribution function P(r) (Svergun, 1992). The P(r) is generated through an indirect Fourier transform of the scattering curve and provides information about the distances between electrons in the scattering particles in the sample. Figure 3.6C shows the P(r) distribution for $Swc2_{1-179}$ (gray) with a D_{max} of 141Å. The P(r) curve is asymmetric with an early maximum near 40Å, followed by a long tail that decreases at larger r. The R_g derived from the P(r) function is 41.5Å and is in close agreement with the R_g derived from the Guinier plot 41.2Å (Table 3.4). Both the D_{max} and R_g values are rather large for a 23kDa molecular mass, suggesting an extended conformation.

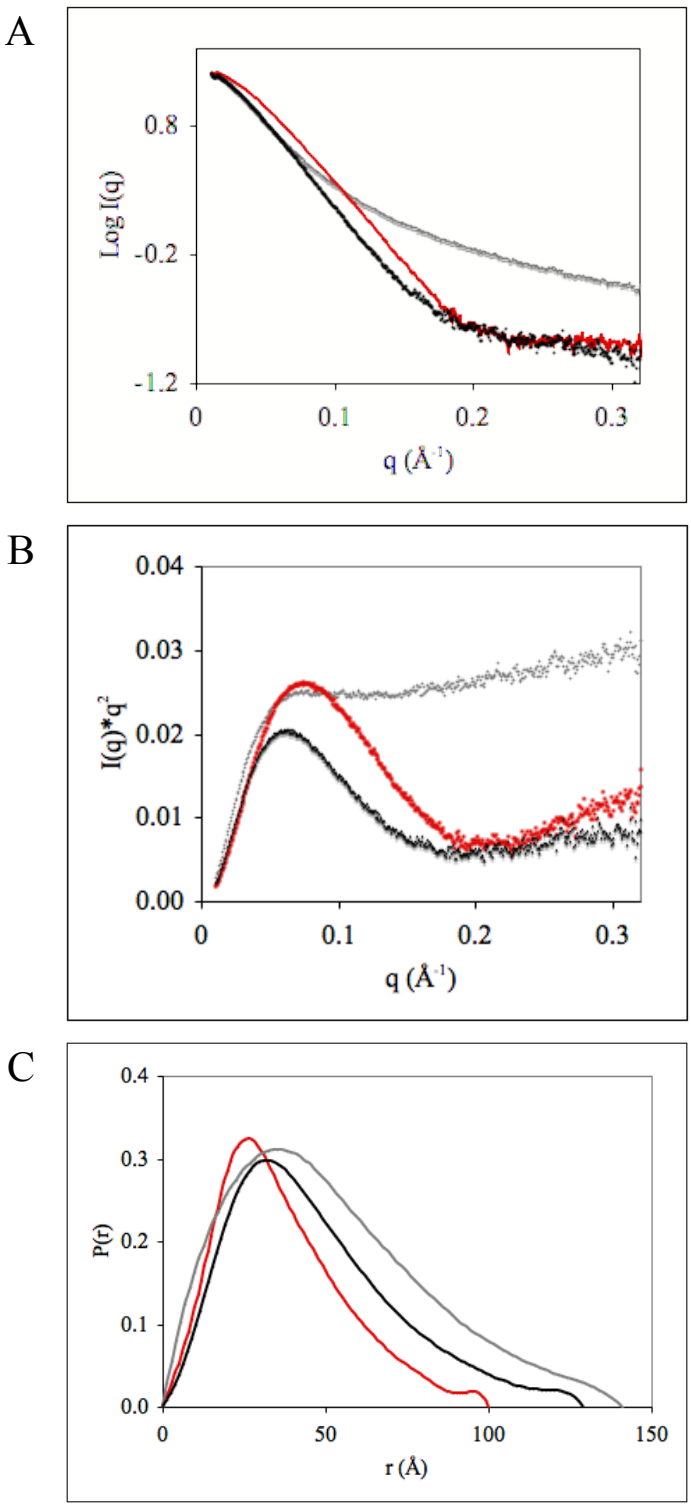

Figure 3.6: Experimental SAXS curves.
(A) Scattering curves of $Swc2_{1-179}$ (gray), H2A.Z-H2B (red) and $Swc2_{1-179}$-H2A.Z/H2B (black). **(B)** Kratky plots of $Swc2_{1-179}$ (gray), H2A.Z-H2B (red) and $Swc2_{1-179}$-H2A.Z/H2B (black). **(C)** P(r) functions of $Swc2_{1-179}$ (gray), H2A.Z-H2B (red) and $Swc2_{1-179}$-H2A.Z/H2B (black).

Ensemble optimization method (EOM) was used to create structural models of $Swc2_{1\text{-}179}$ (Bernado et al., 2007). RanCh (Ran*dom* Ch*ain*) generates the pool of random models of intrinsically unfolded proteins. The program GAJOE (G*enetic* A*lgorithm* J*udging* O*ptimization of* E*nsembles*) is the selection program. Figure 3.7A illustrates that the GAJOE selected ensemble fits the scattering data very well (average $\chi^2 = 1.0$). In figure 3.7B, the R_g distribution of the GAJOE selected conformations in red is compared to the distribution of the pool of all curves-structures created by RanCh in black. The average R_g is 45Å for the selected ensemble and the RanCH pool average R_g is 39Å. The D_{max} distribution histograms for the RanCH pool compared to the distribution of the curves-structures selected by GAJOE can be seen in Figure 3.7C. The average D_{max} is 119Å for the pool and the average D_{max} is 137Å for the selected curves. The selected R_g and D_{max} distributions were shifted to values larger than the pool which indicates they have a very extended structure (more extended than that of a random coil). Figure 3.7D shows an overlay of 20 representative conformers of $Swc2_{1\text{-}179}$ that were selected by GAJOE from the RanCh pool. Analysis of the normalized spatial discrepancy (NSDs) of the individual structures affirms the lack of a strongly preferred orientation for $Swc2_{1\text{-}179}$. For ideally superimposed samples the NSD nears 0 and NSDs significantly exceeding 1 indicates large variances. The EOM-generated conformers for $Swc2_{1\text{-}179}$ had an average NSD of 3.10, indicating there is no strongly preferred conformation for $Swc2_{1\text{-}179}$ (Figure 3.7D).

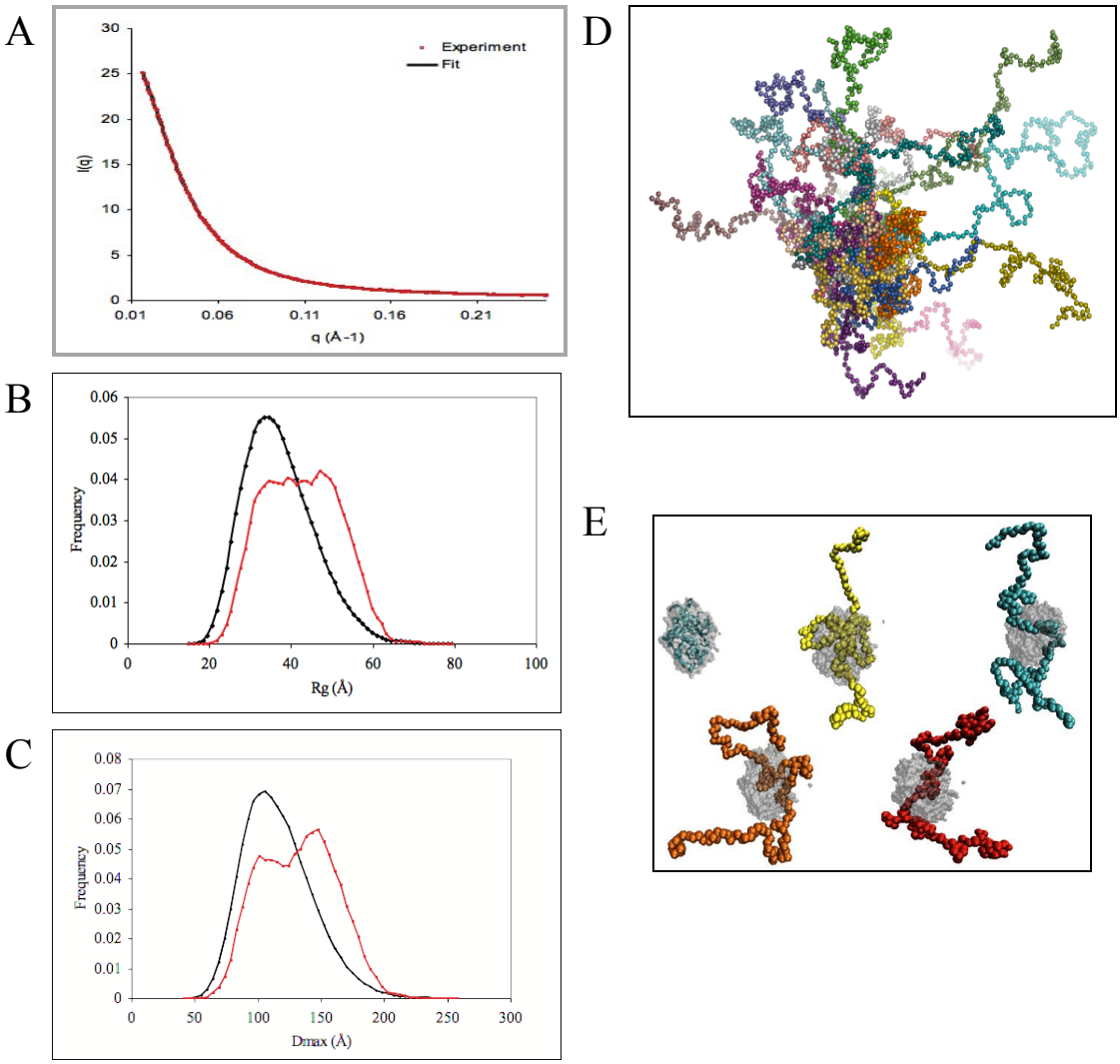

Figure 3.7: Solution structure of Swc2$_{1-179}$.
(A) The fit of the selected ensemble to the experimental data. The average $\chi 2$ is1.0 and the experimental data are represented by red dots and a black line represents the ensemble fit. **(B)** The R_g distribution histogram for Swc2$_{1-179}$. The black line corresponds to the pool of conformers generated by RanCH and the red line corresponds to the ensemble of curves/structures selected by the genetic algorithm GAJOE. **(C)** Distribution of Swc2$_{1-179}$ distances. The black line corresponds to the distances generated by RanCH (pool) and the red line represents the ensemble of curves/structures selected by GAJOE. **(D)** Overlay of the 20 Swc2$_{1-179}$ (3.5 mg/ml) structures selected by EOM (Bernado et al., 2007). Each of the 20 different conformers is depicted in a different color. **(E)** Representative Swc2$_{1-179}$ structures; each conformer is a different color. The model of a folded protein with a similar number of residues in the crystal structure (Actinidin, 2ACT) is displayed as a cyan ribbon for comparison. The 3D surface representation of Actinidin (semitransparent gray) is positioned at the approximate center of each model for comparison.

3.4.8 Solution structure of H2A.Z/H2B

The scattering profile for H2A.Z/H2B is shown in Figure 3.6A (red). The Kratky plot for H2A.Z/H2B (red) is in Figure 3.6B. Unlike the plot for $Swc2_{1-179}$, the Kratky plot doesn't plateau and is more bell-shaped. This is typical for a compact or globular structure that is at least partially folded. Figure 3.6C is the P(r) distribution curve for H2A.Z/H2B (red) with a D_{max} of 100Å. The distribution is smooth and asymmetric with maximum near 30Å and with a tail extending to longer distances. The shape of this distribution suggests that H2A.Z/H2B is globular with a slightly extended structure, most likely due to the histone tails. The R_g derived from the P(r) function is 29.1Å and is in very close agreement with R_g derived from the Guinier plot 28.9 Å (Table 3.4).

GASBOR was used for *ab initio* SAXS envelope reconstruction of H2A.Z/H2B. In GASBOR, the protein is represented by an ensemble of dummy residues forming a chain-compatible model (Svergun et al., 2001). Keeping in mind that SAXS scattering profiles do not yield one unique structural solution, multiple models are generated. In figure 3.8A, 3 of the 15 bead models generated by GASBOR for H2A.Z/H2B can be seen. The fit to the raw scattering data has χ^2 values ranging from 1.25 - 1.36, indicating that the models fit the raw data well. The 15 bead models of H2A.Z/H2B were averaged and filtered; the resulting envelope is depicted in Figure 3.8B (Svergun, 2003b).

Situs software was then utilized to create a 3D volumetric model of the averaged and filtered H2A.Z/H2B envelope. This allows for better visualization when docking rigid body structures (Wriggers et al., 1999). The contoured surface of the SAXS H2A.Z/H2B model with the crystal structure of H2A.Z/H2B (from the H2A.Z containing

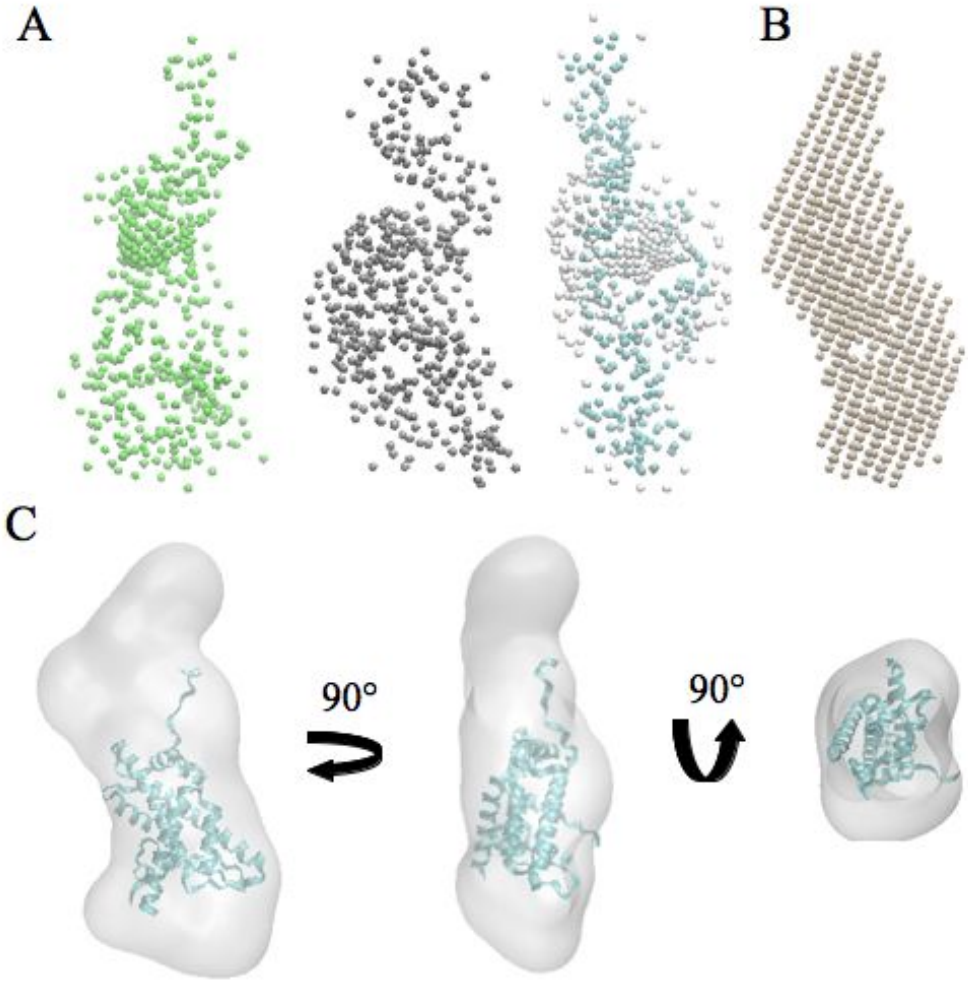

Figure 3.8: Solution structure of H2A.Z/H2B.
(A) Three different GASBOR reconstructions showing variations among the H2A.Z/H2B structures (Svergun et al., 2001). **(B)** The averaged *ab-initio* SAXS envelope calculated from 15 different GASBOR runs on left (gray) using the program DAMAVER (Svergun, 2003b). **(C)** Chains C and D (H2A.Z-H2B) from the nucleosome crystal structure (1F66), represented as a blue ribbon, were manually docked into the volumetric map of H2A.Z/H2B using *Situs* and VMD (Wriggers et al., 1999). The histone dimer structure fits within the SAXS H2A.Z/H2B model.

nucleosome structure IF66) manually docked inside can be seen in Figure 3.8C (Wriggers et al., 1999). The crystal structure of H2A.Z/H2B has a shape similar to the SAXS generated volumetric map. We attribute the excess volume to the fact that the crystal structure is missing 57 amino acids from the histone tails. Furthermore, it is unknown whether the structure of H2A.Z/H2B is the same in a non-nucleosomal context.

3.4.9 Solution structure of $Swc2_{1-179}$-H2A.Z/H2B

The scattering profile for $Swc2_{1-179}$-H2A.Z/H2B is shown in Figure 3.6A (black). Figure 3.6B is a Kratky plot of $Swc2_{1-179}$ - H2A.Z/H2B (black), unlike $Swc2_{1-179}$, this curve doesn't plateau at large q-values, but exhibits a bell shaped curve. This is evidence that the complex is a partially folded structure that is less elongated than $Swc2_{1-179}$ in the absence of histones. Figure 3.6C shows the P(r) distribution curve for $Swc2_{1-179}$ - H2A.Z/H2B with a D_{max} of 129Å. The P(r) distribution is asymmetric with a maximum near 40Å (like $Swc2_{1-179}$) and a tail extending to longer distances. The R_g derived from the P(r) function is 37.2Å and in close agreement to the R_g derived from the Guinier plot 37.5Å (Table 3.4). Notably, $Swc2_{1-179}$-H2A.Z/H2B is almost twice the molecular mass of $Swc2_{1-179}$ (Table 3.3), but the structural parameters R_g and D_{max} are smaller.

GASBOR was used for *ab initio* SAXS envelope reconstruction of $Swc2_{1-179}$-H2A.Z/H2B complex (Svergun et al., 2001). Figure 3.9A depicts 3 of the 15 GASBOR structures generated for $Swc2_{1-179}$-H2A.Z/H2B. The models are all similar in structure (χ^2 values of 1.2 – 1.3). The 15 bead models of $Swc2_{1-179}$ - H2A.Z/H2B were averaged and filtered as seen in Figure 3.9B (Svergun, 2003b).

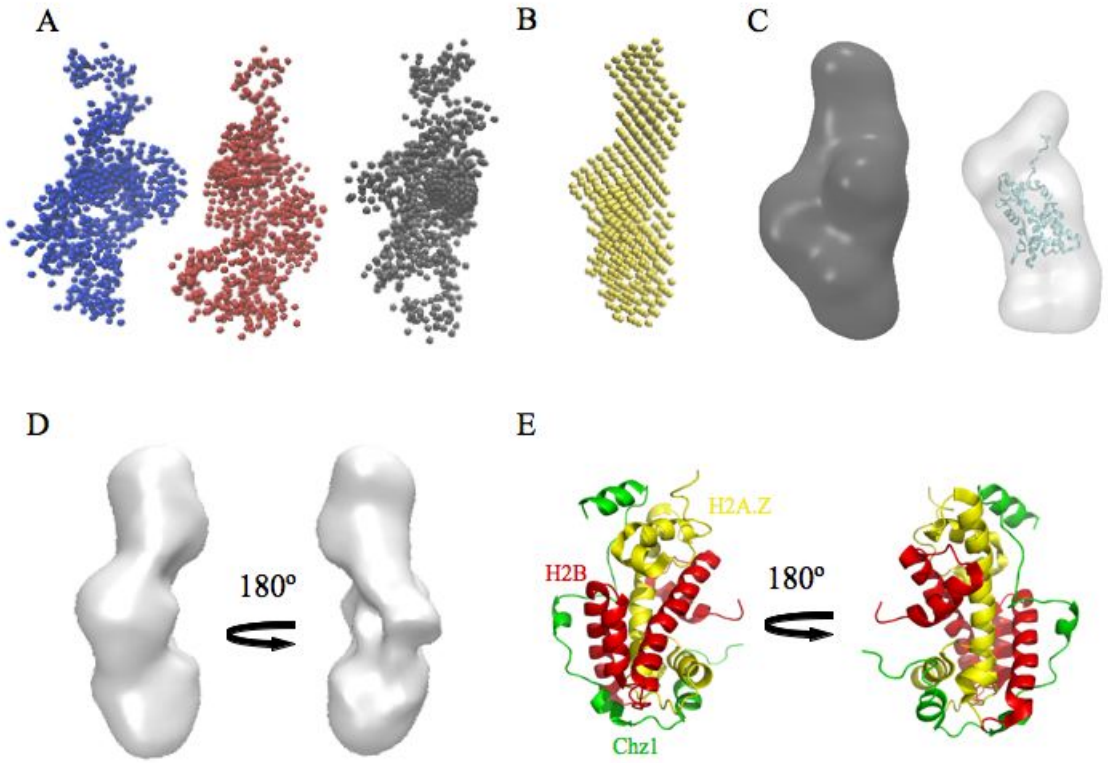

Figure 3.9: *Ab initio* reconstructions of Swc2$_{1-179}$-H2A.Z/H2B.
(A) Three different GASBOR reconstructions showing variations among the Swc2$_{1-179}$-H2A.Z/H2B structures (Svergun et al., 2001). **(B)** The averaged *ab-initio* SAXS envelope calculated from 15 different GASBOR models using the program DAMAVER (Svergun, 2003b). **(C)** Comparison of H2A.Z/H2B averaged volumetric model (white with docked H2A.Z/H2B crystal structure) to Swc2$_{1-179}$-H2A.Z/H2B averaged model in grey. **(D)** The volumetric envelope difference (Swc2$_{1-179}$-H2A.Z/H2B – H2A.Z/H2B) generated using voldiff program in (Wriggers, 2010). **(E)** The Chz1 core forms a long irregular chain capped by two short helices (green) which wrap around the histone dimer. The core makes broad contacts with H2A.Z (yellow) and H2B (red) (Zhou et al., 2008).

Using *Situs*, the filtered structure of the complex was converted to 3D volume representation (Wriggers, 2010). The volumetric molecular envelope of $Swc2_{1-179}$-H2A.Z/H2B is slightly larger than the volumetric envelope of H2A.Z/H2B (Figure 3.9C). The volumetric difference program (Wriggers, 2010) allows one to compute and visualize the difference density map (discrepancy map) of two volume data sets. A difference model was created (using $Swc2_{1-179}$-H2A.Z/H2B and H2A.Z/H2B volumetric maps) and is depicted in Figure 3.9D. The difference map shows the putative binding positioning of $Swc2_{1-179}$ in the heterotrimeric complex. When compared to the NMR structure of Chz1-H2A.Z/H2B depicted in Figure 3.9E, a similar mode of binding is suggested.

3.4.8 Neither $Swc2_{1-179}$ nor Chz1 affect the nucleosome structure.

Nucleosomes reconstituted onto 146 base pairs of 5S rDNA sequence (Dyer et al., 2004) were incubated with increasing molar amounts of $Swc2_{1-179}$ or Chz1 (1 - 10 fold molar excess). After incubation for 12 hours at 4°C, neither $Swc2_{1-179}$ nor Chz1 were able to remove the histone dimer (H2A/H2B) from the preformed nucleosomes (Figure 3.10A,B). Neither of the proteins were able to shift the nucleosome band, indicating that under our conditions, they do not stably bind to the nucleosomes. Notably, at higher concentrations of $Swc2_{1-179}$, the nucleosome band does smear, but this could be a gel artifact. The Coomassie-stained gel (Figure 3.10 C,D) shows an increase in Swc2 $_{1-179}$ or Chz1 staining as the concentration increases.

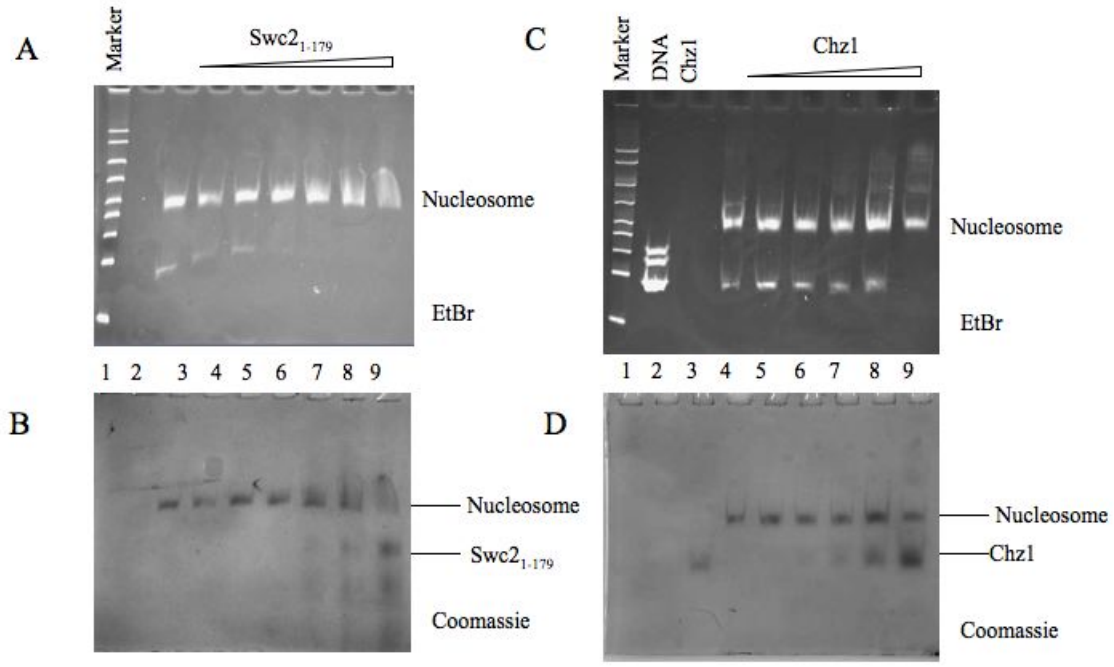

Figure 3.10: Swc2 $_{1\text{-}179}$ and Chz1 are unable to affect nucleosome structure.
(A) 5μM nucleosomes (NCP) reconstituted with canonical histones were incubated with increasing molar amounts of Swc2$_{1\text{-}179}$ (*lane* 1, marker, *lane* 2, Swc2$_{1\text{-}179}$, *lane* 3, no Swc2$_{1\text{-}179}$, *lanes* 4-9, 0-, 1-, 2-, 4-, 6- and 10-fold molar ratio of Swc2$_{1\text{-}179}$ to NCP). Samples were incubated at 4°C for 12 hours and analyzed by 5% native PAGE. **(B)** Coomassie staining of the 5% native gel in A. **(C)** 5μM nucleosomes (NCP) reconstituted with canonical histones were incubated with increasing molar amounts of Chz1 (*lane* 1, marker, *lane* 2, 146bp DNA, *lane* 3 Chz1, *lane* 4 no Chz1 *lanes* 5-9, 1-, 2-, 4-, 6- and 10-fold molar ratio of Chz1 to NCP). Samples were incubated at 4°C for 12 hours and analyzed by 5% native PAGE. **(D)** Coomassie staining of the 5% native gel in C.

3.5 Discussion

Both Swc2 and Chz1 bind histone H2A.Z *in vivo* as shown by immunoprecipitations. Chz1 (Chaperone for H2A.Z/H2B) has been classified as the first discovered histone variant chaperone. Although some redundancy exists *in vivo* with Nap1, it serves to bind histones H2A.Z/H2B and presumably prevent improper interactions with DNA. *In vitro* studies have shown that Chz1 can supply the H2A.Z/H2B dimer to the SWR1 complex for histone variant exchange. Swc2 is a key member of the SWR1 complex and previous studies have shown that Swc2 is essential for binding and transfer of H2A.Z. Mechanistically, it's thought that Chz1 hands the variant dimer to Swc2 which can supply it to the SWR1 complex for exchange into nucleosomes. Thus Swc2, like Chz1, is thought to selectively recognize H2A.Z.

Here we analyzed how two intrinsically disordered histone modules interact with variant dimers. We provide new information about the extended conformations of the N-terminus of Swc2. We utilized bioinformatics, proteolytic degradation susceptibility, CD spectroscopy and solution scattering to conclude that $Swc2_{1\text{-}179}$, like Chz1, is an intrinsically disordered protein (IDP). The structural characterization of an IDP by x-ray diffraction techniques is difficult and therefore requires a solution state study. Small-angle x-ray scattering (SAXS) is a technique that allows for the low-resolution determination of molecular shape. Our SAXS studies produced the first structural conformers of an intrinsically disordered histone-binding protein, in the absence of histones. When compared to a typical globular protein of similar size (actinidin 220 residues) the extended nature and structural flexibility of $Swc2_{1\text{-}179}$ is highly evident (Figure 3.7E). Interestingly, a structural characterization of over 300 globular proteins

from the SCOP database revealed that folded proteins with 200-250 residues have an R_g between 18-20Å (Lobanov et al., 2008). This is much smaller than the SAXS obtained R_g value for $Swc2_{1-179}$ (41Å). Chz1 and $Swc2_{1-179}$ are unusual amongst histone binding proteins in that they lack a folded structure in the absence of histones. In contrast, previously characterized histone chaperones such as Nap1 (Park and Luger, 2006b), Vps75 (Park et al., 2008b), Asf1 (Daganzo et al., 2003) and Nucleoplasmin (Dutta et al., 2001) have well-defined secondary structures even in the absence of histones.

Several reviews describe in great detail the function and structure of natively disordered proteins (Dunker et al., 2002; Dunker et al., 2001; Tompa, 2002, 2005). Intrinsic disorder has been highly correlated in functional areas such as transcription, DNA binding and protein interaction networks, regulation of the cell cycle, and signaling proteins (Vucetic et al., 2007; Ward et al., 2004; Xie et al., 2007a; Xie et al., 2007b).

Our results established that both $Swc2_{1-179}$ and Chz1 are intrinsically disordered and capable of binding histones. We then studied how binding to H2A.Z/H2B affected the structure of the IDPs. AUC and ITC studies revealed Chz1 and $Swc2_{1-179}$ are monomeric in solution and they bind H2A.Z/H2B in a 1:1:1 ratio. CD spectroscopy analysis affirmed that both Chz1 and $Swc2_{1-179}$ become more ordered upon interacting with the histone variant dimer. Using SAXS we show that $Swc2_{1-179}$ undergoes a change in structural parameters and the complex (higher molecular mass) has a smaller maximum dimension and radius of gyration than $Swc2_{1-179}$ alone. These results indicate that $Swc2_{1-179}$ becomes less elongated (or more ordered) upon binding H2A.Z/H2B, which would be expected for an IDP. Importantly, our SAXS models also suggest that

$Swc2_{1-179}$ wraps around the H2A.Z/H2B dimer, binding a large area and perhaps making many contacts.

How are two intrinsically disordered proteins capable of selectively identifying and binding yeast H2A.Z over H2A? Although binding to the variant dimer had been established, no relative binding affinity comparing wild type and variant histones had been published. Our studies show that $Swc2_{1-179}$ does not have a preference for H2A.Z and it binds with low μM affinity to histone heterodimers H2A/H2B and H2A.Z/H2B. Chz1 has a similar low micromolar binding affinity for H2A/H2B and H2A.Z/H2B. These results indicate that $Swc2_{1-179}$ and Chz1 (at the salt concentration tested) are not histone variant-specific but rather have similar binding affinities for both canonical and variant dimers. When compared to other histone chaperones, this affinity is rather weak. Both Nap1 and Vps75 bind histones with low nanomolar affinity under the same conditions tested (Andrews et al., 2008; Park et al., 2008b). The affinity of Chz1 for H2A.Z/H2B heterodimers was ascertained by isothermal titration calorimetry (ITC) and relaxation dispersion NMR spectroscopy (Hansen et al., 2009). The reported dissociation constant (Kd) for Chz1 binding to H2A.Z/H2B was ~0.2μM (Hansen et al., 2009). There is a 10-fold difference between reported Kds, but this could be attributed to differences in assays used (different salt concentrations, buffer conditions and temperature were noted). Additionally, the previously published study utilized only the Chz1 core (71-32) and tail-less histones constructed as a single chain. The published structure of Chz1-H2A.Z/H2B does not support the hypothesis that Chz1 has a structural preference for H2A.Z (Zhou et al., 2008). All of the unique residues of H2A.Z were analyzed in the NMR complex structure. There is no indication that these residues are poised to interact with Chz1.

Much like previously characterized chaperones, $Swc2_{1-179}$ and Chz1 appear to lack histone variant specificity.

$Swc2_{1-179}$ and Chz1 are not histone variant-specific, although *in vivo*, they are found in complex with yeast H2A.Z/H2B. Unlike other characterized chaperones such as Nap1, neither protein could affect canonical nucleosome structure (Park et al., 2005). Their inability to affect the nucleosome, combined with the low binding affinity for histones, leads us to believe that neither Chz1 nor $Swc2_{1-179}$ function as "true" histone chaperones, defined as preventing improper histone-DNA interactions (Andrews et al., 2010; Laskey et al., 1978). Interestingly, a genetic interaction summary reveals that Swc2 has over 500 genetic and physical interactions partners *in vivo* (yeastgenome.org). Perhaps the intrinsic disorder allows the proteins to adopt a multitude of structural states therefore facilitating many different interactions and functions.

3.6 Acknowledgements

Special thanks are given to Kris Hite and Young-Jun Park who designed the Swc2 constructs utilized in this paper. Steve McBryant was instrumental in helping with the AUC and CD data. We thank Teri McLain from the W.M. Keck facility for the purified histones. Mary Robinson, Andy Andrews, Wayne Lilyestrom and Mark Van der Woerd offered advice and help when needed. This research was supported by a predoctoral grant from the American Heart Association.

CHAPTER IV

A Role for the N-terminal Domain of Swc2, a Subunit of SWR1 Complex, in DNA Damage Recognition

Sudhoff KB, Campbell A, and Luger K.

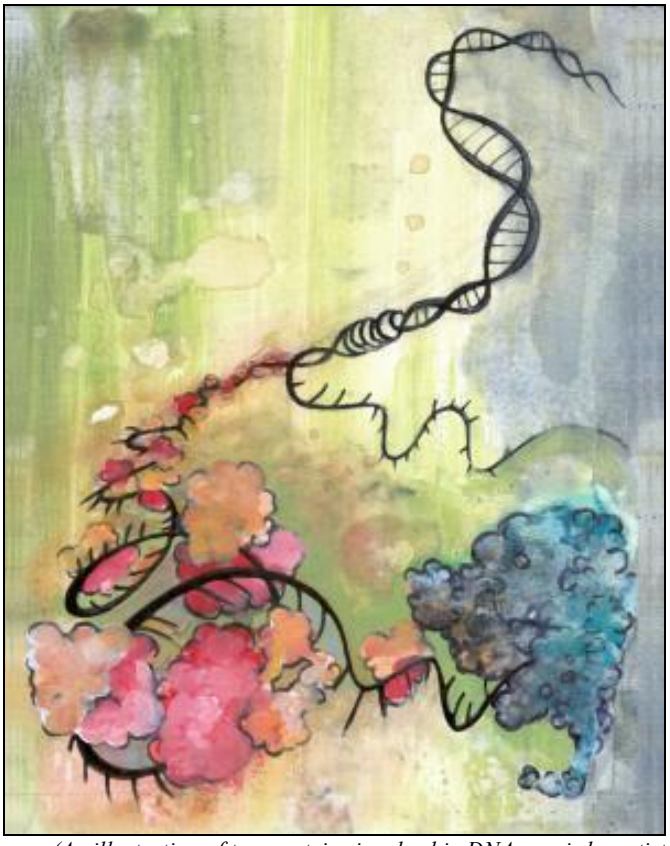

(An illustration of two proteins involved in DNA repair by artist Amy VanDonsel.)

K.B.S. did all the experiments; A.C. prepped the proteins and DNA and provided supporting data; K.L. and K.B.S. planned and supervised the experimental sections.

4.1 Abstract

SWR1 is the first characterized ATP-dependent chromatin-remodeling complex that catalyzes incorporation of H2A.Z into nucleosomes. Published research has identified a role for the SWR1 complex in DNA damage repair that is unrelated to its histone exchange function. Swc2 (Swr1 complex 2) is a subunit of the multi-subunit SWR1 complex. Here we show that $Swc2_{1-179}$, despite its overall acidic charge, can bind dsDNA - in particular, 3-way and 4-way junction DNA. These junctions are thought to mimic the central intermediates found in DNA damage repair. This characteristic is unique to $Swc2_{1-179}$ and not associated with any other histone chaperone tested. Furthermore, yeast phenotypic assays have revealed a role for *SWC2* in DNA damage repair, as indicated by sensitivity to DNA damaging agent methyl methanesulfonate. Thus, our data has exposed a novel role for Swc2 in DNA damage repair. This has important implications, as it may be the missing link between the presence of SWR1 at double strand breaks (DSBs) and its role in DNA repair.

4.2 Introduction

The nucleosome is the basic repeating unit of chromatin and consists of 146bp of DNA wrapped in superhelical turns around a histone octamer of two (H2A/H2B) heterodimers and an $(H3\text{-}H4)_2$ tetramer (Luger et al., 1997). Chromatin assembly is a stepwise process that begins when one tetramer of $(H3\text{-}H4)_2$ binds the central ~70 base pairs of DNA, followed by binding of two (H2A/H2B) dimers, each organizing approximately 40 base pairs of peripheral DNA (Luger and Richmond, 1998a). Despite its apparent stability and the high degree of chromatin compaction in the nucleus, chromatin is surprisingly dynamic (Luger, 2006). The histone-DNA interactions inside

the nucleus are altered in response to protein complexes that regulate gene expression, DNA replication, recombination and repair (Akey and Luger, 2003).

Substitution of one or more of the core histones with the corresponding histone variant has the potential to exert considerable influence on the structure and function of nucleosomes and chromatin (Jin et al., 2005). In contrast to canonical histones, variant histones are incorporated into chromatin independent of DNA replication. To date, histone variants for H2A, H3 and H1 have been characterized, and to a lesser extent, H2B variants (Bernstein and Hake, 2006). The histone H2A variant H2A.Z is found in all eukaryotes from *Saccharomyces cerevisiae* to humans (Redon et al., 2002).

A protein complex has been identified which can specifically exchange H2A with H2A.Z in yeast chromatin in a replication-independent manner (Kobor et al., 2004; Krogan et al., 2003; Mizuguchi et al., 2004). SWR1 is the first characterized ATP-dependent chromatin-remodeling complex that catalyzes incorporation of H2A.Z into nucleosomes. Phenotypic studies of the *htz1*Δ and *swr1*Δ mutants revealed a similar phenotypic sensitivity to DNA damaging UV radiation and methyl methanesulfonate (MMS), as well as caffeine, indicating a role for the two proteins in DNA damage repair (Kobor et al., 2004; Mizuguchi et al., 2004).

Cells constantly battle harmful DNA lesions; some are potentially lethal. DNA DSBs are the most deleterious to cell viability. The inability to repair these lesions can result in mutations, cancer, cell death or chromosomal mutations (Finkel and Holbrook, 2000; Peltomaki, 2001). Two evolutionarily conserved pathways have been described for the repair of DSB: homologous recombination (HR) and non-homologous end joining

(NHEJ). After DNA damage, yeast H2A (the histone variant H2A.X in mammals) is phosphorylated on Serine 129 within ~50 kb of a single double strand break (DSB) immediately by the ATM and ATR checkpoint kinases (Tel1 and Mec1) (Burma et al., 2001; Downs et al., 2000; Redon et al., 2003). Intriguingly, the SWR1 complex is recruited to DSBs, but the occupancy of H2A.Z surrounding an HO-endonuclease induced cut site decreases for up to four hours (van Attikum et al., 2007). Therefore, the SWR1 complex doesn't function to exchange γ-H2AX for H2A.Z at DSBs.

Previous experiments performed on the non-essential subunits of the SWR1 complex established the N-terminal 1-281 amino acids of Swc2 as a binding module for H2A.Z (Wu et al., 2005). Partial SWR1 complexes purified from Δ*swc2* strains had severely reduced histone exchange activity, as indicated by little transfer of H2A.Z-Flag to immobilized nucleosomes, and showed an approximately two-fold decrease in nucleosome binding compared to wild-type SWR1 complexes (Wu et al., 2005). Our own studies (Chapter 3) revealed that $Swc2_{1\text{-}179}$ does not exhibit preferential binding to histone dimers comprised of H2A.Z/H2B. Rather, it binds with comparatively low affinity to wild-type and histone variant dimers.

In this study, we demonstrate that $Swc2_{1\text{-}179}$ does not bind nucleosomes nor can it remove the histone dimer H2A/H2B from preformed nucleosomes. However, we discovered that $Swc2_{1\text{-}179}$ forms defined complexes with free DNA. Importantly, our data suggests that $Swc2_{1\text{-}179}$ binds DNA structures that are characteristic of sites of DNA repair. These include 3-way and 4-way junction DNA structures, but not DNA nicks or overhangs (Khuu et al., 2006; Walker et al., 2001). In addition, we have evidence that

the DNA binding ability of $Swc2_{1-179}$ is relevant *in vivo*. We show that a *SWC2* gene deletion is sensitive to DNA damaging agent methyl methanesulfonate.

4.3 Materials and Methods

4.3.1 Expression and purification of proteins

$Swc2_{1-179}$ and Chz1 were purified as follows. The plasmids were transformed into Bl21 (43) competent cells by electroporation or heat shock. The cells were then grown in 2XYT media and induced at an OD_{600} of 0.6 with 0.7mM IPTG for 5 hours. Lysates were purified using batch Ni resins, gel-filtration chromatography on Superdex S200 16/60, and ion exchange on MonoQ HR5/5. To prepare the fluorescently labeled protein, purified $Swc2_{1-179}$ S4C mutant was labeled with Alexa488. Nap1 was expressed and purified as previously described by (Park and Luger, 2006b). Vps75 was expressed and purified as previously described by (Park et al., 2008b). The molar concentrations of Vps75 and Nap1 reported in this paper are based on the dimeric nature of the proteins. We tested the purity of individual proteins on 15% SDS-PAGE and stained with Coomassie brilliant blue. Recombinant histones (yeast and *Xenopus*) H2A, H2B, H3 and H4 were generated in bacteria as described and refolded to form histone octamer (Dyer et al., 2004).

4.3.2 Preparation of DNA, nucleosomes, and nucleosomal arrays

The 146 bp fragment from a 5S rRNA gene (Simpson and Stafford, 1983) and the 146 and 207 bp fragments of the 601 sequence (Lowary and Widom, 1998) were purified as described (Dyer et al., 2004). The 208-12 5S rDNA sequence used to prepare nucleosomal arrays was purified following published procedures (Schwarz and Hansen,

1994). The oligonucleotides for the 3-way junction were ordered from Integrated DNA technologies and the sequences are as follows: 21 bp (5' GTT TTT AGT TTA TTG GGC GCG 3') and for the 35 bp (5' CGC GCC CAG CTT TCC CAG CTA ATA AAC TAA AAA C 3') (Walker et al., 2001). The oligonucleotides were reconstituted to a final concentration of 500μM in TE; equimolar amounts of each primer were then incubated together at 95°C for 10 minutes. The DNA was annealed by slowly equilibrating to room temperature overnight. To ensure complex formation, the junction DNA was analyzed by 5% native PAGE and compared to single stranded primers. Further analysis using size-exclusion chromatography multi-angle light scattering confirmed a homogenous complex of 16.3kDA, the expected size for complexed 3-way junction DNA (Supplementary Figure 4.1). The oligonucleotide sequences used for the asymmetric 4-way junction are as follows: A (5' TAGGGGCCGA 3'), B (5' CCGAGTCCTA 3'), C (5' TCGGCCTGAG 3'), and D (5' CTCAACTCGG 3') (Khuu and Ho, 2009). The 4-way junction DNA was annealed using the same procedures described for the 3-way junction DNA. Nucleosomes were reconstituted by dialysis against decreasing salt concentrations as described in (Dyer et al., 2004) and analyzed by native PAGE. Nucleosomal arrays were reconstituted onto 208-12 5S rDNA with canonical histones as described in (Hansen et al., 1991).

4.3.3 Multi-Angle Light Scattering

Samples of $Swc2_{1-179}$ (2mg/ml) or 3-way junction DNA (2.5mg/ml) in 20mM Tris pH7.5, 300mM NaCl and 5% glycerol were loaded onto an AKTA purified HPLC system. Samples were run over a SHODEX-803 size-exclusion column at 0.3ml/min, prior to flowing into a Wyatt Dawn Heleos II multi-angle light scattering instrument,

followed by a rEX refractive index detector (Wyatt Technologies). To determine the concentrations of the $Swc2_{1-179}$, we used a differential index of diffraction (dn/dc) of 0.185 and (dn/dc) of 0.175 for DNA.

4.3.4 Gel-shift binding assays with nucleosomes and nucleosome arrays

5 μM nucleosomes, reconstituted as described in (Dyer et al., 2004), were mixed with increasing molar ratios of $Swc2_{1-179}$ or Chz1, and incubated at 4° C for 12 hours in binding buffer (10mM Tris pH7.5, 100mM NaCl and 1mM EDTA). Nucleosome dissociation was analyzed by native PAGE on 5% polyacrylamide gels (acrylamide : bis-acrylamide 59:1) in 0.2 X TBE. The samples were run on a 5% native gel at 150V for 60 minutes. The gel was ethidium bromide-stained, followed by staining with Coomassie blue. When fluorescently labeled $Swc2_{1-179}$ S4C *488 was used, the gel was first photographed without staining to view fluorescence, followed by staining with ethidium bromide. Arrays were reconstituted on 208-12 rDNA with wild-type *Xenopus* octamer. The samples were run on a 0.6% agarose gel at 60V for 120 minutes in 1X TAE buffer. The experiment was repeated multiple times in binding buffers containing TE with 10, 20, 50 or 100mM NaCl.

4.3.5 DNA electrophoretic mobility shift assay

The protein and DNA complexes were analyzed by electrophoretic mobility shift assays (EMSAs) under native conditions. EMSAs were performed by incubating Chz1 or $Swc2_{1-179}$ in a 10 μl reaction with the indicated concentrations of DNA at 4°C for 12 hours (in binding buffer 10 mM Tris, pH 7.5, 100 mM NaCl, 1 mM EDTA and 1 mM DTT). The samples were loaded onto an acrylamide, 0.2× Tris-borate with EDTA (TBE)

gel, electrophoresed for 60 min at 150 V and stained with ethidium bromide, followed by Coomassie brilliant blue. The 4-way junction samples were loaded onto an acrylamide, 0.2x Tris-borate with $CaCl_2$ gel in binding buffer (25mM Tris pH 8.0, 5mM $CaCl_2$, and 200mM NaCl). The 10% native acrylamide gel was run at 60V for 90 minutes prior to staining with ethidium bromide.

4.3.6 Yeast strains, plasmids and media

Yeast strain BY4741 (MATa his3Δ1 leu2Δ0 met15Δ0 ura3Δ0) was used for all investigations. Deletion mutants in the BY4741 background were purchased from Open Biosystems. BY4741 cells were grown for 48 hours on rich media containing 2% (w/v) glucose. For spot assays, cells were grown in liquid YPD medium (1% yeast extract, 1% bactopeptone and 2% glucose) at 30 °C and then diluted to an absorbance at 600 nm (A_{600}) of 0.1. We made ten-fold serial dilutions of each culture and spotted them onto plates as indicated in Figure 4.7. Cells were allowed to grow for 48−72 h at 30 °C or 38 °C. The methyl methanesulfonate (MMS) plate was made within 24 hours of use. Plates for DNA damage assays contained YPD with or without 0.025% MMS or 0.2 M hydroxyurea (HU) and were photographed after 3 days of growth at 30 °C.

4.4 Results

4.4.1 $Swc2_{1\text{-}179}$ does not bind the nucleosome, but it does bind free DNA.

To investigate whether $Swc2_{1\text{-}179}$ was capable of partially or completely disassembling nucleosomes, as has been observed with other histone chaperones, we used native gel electrophoresis. Nucleosomes reconstituted onto 146 base pairs of 5S rDNA sequence were incubated with increasing amounts of $Swc2_{1\text{-}179}$ (1 - 10 fold molar

excess). The intensity and migration of the nucleosome band remained unchanged throughout the entire titration series (Figure 4.1A). Thus, $Swc2_{1-179}$ did not bind the nucleosome, nor did it remove histone dimers from the preformed NCP.

The experiment was repeated with nucleosomes containing a slight excess of 146 bp 5S DNA (1:1.3 ratio of octamer to DNA). Notably, the free DNA shifted upwards as $Swc2_{1-179}$ concentrations increased (Figure 4.1B top panel lanes 5-9), yet the mobility of the NCP was unaffected. A 5:1 mixture of $Swc2_{1-179}$ and DNA (in the absence of nucleosome) was run on the gel as a control (lane 10) and this band also experienced upwards mobility when compared to the free DNA (lane 2). This indicated that $Swc2_{1-179}$ was forming a complex with 146 bp DNA (denoted S-D on the gel). The results were confirmed when Coomassie blue staining revealed that $Swc2_{1-179}$ mobility decreased as it formed a complex with DNA (Figure 4.1B lower panel).

This represented an intriguing and unexpected finding because the isoelectric point of $Swc2_{1-179}$ is 4.2 and thus the protein is not expected to bind DNA. To gain insight into the DNA sequence and length requirements for this interaction we tested various other lengths and sequences of DNA using qualitative gel shifts (Table 4.1). Three different lengths of DNA (30, 84, or 146 bp) were incubated with increasing molar ratios of $Swc2_{1-179}$ (1-5 fold molar excess). As indicated in Figure 4.2 panel A, $Swc2_{1-179}$ was unable to shift the 30 bp DNA; the intensity of the DNA band remained constant and the mobility was unaffected. Coomassie blue staining did reveal the presence of free $Swc2_{1-179}$ in the gel (data not shown). However, both the 84 and 146 bp DNA exhibited a clear supershift when incubated with $Swc2_{1-179}$ (Figure 4.2 panels B and C, lanes 5-10).

A comprehensive list of the DNAs assayed for $Swc2_{1-179}$ binding can be seen in Table 4.1.

Chz1 (Chaperone for H2A.Z/H2B), like $Swc2_{1-179}$, is a highly acidic, intrinsically disordered protein. In previous studies (see Chapter 3) the two proteins have been shown to bind histones with similar affinities. We wondered if perhaps DNA binding was a general property of negatively charged, intrinsically disordered proteins. To test this idea, we analyzed the ability of Chz1 to bind 5S 146 bp DNA. Our results confirm that Chz1 is unable to bind and form a complex with 146 bp DNA when subjected to the same conditions that result in $Swc2_{1-179}$ being supershifted (Supplementary Figure 4.2 A).

Two other histone chaperones, Vps75 and Nap1, were assayed for DNA binding using EMSAs. Both chaperones are highly acidic, however, they have clearly defined tertiary structure in the absence of histones (Park and Luger, 2006b; Park et al., 2008b). Our results indicate that neither histone chaperone is capable of binding to 5S 146 bp DNA (Supplementary Figure 4.2 C, D). Our results suggest that $Swc2_{1-179}$ forms a single complex with DNA; this is a unique property of $Swc2_{1-179}$.

4.4.2 $Swc2_{1-179}$ doesn't bind nucleosomes with linker DNA or nucleosome arrays

We had established a length requirement for $Swc2_{1-179}$ binding to DNA. Using native gel electrophoresis we discovered that $Swc2_{1-179}$ could bind to 53 bp of DNA, but not 40 bp (Table 4.1). To investigate whether $Swc2_{1-179}$ nucleosome binding requires linker DNA, we assayed $Swc2_{1-179}$ binding to nucleosomes that are centrally positioned on 207 base pairs of 601 DNA. These nucleosomes contain 30bp of excess DNA on each end protruding from the nucleosome (60 bp total).

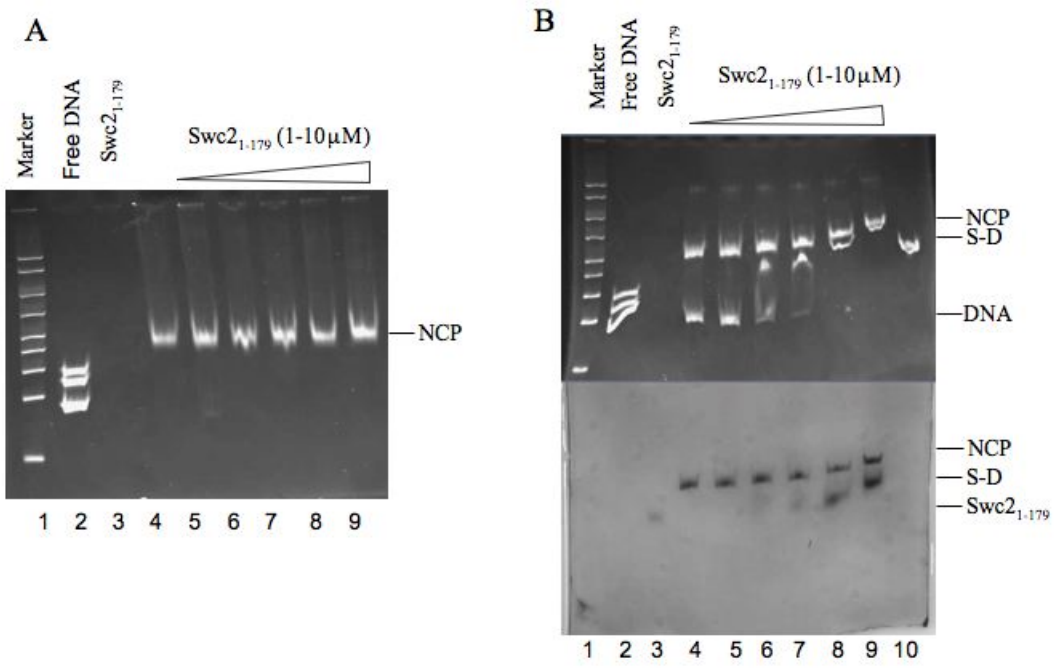

Figure 4.1: $Swc2_{1-179}$ binds free DNA, but not nucleosomes.
(A) 5μM nucleosomes (NCP) reconstituted with canonical histones were incubated with increasing molar amounts of $Swc2_{1-179}$ (*lane* 1, marker, *lane* 2 146bp DNA, *lane* 3 $Swc2_{1-179}$, *lanes* 4-9, 0-, 1-, 2-, 4-, 6- and 10-fold molar excess of $Swc2_{1-179}$ to NCP). Samples were incubated at 4°C for 12 hours and analyzed by 5% native PAGE. The gel was stained in ethidium bromide. The NCP is indicated on the gel. **(B)** 5μM nucleosomes reconstituted with excess DNA (1:1.3 ratio of octamer:DNA) were incubated with increasing molar amounts of $Swc2_{1-179}$ (*lane* 1 marker, *lane* 2 146bp DNA, *lane* 3 $Swc2_{1-179}$, *lanes* 4-9, 0-, 1- , 2-, 4-, 6- and 10-fold molar ratio of $Swc2_{1-179}$ to NCP and *lane* 10, 1:5 ratio of DNA:$Swc2_{1-179}$). Samples were incubated at 4°C for 12 hours and then analyzed by 5% native PAGE. The gel was first stained with ethidium bromide (top panel), then Coomassie blue (lower panel). The free DNA shifts upwards as the concentration of $Swc2_{1-179}$ increases and forms a complex (denoted S-D) as seen in the top panel. Furthermore, $Swc2_{1-179}$ shifts upward when complexed with DNA as indicated on the Coomassie stained gel (lower panel).

Table 4.1: $Swc2_{1-179}$ binding to various DNA constructs

DNA	Binding to $Swc2_{1-179}$
146 bp α-satellite	Yes
146 bp 5S	Yes
146 bp 601	Yes
84 bp 5S	Yes
80 bp 7S	Yes
64 bp SELEX	Yes
53 bp	Yes
3-way junction (28/42)	Yes
3-way junction (21/35)	Yes
3-way junction (14/28)	Yes
4-way junction	Yes
30 bp	No
40 bp	No
30/41 3' overhang	No
Nicked 22 bp	No
Looped 33 bp	No
Poly dAdT 31 bp	No
Poly dGdC 31 bp	No
48 bp single stranded	No

The constructs were assayed for $Swc2_{1-179}$ binding using electrophoretic mobility gel shift assays, as described in Methods.

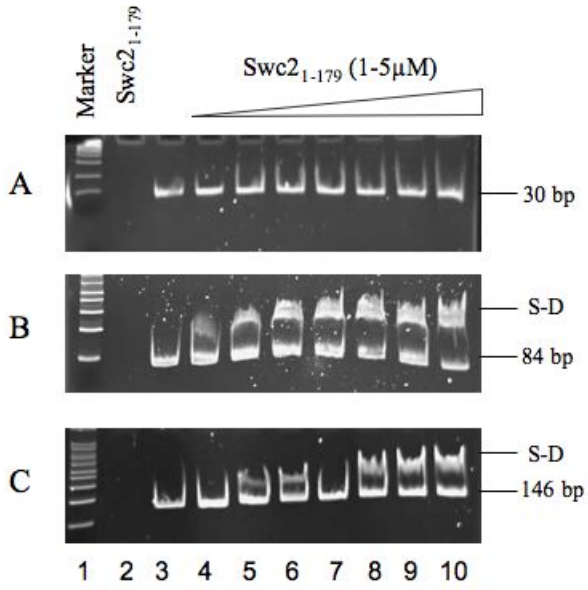

Figure 4.2: Swc2$_{1-179}$ binds DNA, but has a length requirement.
(A) 1μM 30 bp blunt dsDNA was incubated with increasing molar amounts of Swc2$_{1-179}$ (*lane* 1 marker, *lane* 2, Swc2$_{1-179}$, *lane* 3, no Swc2$_{1-179}$, *lanes* 4-10, 1-, 2-, 3-, 3.5-, 4-, 4.5- and 5-fold molar ratio of Swc2$_{1-179}$ to DNA). Samples were incubated at 4°C for 12 hours and analyzed by 20% native PAGE. The gel was stained in ethidium bromide. The DNA did not shift, as indicated on the gel. **(B)** 5S 84 bp dsDNA was incubated with increasing molar amounts of Swc2$_{1-179}$ (*lane* 1 marker, *lane* 2, Swc2$_{1-179}$, *lane* 3, no Swc2$_{1-179}$, *lane*s 4-10, 1-, 2-, 3-, 3.5-, 4-, 4.5- and 5-fold molar ratio of Swc2$_{1-179}$ to DNA). Samples were incubated at 4°C for 12 hours and analyzed by 10% native PAGE. The Swc2$_{1-179}$-DNA complex is denoted as S-D on the gel. **(C)** 5S 146 bp dsDNA was incubated with increasing molar amounts of Swc2$_{1-179}$ (*lane* 1 marker, *lane* 2, Swc2$_{1-179}$, *lane* 3, no Swc2$_{1-179}$, *lane*s 4-10, 1-, 2-, 3-, 3.5-, 4-, 4.5- and 5-fold molar ratio of Swc2$_{1-179}$ to DNA). Samples were incubated at 4°C for 12 hours and analyzed by 10% native PAGE. Swc2$_{1-179}$ formed a complex with the DNA and is depicted as S-D on the gel.

5μM nucleosomes, reconstituted with 207 bp of 601 positioning sequence DNA (Lowary and Widom, 1998), were incubated with increasing molar ratios of fluorescently labeled $Swc2_{1-179}$. The unstained gel was first visualized by UV light for fluorescence, as depicted in Figure 4.3A. The fluorescently labeled $Swc2_{1-179}$ is the only band visible and its mobility does not change (lanes 2-7). In Figure 4.3B, the ethidium bromide-stained 5% native PAGE (from 4.3A) reveals that the mobility of the 207 nucleosomes also remains unchanged, even when incubated with a 10-fold molar excess of $Swc2_{1-179}$ (lane 7). This experiment was repeated using unlabeled Swc_{21-179} on a 1% native agarose gel. The results were the same (data not shown). We conclude that $Swc2_{1-179}$ does not bind nucleosomes even if they contain 2x30 base pairs of linker DNA.

To obtain qualitative information about the interaction of $Swc2_{1-179}$ with chromatin, we used native EMSAs. Tandem arrays of (N=12) 208 bp sequences from 5S rDNA were reconstituted with canonical histones. The nucleosome array (NA) was subsaturated and contained only 5-6 nucleosomes, leaving large stretches of accessible DNA for putative $Swc2_{1-179}$ binding. The mobility of the band corresponding to the NA does not shift with increasing molar ratios of $Swc2_{1-179}$ (Figure 4.4A, lanes 2-5) or Chz1 (Figure 4.4A, lanes 6-9). Conversely, full length MeCP2 (a known chromatin interaction partner) experienced a large mobility shift when interacting with nucleosomal arrays at low molar ratios (Figure 4.4A lane 10) (Ghosh et al., 2010).

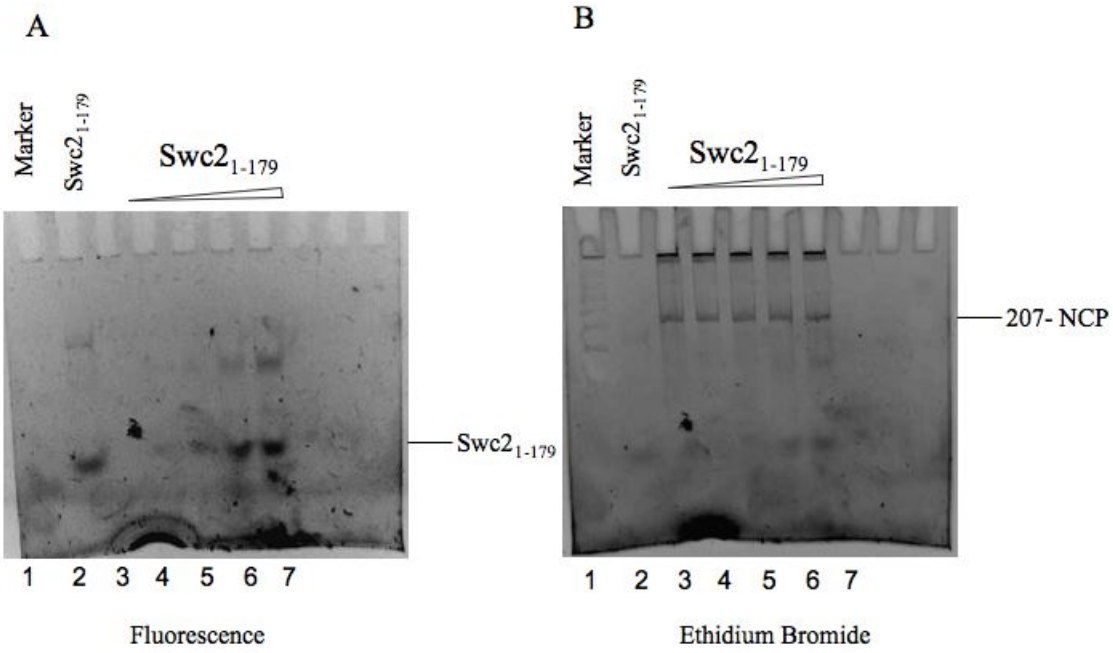

Figure 4.3: $Swc2_{1-179}$ does not bind nucleosomes with linker DNA.
(A) 5μM nucleosomes 601 DNA (NCP) reconstituted with canonical histones were incubated with increasing molar amounts of $Swc2_{1-179}$ S4C labeled with Alexa488 (*lane* 1, marker, *lane* 2 $Swc2_{1-179}$, *lanes* 3-7, 0-, 5-, 10-, 15-, 20-fold molar ratio of $Swc2_{1-179}$ to NCP). Samples were incubated at 4°C for 12 hours and analyzed by 5% native PAGE. The gel from was first photographed with the Biorad Gel Doc to view fluorescence. Alexa488 labeled $Swc2_{1-179}$ is marked on the gel. The mobility of $Swc2_{1-179}$ does not change when incubated with 207 bp nucleosomes. **(B)** The gel was stained in ethidium bromide. The NCP is indicated on the gel.

These experiments were repeated with more saturated nucleosome arrays (24S and 31S), varied binding buffer salt concentrations (10-100mM NaCl), different native agarose percentages (0.6% -1%) and with fluorescently labeled $Swc2_{1-179}$ (data not shown). None of these conditions resulted in a stable interaction of $Swc2_{1-179}$ with chromatin.

4.4.3 $Swc2_{1-179}$ binds three-way and four-way junction DNA

In nucleosome arrays, the nucleosomes are often positioned at the ends of the DNA, even if the arrays are subsaturated (Yodh et al., 2002). The inability of Swc_{1-179} to bind undersaturated nucleosome arrays implies that the ends of DNA might be necessary for complex formation. If $Swc2_{1-179}$ prefers to bind DNA ends, this could be evidence for a role in DNA damage recognition. To test this hypothesis, we constructed a model 3-way junction DNA (detailed in Methods, Supplementary Figure 4.1). This junction had previously been crystallized with the yeast DNA repair proteins ku70/ku80 (Walker et al., 2001).

Gel shift assays were utilized to investigate $Swc2_{1-179}$ binding to three-way junction DNA. The structural features of the three-way junction include: a 14 bp AT rich stem and a junction comprised of a 14 bp loop region and a 7 bp short G-rich stem (Figure 4.5A). We discovered that $Swc2_{1-179}$ is able to form a complex with three-way DNA (Figure 4.5B denoted S-D). Importantly, even at high molecular ratios of $Swc2_{1-179}$ to DNA, only one type of complex is formed as indicated by the presence of only one band on the ethidium bromide stained gel (Figure 4.5B left panel lanes 2,3). To better characterize $Swc2_{1-179}$ binding to the three-way junction, we designed additional DNA constructs and conducted gel shift assays.

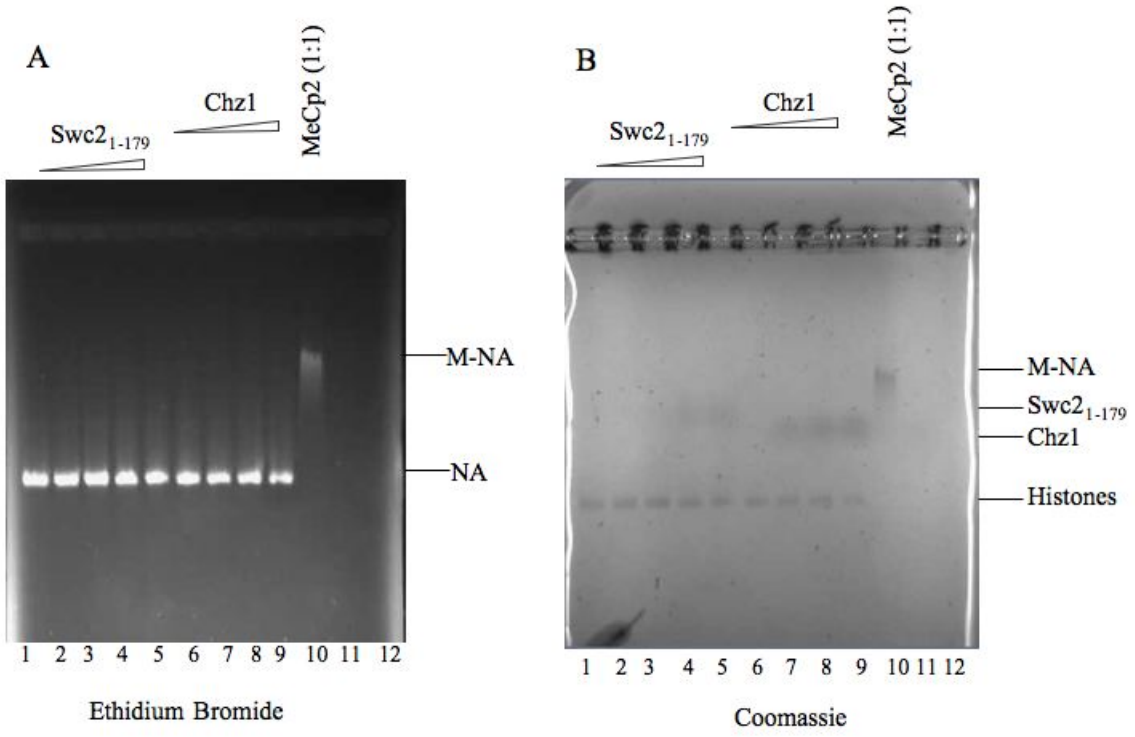

Figure 4.4: $Swc2_{1-179}$ does not bind nucleosome arrays.
(A) 1.6μM/repeat of 16.5S nucleosome arrays reconstituted with canonical histones were incubated with increasing molar amounts of $Swc2_{1-179}$ or Chz1 (*lane* 1, no $Swc2_{1-179}$ or Chz1, *lanes* 2-5, 1-, 5-, 10-, and 15- fold molar ratio of $Swc2_{1-179}$ to arrays, *lanes* 6-9, 1-, 5-, 10- and 15- fold molar ratio of Chz1 to array, *lane* 10, 1:1 ratio of MeCP2 to array, *lane* 11 Chz1, *lane* 12 $Swc2_{1-179}$). Samples were incubated at 4°C for 12 hours and analyzed on a 0.6% agarose gel stained with ethidium bromide. The nucleosome array is indicated on the gel as NA. Only MeCP2 shifted the arrays and the complex is labeled M-NA on the agarose gel. **(B)** The gel from A stained in Coomassie blue. $Swc2_{1-179}$ and Chz1 are indicated on the gel; both are incapable of binding the subsaturated arrays.

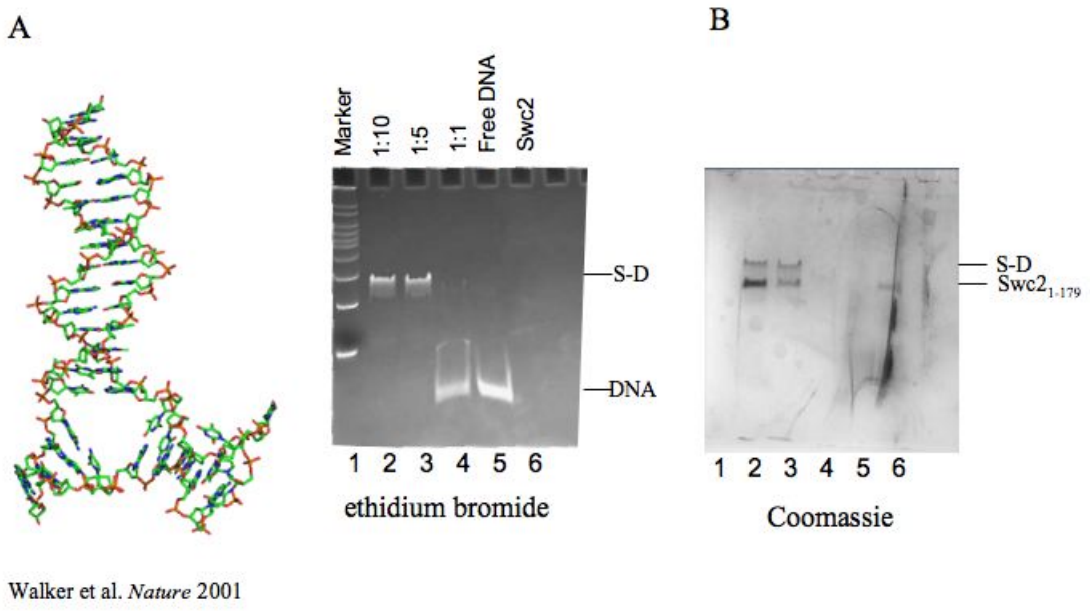

Figure 4.5: $Swc2_{1-179}$ binds three-way junction DNA.
(A) Crystal structure of the three-way junction DNA (from 1JEY) (Walker et al., 2001) used for EMSAs in B. **(B)** 5μM three-way junction DNA was incubated with increasing molar amounts of $Swc2_{1-179}$ (*lane* 1 marker, *lanes* 2-4, 10-, 5-, and 1- fold molar excess of $Swc2_{1-179}$ to DNA, *lane* 5 DNA, and *lane* 6 $Swc2_{1-179}$). Samples were incubated at 4°C for 2 hours and analyzed by 10% native PAGE. The gel was stained in ethidium bromide on the left and with Coomassie blue on the right. The $Swc2_{1-179}$-DNA complex is labeled S-D on the gels.

The first construct tested was the 14 bp AT rich stem of the junction DNA. We observed that $Swc2_{1\text{-}179}$ could not bind the AT rich stem, nor could it bind 31 base pair poly dAdT (data not shown). This is consistent with our data demonstrating a minimum of 40 bp of linear DNA. From this, we conclude that the stem is not the structural region necessary for $Swc2_{1\text{-}179}$ binding. The other structural feature of the 3-way junction is the DNA loop. Using EMSAs, we discerned that $Swc2_{1\text{-}179}$ is incapable of binding to 30 bp looped DNA. We then designed three-way junction DNA in which the stem region was reduced by 1/2 the length (while maintaining the junction comprised of a 14 bp loop region and a 7 bp short G-rich stem). $Swc2_{1\text{-}179}$ could bind shorter segments of DNA that contained the three-way junction.

Four-way (Holliday) junction DNA is a structural intermediate in homologous recombination. Homologous recombination is involved in a variety of cellular processes including repair of DNA lesions (Smith, 2004). To investigate $Swc2_{1\text{-}179}$ interactions with 4-way junction DNA, we utilized an asymmetric junction with an anti-parallel stacked X-form (Khuu and Ho, 2009) (Figure 4.6A,B). $Swc2_{1\text{-}179}$ is able to form a complex with 4-way DNA (Figure 4.6C) using native gel electrophoresis. The four-way junction DNA exhibits a clear decrease in mobility when incubated with increasing molar ratios of $Swc2_{1\text{-}179}$ (Figure 4.6C lanes 3-5). We tested other constructs of dsDNA that mimic sites of DNA damage in the cell, including DNA containing nicks as well as a 3' overhang (Table 4.1). $Swc2_{1\text{-}179}$ is incapable of binding to these DNA constructs (data not shown). Thus, we have established a clear preference for $Swc2_{1\text{-}179}$ for linear, blunt ended DNA fragments greater than 40 bp and for three- and four-way junction DNA.

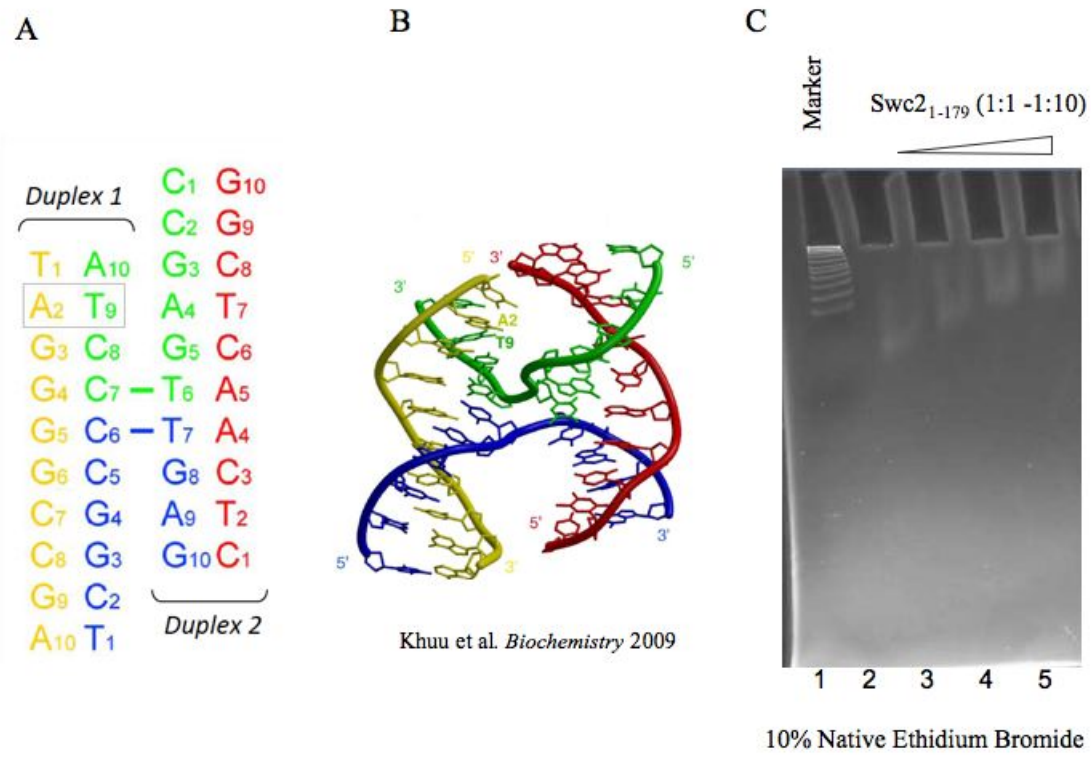

Figure 4.6: Swc2$_{1-179}$ binds four-way junction DNA.
(A) Sequence assignments of the asymmetric Holliday junction. **(B)** Crystal structure of the 4-way junction DNA (Khuu and Ho, 2009) used for EMSAs in C. **(C)** 5μM 4-way junction DNA was incubated with increasing molar amounts of Swc2$_{1-179}$ (*lane* 1 marker, *lanes* 2-5, 0-, 1-, 5-, and 10- fold molar excess of Swc2$_{1-179}$ to DNA). Samples were incubated at 4°C for 12 hours and analyzed by 10% native PAGE. The gel was stained in ethidium bromide.

4.4.4 A *SWC2* gene deletion is sensitive to DNA damaging agents

To establish an *in vivo* role for Swc2 in DNA repair, we analyzed the phenotypes associated with a *SWC2* gene deletion in yeast *S. cerevisiae*. A yeast strain in which the *swc2* open reading frame (ORF) was replaced with KanMx was spotted onto several different types of yeast media in order to determine the phenotypes associated with a*swc2*Δ mutant.

We discovered that the *swc2*Δ mutant strain displayed sensitivity to hydroxyurea (HU 200mM), methyl methanesulfonate (MMS 0.025%) and caffeine (8mM); additionally, the deletion strain displayed a conditional phenotype (high temperature on YPD at 38°C). Sensitivity to high temperatures functionally implies a general protein defect and quite often it is indicative of genes that are essential for viability (Hampsey, 1997). HU and MMS sensitivity implies that the *swc2*Δ mutant strain is defective in induced DNA-damage repair and DNA replication (Hampsey, 1997). Caffeine impacts many cellular responses and metabolic activities (Hampsey, 1997). Importantly, our results shed new light on a broad role for Swc2 in DNA damage repair and genotoxic stress.

4.5. Discussion

SWC2 has been shown to play an important role in H2A.Z deposition *in vivo* and natively purified SWR1 complexes lacking Swc2 show reduced histone exchange and nucleosome binding (Wu et al., 2005). $Swc2_{1\text{-}179}$ was shown to bind histones H2A/H2B and H2A.Z/H2B *in vitro* (Chapter 3, section 3), but it was unknown if this fragment could

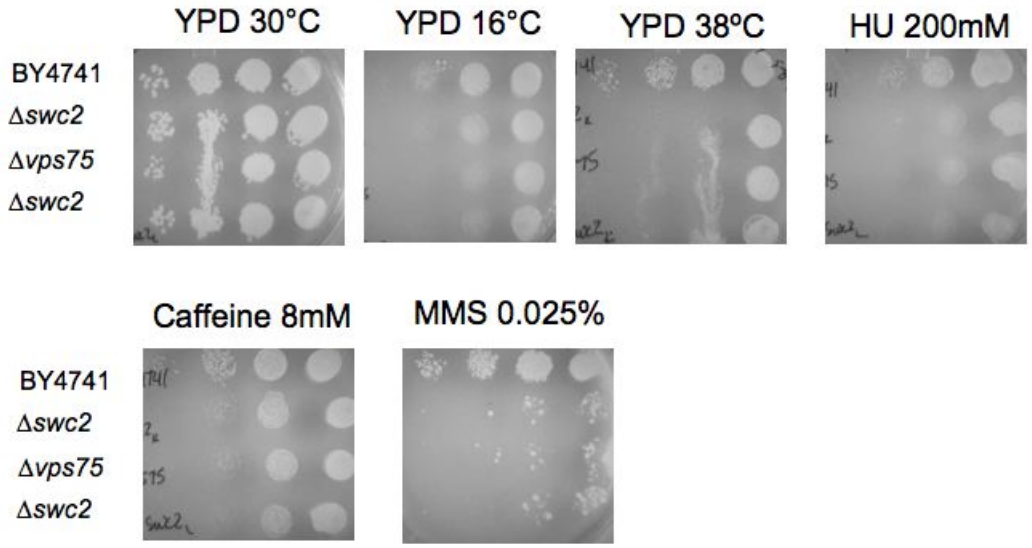

Figure 4.7: Swc2$_{1-179}$ has a DNA damage repair phenotype.
The three strains used in this comparison include BY4741 (wild-type), *swc2Δ,* and *vps75Δ*. For phenotypic studies, 10-fold serial dilutions of strains were applied as spots to plates containing rich medium containing either glucose (YPD), hydroxyurea (200mM), caffeine (8mM) or MMS (0.025%) and incubated at 30°C or 38°C (as indicated). The YPD plate incubated at 30°C was the control and all the strains had the same growth pattern as seen on the plate. On the MMS, HU and caffeine plates, as well as the YPD plate incubated at 38°C, the *swc2Δ* and *vps75Δ* strains had severely reduced growth.

bind nucleosomes or remove histone dimers for exchange, as has been observed for Nap1 (Park et al., 2005). Using EMSAs we show that $Swc2_{1-179}$ does not bind nucleosomes, nor can it remove histone dimers from preformed NCPs. However, we did discover that $Swc2_{1-179}$ is capable of binding free DNA. This is an unexpected property for an acidic, histone-associated protein and prompted further investigations.

Using gel shifts we discovered that Swc_{1-179} binds many different sequences of DNA, but it does have a clear length requirement (Table 4.1). Our results reveal that $Swc2_{1-179}$ does not bind linear dsDNA that is less than 40 bp. This is a surprisingly large DNA fragment for a relatively small protein. Why would this selective binding exist? Perhaps $Swc2_{1-179}$ binds longer DNA because it exhibits a curvature not found in shorter sequences (or conversely perhaps longer sequences are more amenable to bending upon interactions with Swc_{21-179}). We assayed both three- and four-way junction DNA for $Swc2_{1-179}$ binding. These structures have loops, bends, and crossed DNA. Although the junctions were assembled with short pieces of DNA (10 bp for the 4-way), $Swc2_{1-179}$ was able to interact with them. From these studies, we believe that $Swc2_{1-179}$ may preferentially interact with junction DNA. However, a careful analysis of the binding affinities is required to resolve the issue of nucleic acid preference.

Initially, we theorized that perhaps the role of Swc2 was not in histone variant recognition or binding, but rather in competing the free DNA from the nucleosome. This would allow the rest of the SWR1 complex better access for histone exchange and removal. One could broadly imagine the DNA at the entry and exit points of the nucleosome resembling the four-way junction. Our results indicated that $Swc2_{1-179}$

requires at least 40 bp of linear DNA for binding. However, we found that $Swc2_{1-179}$ was unable to bind 207 bp nucleosomes or subsaturated nucleosome arrays that contain at least 200 free base pairs flanked by nucleosomes. If the two ends of the 207 bp nucleosomal DNA existed in an open, uncrossed conformation, then only 30 bp of free DNA would exist for putative $Swc2_{1-179}$ binding, which our data indicates is not long enough. However, this wouldn't explain why $Swc2_{1-179}$ failed to bind NAs. It is known however, that nucleosomes first form on the ends of DNA (Yodh et al., 2002). This may indicate that $Swc2_{1-179}$ prefers free DNA ends.

Our in vitro binding studies revealed that $Swc2_{1-179}$ could bind to intermediates found during DNA-damage repair. To establish an *in vivo* role for Swc2 in DNA repair, we analyzed the phenotypes associated with a *SWC2* gene deletion in yeast *S. Cerevisiae*. We discovered that *swc2Δ* displayed sensitivity to HU, MMS, caffeine and conditional high temperatures. These phenotypes are broadly associated with a role in DNA-damage repair and resistance to genotoxic stress.

Intriguingly, the SWR1 complex is recruited to DSBs, but the occupancy of H2A.Z surrounding an HO-endonuclease induced cut site decreases for up to four hours (van Attikum et al., 2007). Therefore, the SWR1 complex association at DSBs doesn't function to exchange γ-H2AX for H2A.Z, nor does it function to remove γ-H2AX or histone core proteins (van Attikum et al., 2007). This means that at DSBs, the SWR1 complex has a novel, yet undefined function. Interestingly, it was reported that a *SWR1* gene deletion negatively affected the binding of yKu80 (van Attikum et al., 2007). The Ku heterodimer comprising yKu70 and yKu80 is involved in telomere maintenance and

DNA repair by the pathway of non-homologous end joining. The crystal structure of yKu70/Ku80 bound to DNA (Walker et al., 2001) utilized the same 3-way junction we did for our $Swc2_{1-179}$ binding assays. This could provide a clue as to why the SWR1 complex is found at cites of DSBs where it serves a function unrelated to H2A.Z incorporation.

4.6 Acknowledgements

Wayne Lilyestrom was very supportive and provided the three-way and four-way junction used in the gel shift assays. Mary Robinson touted the ease with which we could take this project *in vivo* and provided great encouragement. We thank Alison White and Pamela Dyer for help with DNA and protein preparation, and Teri McLain from the W.M. Keck Protein Expression and Purification facility for purified histones. Troy Sorenson provided the nucleosome arrays used in this study. This work was supported by a pre-doctoral grant from the American Heart Association.

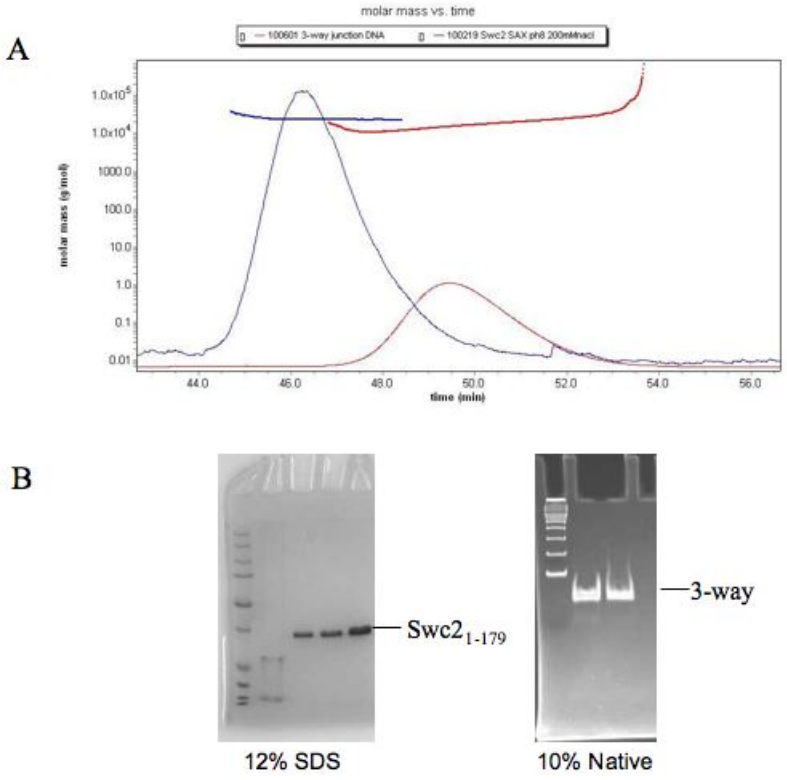

Supplementary Figure 4.1: Verification of 3-way DNA complex formation.
(A) Chromatograph illustrating the molar mass (g/mol) versus the elution time (min) for $Swc2_{1-179}$ and the 3-way junction DNA. Swc2 $_{1-179}$ (2 mg/ml) was analyzed using size-exclusion chromatography in line with multi-angle light scattering (SEC-MALS). The elution profile can be seen in blue and the molecular mass is represented as a line across the peak (~22kDa). The molecular mass is consistent across the peak. The 3-way junction DNA (2 mg/ml) eluted later than $Swc2_{1-179}$ and is represented by the red line. The molar mass of the 3-way junction is ~16kDa, which is the expected size for the DNA. **(B)** 10% native gel depicting the 3-way junction DNA and a 12%SDS-PAGE gel which shows the purity of $Swc2_{1-179}$ before analysis by SEC-MALS.

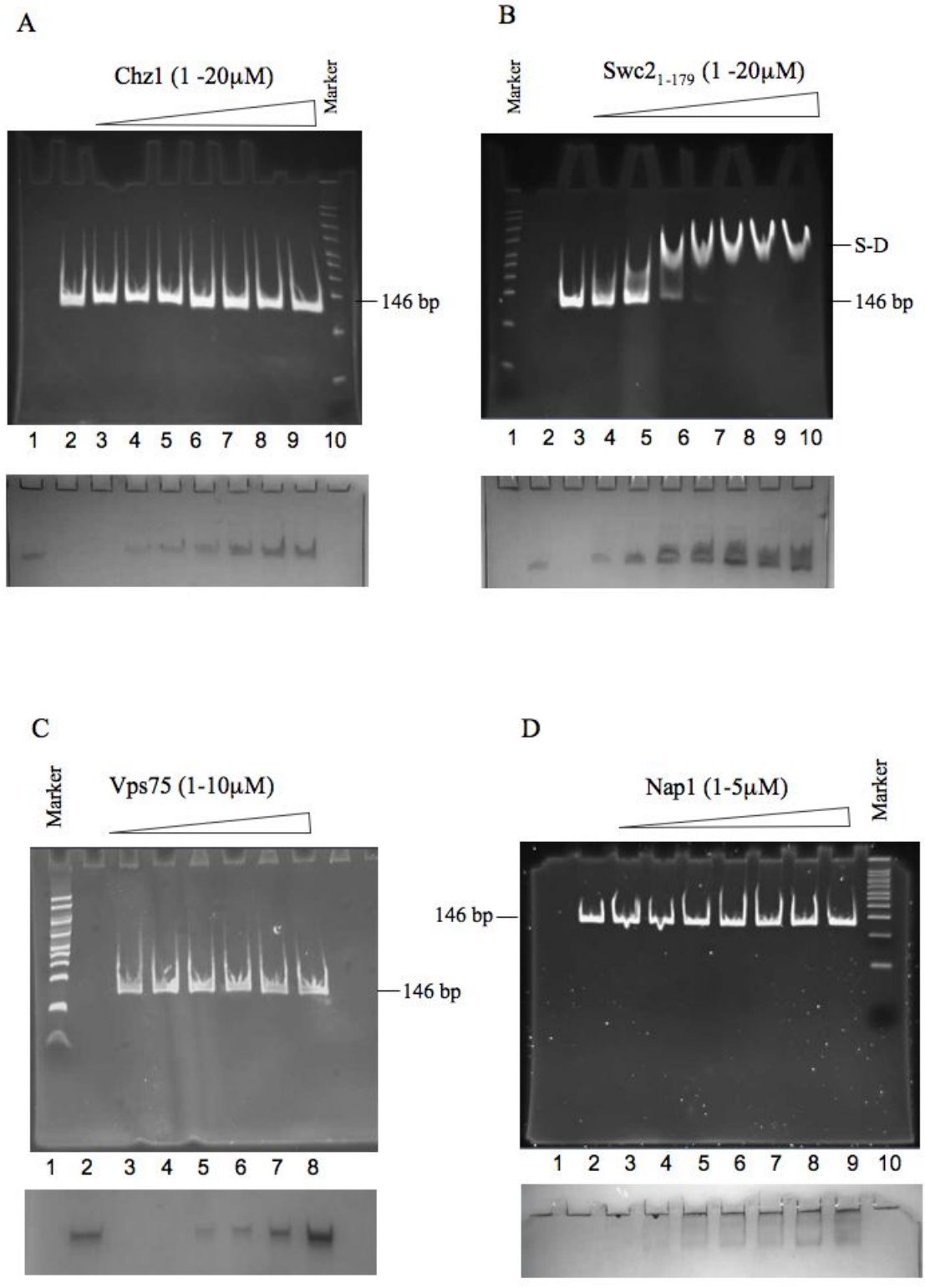
A
Chz1 (1 -20μM)
Marker
146 bp
1 2 3 4 5 6 7 8 9 10
B
Marker
Swc2$_{1-179}$ (1 -20μM)
S-D
146 bp
1 2 3 4 5 6 7 8 9 10
C
Marker
Vps75 (1-10μM)
146 bp
1 2 3 4 5 6 7 8
D
Nap1 (1-5μM)
Marker
146 bp
1 2 3 4 5 6 7 8 9 10

Supplementary Figure 4.2: Swc2$_{1-179}$ binds DNA, but Chz1, Vps75, and Nap1 do not. **(A)** 1μM α-sat 146bp dsDNA was incubated with increasing molar amounts of Swc2$_{1-179}$ (*lane* 1 marker, *lane* 2 Swc2$_{1-179}$ **,** *lane* 3 no Swc2$_{1-179}$, *lanes* 4-10, 1-, 2-, 4-, 8-, 10-, 16- and 20-fold molar ratio of Swc2$_{1-179}$ to DNA). Samples were incubated at 4°C for 2 hours and analyzed by 10% native PAGE. The gel was stained in ethidium bromide. The Swc2-DNA complex is denoted as (S-D) on the gel. **(B)** 1μM α-sat 146bp dsDNA was incubated with increasing molar amounts of Chz1 (*lane* 1 Chz1**,** *lanes* 2-9, 0-, 1-, 2-, 4-, 8-, 10-, 16- and 20-fold molar ratio of Chz1 to DNA, *lane* 10 marker). Samples were incubated at 4°C for 2 hours and analyzed by 10% native PAGE. The gel was stained in ethidium bromide. The DNA did not shift, as indicated on the gel. **(C)** 1μM α-sat 146bp dsDNA was incubated with increasing molar amounts of Vps75 (*lane* 1 marker, *lane* 2 Vps75**,** *lane* 3 no Vps75, *lanes* 4-8, 0.5-, 1-, 2-, 4-, and 10-fold molar ratio of Vps75 to DNA). The DNA did not shift, as indicated on the 10% native PAGE gel. **(D)** 1μM α-sat 146bp dsDNA was incubated with increasing molar amounts of Nap1 (*lane* 1 marker, *lane* 1 Nap1**,** *lanes* 2-9, 0-, 1-, 2-, 3-, 3.5-, 4-, 4.5 and 5- fold molar ratio of Nap1 to DNA, *lane* 10 Marker). The DNA did not shift, as indicated on the 10% native PAGE gel.

Chapter V

Summary and Future Directions

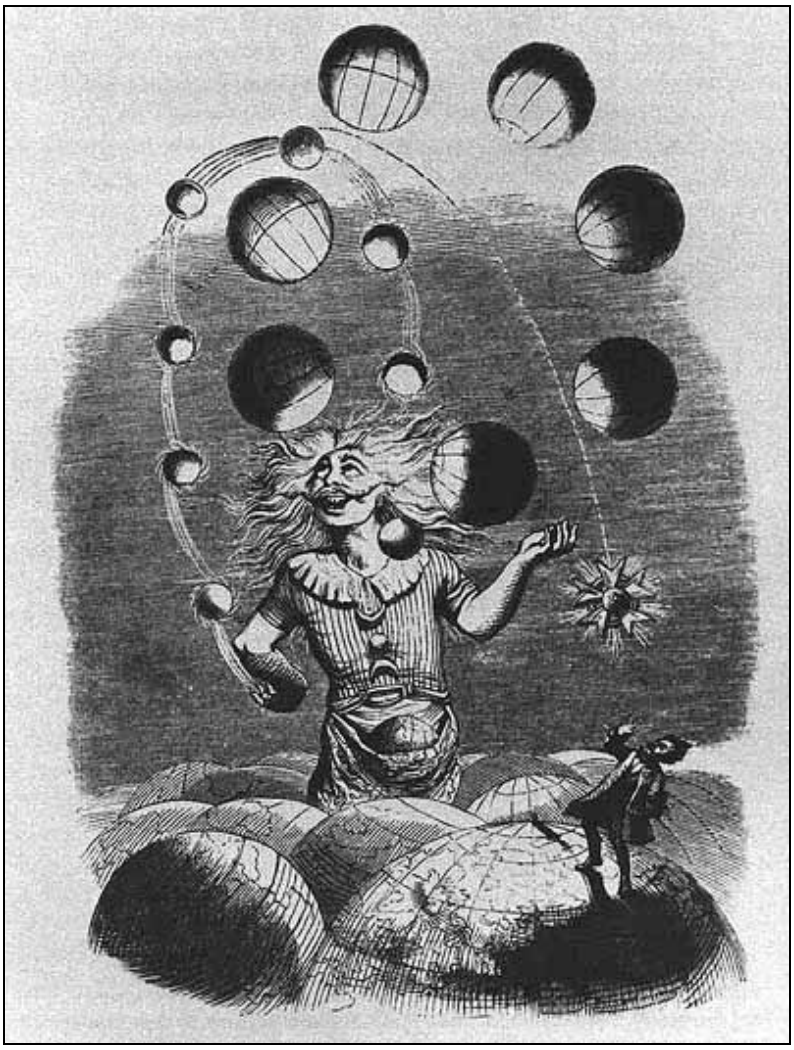

(J.J Grandville's Another World 1844)

The primary objective of my thesis work was to study histone chaperones Vps75, Nap1, Chz1, and $Swc2_{1-179}$. Using yeast genetics, biophysics, structural, and fluorescence studies we probed the structural and functional aspects of three yeast histone chaperones. The primary conclusion that can be drawn from this dissertation is that two structurally similar chaperones can possess different and unique functionalities. Nap1 and Vps75 are structural homologs and both bind histones and Rtt109 (Park and Luger, 2006). However, we found functional differences *in vivo* and *in vitro*. In the case of Vps75, we determined that its unique functions could be attributed to the C-terminal acidic tail. Chz1 and $Swc2_{1-179}$ are both intrinsically disordered proteins and they both bind H2A.Z/H2B *in vivo*. However, we discovered a functional difference between these very similar proteins. $Swc2_{1-179}$ has the ability to bind dsDNA *in vitro*, whereas Chz1 does not. We also conclude that histone chaperones seem to bind non-discriminately to histones (regardless of tertiary structure). It is becoming increasingly clear that *in vitro*, under physiological conditions, histone chaperones and histone-associated proteins fail to possess histone specificity, variant or otherwise (Andrews et al., 2008; Park et al., 2008).

In Chapter II, published in its present form in 2008, we studied two structurally similar histone chaperones Vps75 and Nap1. Here we describe the crystal structure of *Saccharomyces cerevisiae* Vps75 and compare its structural and functional properties to those of *S. cerevisiae* Nap1. Both chaperones (the only two known Nap1 family members in yeast) bind histones with similarly high affinities, and both proteins stably interact with Rtt109; however, only Vps75 is capable of stimulating Rtt109 HAT activity. In addition, deletion of *VPS75* results in dramatic and diverse mutant phenotypes, in contrast to the

lack of effects observed for the deletion of *NAP1*. The flexible C-terminal domain of Vps75 is important for the *in vivo* functions of Vps75 and modulates Rtt109 activity *in vitro*. Together, our data demonstrate a remarkable specialization of Vps75 for the interaction with and stimulation of Rtt109.

The structurally unrelated histone chaperone Asf1 is also a pertinent player in Rtt109 HAT activity (Han et al., 2007; Tsubota et al., 2007). Asf1 was crystallized with an H3/H4 dimer; therefore the H3/H4 dimer is the assumed binding partner *in vivo* (English et al., 2006*)*. How do Rtt109, Vps75, Asf1 and H3 and H4 work together to achieve acetylation of H3K56? Future studies for this project could include characterizing the association between Vps75, Rtt109 and the $(H3/H4)_2$ tetramer or H3/H4 dimer. It is currently unknown if Vps75, Rtt109, and H3/H4 form a ternary complex, nor has the stoichiometry between Vps75 and Rtt109 been clearly elucidated. This could have important implications for the mechanism of Vps75-mediated Rtt109 HAT activity. These questions remain unsolved, but analytical ultracentrifugation or dynamic light scattering could yield valuable quantitative information about the stoichiometries.

In Chapter III, we utilized biophysical and structural studies to determine that Chz1 and $Swc2_{1\text{-}179}$ are intrinsically disordered, but become more ordered upon binding H2A.Z/H2B heterodimers. Importantly, we discovered that Chz1 and $Swc2_{1\text{-}179}$ are not histone variant-specific as previously reported by others; in fact, they bind histones with an affinity lower than that of previously described histone chaperones. We determined that due to their inability to affect nucleosome structure, these proteins should not be

classified as chaperones, but rather may function as simple histone-binding proteins (see below). We used small angle x-ray scattering (SAXS) to examine the structure of the N-terminus of $Swc2_{1-179}$ and $Swc2_{1-179}$ -H2A.Z/H2B in solution. Our SAXS data reveals the N-terminus of $Swc2_{1-179}$ is intrinsically disordered with an extended and flexible conformation. The $Swc2_{1-179}$-H2A.Z/H2B complex has a significantly smaller maximum dimension and radius of gyration when compared to $Swc2_{1-179}$ alone, indicating that perhaps $Swc2_{1-179}$ envelops the H2A/H2B dimer, much like Chz1.

Future plans for this project include further investigating the apparent histone chaperone activity of Chz1. Simple gel-shift binding studies will reveal if Chz1 is capable of removing histone H2A.Z/H2B dimers from DNA. Based on the low binding affinity of Chz1 for histones, in comparison to Nap1 or Vps75, (Andrews et al., 2008; Park et al., 2008) we predict that Chz1 will not affect the histone-DNA complex. This has important implications because a recent paper from our laboratory presents evidence for nucleosome assembly via histone chaperone removal of nonnucleosomal histone-DNA contacts (Andrews et al., 2010).

In Chapter IV, we discovered that $Swc2_{1-179}$ forms defined complexes with free DNA. Importantly, our data suggests that $Swc2_{1-179}$ binds DNA structures that mimic sites of DNA repair. These include 3-way and 4-way junction DNA structures, but not DNA nicks or overhangs. We also have evidence that at least one free DNA end is required for binding In addition, we have evidence that the DNA-binding ability of $Swc2_{1-179}$ is relevant *in vivo*. We show that a *SWC2* gene deletion is sensitive to DNA

damaging agent methyl methanesulfonate. This is an intriguing finding and there are numerous directions into which this could lead.

Importantly, we need to first establish that the phenotypes observed are due to deletion of *SWC2*. Current work is underway to create a shuttle vector that encodes the full-length copy of the genomic DNA sequence for *SWC2* as well as a selectable marker *URA3*. Once the phenotypes are recovered, we will make a shuttle vector encoding amino acids 180-795, and assay for sensitivity to genotoxic agents (1-179 is the region which binds DNA). This will allow us to determine if the N-terminal residues of Swc2 (which recognized damaged DNA) are responsible for the DNA damage-repair phenotypes. Future work should also determine the binding affinity of $Swc2_{1\text{-}179}$ for DNA, and the precise type of DNA damage that is preferentially recognized. Such studies will pave the way for crystallization attempts, with the ultimate goal of determining the structure of $Swc2_{1\text{-}179}$ complexed with DNA.

References

Adam, M., Robert, F., Larochelle, M., and Gaudreau, L. (2001). H2A.Z is required for global chromatin integrity and for recruitment of RNA polymerase II under specific conditions. Molecular and cellular biology *21*, 6270-6279.

Adkins, M.W., Carson, J.J., English, C.M., Ramey, C.J., and Tyler, J.K. (2007). The histone chaperone anti-silencing function 1 stimulates the acetylation of newly synthesized histone H3 in S-phase. The Journal of biological chemistry *282*, 1334-1340.

Akey, C.W., and Luger, K. (2003). Histone chaperones and nucleosome assembly. Current opinion in structural biology *13*, 6-14.

Andrews, A.J., Chen, X., Zevin, A., Stargell, L.A., and Luger, K. (2010). The histone chaperone Nap1 promotes nucleosome assembly by eliminating nonnucleosomal histone DNA interactions. Molecular cell *37*, 834-842.

Andrews, A.J., Downing, G., Brown, K., Park, Y.J., and Luger, K. (2008). A thermodynamic model for Nap1 - histone interactions. The Journal of biological chemistry.

Arents, G., Burlingame, R.W., Wang, B.C., Love, W.E., and Moudrianakis, E.N. (1991). The nucleosomal core histone octamer at 3.1 A resolution: a tripartite protein assembly and a left-handed superhelix. Proceedings of the National Academy of Sciences of the United States of America *88*, 10148-10152.

Arents, G., and Moudrianakis, E.N. (1995). The histone fold: a ubiquitous architectural motif utilized in DNA compaction and protein dimerization. Proceedings of the National Academy of Sciences of the United States of America *92*, 11170-11174.

Avery, O.T., Macleod, C.M., and McCarty, M. (1944). Studies on the Chemical Nature of the Substance Inducing Transformation of Pneumococcal Types : Induction of Transformation by a Desoxyribonucleic Acid Fraction Isolated from Pneumococcus Type Iii. J Exp Med *79*, 137-158.

Bernado, P., Mylonas, E., Petoukhov, M.V., Blackledge, M., and Svergun, D.I. (2007). Structural characterization of flexible proteins using small-angle X-ray scattering. J Am Chem Soc *129*, 5656-5664.

Bernstein, E., and Hake, S.B. (2006). The nucleosome: a little variation goes a long way. Biochemistry and cell biology = Biochimie et biologie cellulaire *84*, 505-517.

Brunger, A.T., Adams, P.D., and Rice, L.M. (1997). New applications of simulated annealing in X-ray crystallography and solution NMR. Structure *5*, 325-336.

Burma, S., Chen, B.P., Murphy, M., Kurimasa, A., and Chen, D.J. (2001). ATM phosphorylates histone H2AX in response to DNA double-strand breaks. The Journal of biological chemistry *276*, 42462-42467.

Cai, Y., Jin, J., Florens, L., Swanson, S.K., Kusch, T., Li, B., Workman, J.L., Washburn, M.P., Conaway, R.C., and Conaway, J.W. (2005). The mammalian YL1 protein is a shared subunit of the TRRAP/TIP60 histone acetyltransferase and SRCAP complexes. The Journal of biological chemistry *280*, 13665-13670.

Chakravarthy, S., Bao, Y., Roberts, V.A., Tremethick, D., and Luger, K. (2004). Structural characterization of histone H2A variants. Cold Spring Harb Symp Quant Biol *69*, 227-234.

Chang, L., Loranger, S.S., Mizzen, C., Ernst, S.G., Allis, C.D., and Annunziato, A.T. (1997). Histones in transit: cytosolic histone complexes and diacetylation of H4 during nucleosome assembly in human cells. Biochemistry *36*, 469-480.

Clarkson, M.J., Wells, J.R., Gibson, F., Saint, R., and Tremethick, D.J. (1999). Regions of variant histone His2AvD required for Drosophila development. Nature *399*, 694-697.

Collins, S.R., Kemmeren, P., Zhao, X.C., Greenblatt, J.F., Spencer, F., Holstege, F.C., Weissman, J.S., and Krogan, N.J. (2007). Toward a comprehensive atlas of the physical interactome of Saccharomyces cerevisiae. Mol Cell Proteomics *6*, 439-450.

Daganzo, S.M., Erzberger, J.P., Lam, W.M., Skordalakes, E., Zhang, R., Franco, A.A., Brill, S.J., Adams, P.D., Berger, J.M., and Kaufman, P.D. (2003). Structure and function of the conserved core of histone deposition protein Asf1. Curr Biol *13*, 2148-2158.

Dahm, R. (2008). Discovering DNA: Friedrich Miescher and the early years of nucleic acid research. Hum Genet *122*, 565-581.

Davey, C.A., Sargent, D.F., Luger, K., Maeder, A.W., and Richmond, T.J. (2002). Solvent mediated interactions in the structure of the nucleosome core particle at 1.9 a resolution. Journal of molecular biology *319*, 1097-1113.

De Koning, L., Corpet, A., Haber, J.E., and Almouzni, G. (2007). Histone chaperones: an escort network regulating histone traffic. Nature structural & molecular biology *14*, 997-1007.

Demeler, B., and van Holde, K.E. (2004). Sedimentation velocity analysis of highly heterogeneous systems. Anal Biochem *335*, 279-288.

Desmoucelles, C., Pinson, B., Saint-Marc, C., and Daignan-Fornier, B. (2002). Screening the yeast "disruptome" for mutants affecting resistance to the immunosuppressive drug, mycophenolic acid. The Journal of biological chemistry *277*, 27036-27044.

Dhillon, N., Oki, M., Szyjka, S.J., Aparicio, O.M., and Kamakaka, R.T. (2006). H2A.Z functions to regulate progression through the cell cycle. Molecular and cellular biology *26*, 489-501.

Downs, J.A., Allard, S., Jobin-Robitaille, O., Javaheri, A., Auger, A., Bouchard, N., Kron, S.J., Jackson, S.P., and Cote, J. (2004). Binding of chromatin-modifying activities to phosphorylated histone H2A at DNA damage sites. Molecular cell *16*, 979-990.

Downs, J.A., Lowndes, N.F., and Jackson, S.P. (2000). A role for Saccharomyces cerevisiae histone H2A in DNA repair. Nature *408*, 1001-1004.

Driscoll, R., Hudson, A., and Jackson, S.P. (2007). Yeast Rtt109 promotes genome stability by acetylating histone H3 on lysine 56. Science (New York, NY *315*, 649-652.

Dunker, A.K., Brown, C.J., Lawson, J.D., Iakoucheva, L.M., and Obradovic, Z. (2002). Intrinsic disorder and protein function. Biochemistry *41*, 6573-6582.

Dunker, A.K., Lawson, J.D., Brown, C.J., Williams, R.M., Romero, P., Oh, J.S., Oldfield, C.J., Campen, A.M., Ratliff, C.M., Hipps, K.W*., et al.* (2001). Intrinsically disordered protein. Journal of molecular graphics & modelling *19*, 26-59.

Dutta, S., Akey, I.V., Dingwall, C., Hartman, K.L., Laue, T., Nolte, R.T., Head, J.F., and Akey, C.W. (2001). The crystal structure of nucleoplasmin-core: implications for histone binding and nucleosome assembly. Molecular cell *8*, 841-853.

Dyer, P.N., Edayathumangalam, R.S., White, C.L., Bao, Y., Chakravarthy, S., Muthurajan, U.M., and Luger, K. (2004). Reconstitution of nucleosome core particles from recombinant histones and DNA. Methods in enzymology *375*, 23-44.

Eitoku, M., Sato, L., Senda, T., and Horikoshi, M. (2008). Histone chaperones: 30 years from isolation to elucidation of the mechanisms of nucleosome assembly and disassembly. Cell Mol Life Sci *65*, 414-444.

English, C.M., Adkins, M.W., Carson, J.J., Churchill, M.E., and Tyler, J.K. (2006). Structural basis for the histone chaperone activity of Asf1. Cell *127*, 495-508.

English, C.M., Maluf, N.K., Tripet, B., Churchill, M.E., and Tyler, J.K. (2005). ASF1 binds to a heterodimer of histones H3 and H4: a two-step mechanism for the assembly of the H3-H4 heterotetramer on DNA. Biochemistry *44*, 13673-13682.

Fan, J.Y., Gordon, F., Luger, K., Hansen, J.C., and Tremethick, D.J. (2002). The essential histone variant H2A.Z regulates the equilibrium between different chromatin conformational states. Nat Struct Biol *9*, 172-176.

Fillingham, J., Recht, J., Silva, A.C., Suter, B., Emili, A., Stagljar, I., Krogan, N.J., Allis, C.D., Keogh, M.C., and Greenblatt, J.F. (2008). Chaperone control of the activity and specificity of the histone H3 acetyltransferase Rtt109. Molecular and cellular biology *28*, 4342-4353.

Finkel, T., and Holbrook, N.J. (2000). Oxidants, oxidative stress and the biology of ageing. Nature *408*, 239-247.

Fish, R.N., and Kane, C.M. (2002). Promoting elongation with transcript cleavage stimulatory factors. Biochimica et biophysica acta *1577*, 287-307.

Fontana, A., de Laureto, P.P., Spolaore, B., Frare, E., Picotti, P., and Zambonin, M. (2004). Probing protein structure by limited proteolysis. Acta Biochim Pol *51*, 299-321.

Freyer, M.W., and Lewis, E.A. (2008). Isothermal titration calorimetry: experimental design, data analysis, and probing macromolecule/ligand binding and kinetic interactions. Methods Cell Biol *84*, 79-113.

Ghaemmaghami, S., Huh, W.K., Bower, K., Howson, R.W., Belle, A., Dephoure, N., O'Shea, E.K., and Weissman, J.S. (2003). Global analysis of protein expression in yeast. Nature *425*, 737-741.

Ghosh, R.P., Nikitina, T., Horowitz-Scherer, R.A., Gierasch, L.M., Uversky, V.N., Hite, K., Hansen, J.C., and Woodcock, C.L. (2010). Unique physical properties and interactions of the domains of methylated DNA binding protein 2. Biochemistry *49*, 4395-4410.

Giaever, G., Chu, A.M., Ni, L., Connelly, C., Riles, L., Veronneau, S., Dow, S., Lucau-Danila, A., Anderson, K., Andre, B.*, et al.* (2002). Functional profiling of the Saccharomyces cerevisiae genome. Nature *418*, 387-391.

Guillemette, B., Bataille, A.R., Gevry, N., Adam, M., Blanchette, M., Robert, F., and Gaudreau, L. (2005). Variant histone H2A.Z is globally localized to the promoters of inactive yeast genes and regulates nucleosome positioning. PLoS Biol *3*, e384.

Hampsey, M. (1997). A review of phenotypes in Saccharomyces cerevisiae. Yeast (Chichester, England) *13*, 1099-1133.

Hampsey, M., and Reinberg, D. (2003). Tails of intrigue: phosphorylation of RNA polymerase II mediates histone methylation. Cell *113*, 429-432.

Han, J., Zhou, H., Horazdovsky, B., Zhang, K., Xu, R.M., and Zhang, Z. (2007a). Rtt109 acetylates histone H3 lysine 56 and functions in DNA replication. Science (New York, NY *315*, 653-655.

Han, J., Zhou, H., Li, Z., Xu, R.M., and Zhang, Z. (2007b). The Rtt109-Vps75 histone acetyltransferase complex acetylates non-nucleosomal histone H3. The Journal of biological chemistry *282*, 14158-14164.

Hansen, D.F., Zhou, Z., Feng, H., Miller Jenkins, L.M., Bai, Y., and Kay, L.E. (2009). Binding kinetics of histone chaperone Chz1 and variant histone H2A.Z-H2B by relaxation dispersion NMR spectroscopy. Journal of molecular biology *387*, 1-9.

Hansen, J.C. (2002). Conformational dynamics of the chromatin fiber in solution: determinants, mechanisms, and functions. Annual review of biophysics and biomolecular structure *31*, 361-392.

Hansen, J.C., Tse, C., and Wolffe, A.P. (1998). Structure and function of the core histone N-termini: more than meets the eye. Biochemistry *37*, 17637-17641.

Hansen, J.C., van Holde, K.E., and Lohr, D. (1991). The mechanism of nucleosome assembly onto oligomers of the sea urchin 5 S DNA positioning sequence. The Journal of biological chemistry *266*, 4276-4282.

Horn, P.J., and Peterson, C.L. (2002). Molecular biology. Chromatin higher order folding--wrapping up transcription. Science (New York, NY *297*, 1824-1827.

Jessulat, M., Alamgir, M., Salsali, H., Greenblatt, J., Xu, J., and Golshani, A. (2008). Interacting proteins Rtt109 and Vps75 affect the efficiency of non-homologous end-joining in Saccharomyces cerevisiae. Archives of biochemistry and biophysics *469*, 157-164.

Jin, J., Cai, Y., Li, B., Conaway, R.C., Workman, J.L., Conaway, J.W., and Kusch, T. (2005). In and out: histone variant exchange in chromatin. Trends in biochemical sciences *30*, 680-687.

Jones, T.A., Zou, J.Y., Cowan, S.W., and Kjeldgaard, M. (1991). Improved methods for building protein models in electron density maps and the location of errors in these models. Acta Crystallogr A *47 (Pt 2)*, 110-119.

Kelly, T.J., Qin, S., Gottschling, D.E., and Parthun, M.R. (2000). Type B histone acetyltransferase Hat1p participates in telomeric silencing. Molecular and cellular biology *20*, 7051-7058.

Khuu, P., and Ho, P.S. (2009). A rare nucleotide base tautomer in the structure of an asymmetric DNA junction. Biochemistry *48*, 7824-7832.

Khuu, P.A., Voth, A.R., Hays, F.A., and Ho, P.S. (2006). The stacked-X DNA Holliday junction and protein recognition. J Mol Recognit *19*, 234-242.

Kleywegt, G.J. (1996). Use of non-crystallographic symmetry in protein structure refinement. Acta crystallographica *52*, 842-857.

Kobor, M.S., Venkatasubrahmanyam, S., Meneghini, M.D., Gin, J.W., Jennings, J.L., Link, A.J., Madhani, H.D., and Rine, J. (2004). A protein complex containing the conserved Swi2/Snf2-related ATPase Swr1p deposits histone variant H2A.Z into euchromatin. PLoS Biol *2*, E131.

Kornberg, R.D., and Lorch, Y. (1999). Twenty-five years of the nucleosome, fundamental particle of the eukaryote chromosome. Cell *98*, 285-294.

Kossel, A. (1910). The chemical composition of the cell nucleus: Nobel lecture. Nobel Lectures, Physiology or Medicine 1901-1921.

Kossel, A. (1911). Ueber die chemische Beschaffenheit des Zellkerns. Munchen Med Wochenschrift *58*, 65-69.

Krogan, N.J., Baetz, K., Keogh, M.C., Datta, N., Sawa, C., Kwok, T.C., Thompson, N.J., Davey, M.G., Pootoolal, J., Hughes, T.R.*, et al.* (2004). Regulation of chromosome stability by the histone H2A variant Htz1, the Swr1 chromatin remodeling complex, and the histone acetyltransferase NuA4. Proceedings of the National Academy of Sciences of the United States of America *101*, 13513-13518.

Krogan, N.J., Cagney, G., Yu, H., Zhong, G., Guo, X., Ignatchenko, A., Li, J., Pu, S., Datta, N., Tikuisis, A.P.*, et al.* (2006). Global landscape of protein complexes in the yeast Saccharomyces cerevisiae. Nature *440*, 637-643.

Krogan, N.J., Keogh, M.C., Datta, N., Sawa, C., Ryan, O.W., Ding, H., Haw, R.A., Pootoolal, J., Tong, A., Canadien, V.*, et al.* (2003). A Snf2 family ATPase complex required for recruitment of the histone H2A variant Htz1. Molecular cell *12*, 1565-1576.

Krogan, N.J., Kim, M., Ahn, S.H., Zhong, G., Kobor, M.S., Cagney, G., Emili, A., Shilatifard, A., Buratowski, S., and Greenblatt, J.F. (2002). RNA polymerase II elongation factors of Saccharomyces cerevisiae: a targeted proteomics approach. Molecular and cellular biology *22*, 6979-6992.

Krude, T. (1999). Chromatin assembly during DNA replication in somatic cells. European journal of biochemistry / FEBS *263*, 1-5.

Laskey, R.A., Honda, B.M., Mills, A.D., and Finch, J.T. (1978). Nucleosomes are assembled by an acidic protein which binds histones and transfers them to DNA. Nature *275*, 416-420.

Lee, M.W., Kim, B.J., Choi, H.K., Ryu, M.J., Kim, S.B., Kang, K.M., Cho, E.J., Youn, H.D., Huh, W.K., and Kim, S.T. (2007). Global protein expression profiling of budding yeast in response to DNA damage. Yeast (Chichester, England) *24*, 145-154.

Li, X., Romero, P., Rani, M., Dunker, A.K., and Obradovic, Z. (1999). Predicting Protein Disorder for N-, C-, and Internal Regions. Genome informatics *10*, 30-40.

Liu, X., Li, B., and GorovskyMa (1996). Essential and nonessential histone H2A variants in Tetrahymena thermophila. Molecular and cellular biology *16*, 4305-4311.

Lobanov, M., Bogatyreva, N.S., and Galzitskaia, O.V. (2008). [Radius of gyration is indicator of compactness of protein structure]. Molekuliarnaia biologiia *42*, 701-706.

Longtine, M.S., McKenzie, A., 3rd, Demarini, D.J., Shah, N.G., Wach, A., Brachat, A., Philippsen, P., and Pringle, J.R. (1998). Additional modules for versatile and economical PCR-based gene deletion and modification in Saccharomyces cerevisiae. Yeast (Chichester, England) *14*, 953-961.

Lovell, S.C., Davis, I.W., Arendall, W.B., 3rd, de Bakker, P.I., Word, J.M., Prisant, M.G., Richardson, J.S., and Richardson, D.C. (2003). Structure validation by Calpha geometry: phi,psi and Cbeta deviation. Proteins *50*, 437-450.

Lowary, P.T., and Widom, J. (1998). New DNA sequence rules for high affinity binding to histone octamer and sequence-directed nucleosome positioning. Journal of molecular biology *276*, 19-42.

Lu, P.Y., Levesque, N., and Kobor, M.S. (2009). NuA4 and SWR1-C: two chromatin-modifying complexes with overlapping functions and components. Biochemistry and cell biology = Biochimie et biologie cellulaire *87*, 799-815.

Luger, K. (2006). Dynamic nucleosomes. Chromosome Res *14*, 5-16.

Luger, K., Mader, A.W., Richmond, R.K., Sargent, D.F., and Richmond, T.J. (1997). Crystal structure of the nucleosome core particle at 2.8 A resolution. Nature *389*, 251-260.

Luger, K., Rechsteiner, T.J., and Richmond, T.J. (1999). Expression and purification of recombinant histones and nucleosome reconstitution. Methods Mol Biol *119*, 1-16.

Luger, K., and Richmond, T.J. (1998a). DNA binding within the nucleosome core. Current opinion in structural biology *8*, 33-40.

Luger, K., and Richmond, T.J. (1998b). The histone tails of the nucleosome. Curr Opin Genet Dev *8*, 140-146.

Luk, E., Vu, N.D., Patteson, K., Mizuguchi, G., Wu, W.H., Ranjan, A., Backus, J., Sen, S., Lewis, M., Bai, Y.*, et al.* (2007). Chz1, a nuclear chaperone for histone H2AZ. Molecular cell *25*, 357-368.

Matangkasombut, O., Buratowski, R.M., Swilling, N.W., and Buratowski, S. (2000). Bromodomain factor 1 corresponds to a missing piece of yeast TFIID. Genes & development *14*, 951-962.

McBryant, S.J., Park, Y.J., Abernathy, S.M., Laybourn, P.J., Nyborg, J.K., and Luger, K. (2003). Preferential binding of the histone (H3-H4)2 tetramer by NAP1 is mediated by the amino-terminal histone tails. The Journal of biological chemistry *278*, 44574-44583.

Meneghini, M.D., Wu, M., and Madhani, H.D. (2003). Conserved histone variant H2A.Z protects euchromatin from the ectopic spread of silent heterochromatin. Cell *112*, 725-736.

Mertens, H.D., and Svergun, D.I. (2010). Structural characterization of proteins and complexes using small-angle X-ray solution scattering. Journal of structural biology.

Miescher, F. (1871). Ueber die chemische Zusammensetzung der Eiterzellen. Medicinisch-chemische Wintertree *4*, 441-460.

Mizuguchi, G., Shen, X., Landry, J., Wu, W.H., Sen, S., and Wu, C. (2004). ATP-driven exchange of histone H2AZ variant catalyzed by SWR1 chromatin remodeling complex. Science (New York, NY *303*, 343-348.

Morrison, A.J., Highland, J., Krogan, N.J., Arbel-Eden, A., Greenblatt, J.F., Haber, J.E., and Shen, X. (2004). INO80 and gamma-H2AX interaction links ATP-dependent chromatin remodeling to DNA damage repair. Cell *119*, 767-775.

Muto, S., Senda, M., Akai, Y., Sato, L., Suzuki, T., Nagai, R., Senda, T., and Horikoshi, M. (2007). Relationship between the structure of SET/TAF-Ibeta/INHAT and its histone chaperone activity. Proceedings of the National Academy of Sciences of the United States of America *104*, 4285-4290.

Park, Y.J., Chodaparambil, J.V., Bao, Y., McBryant, S.J., and Luger, K. (2005). Nucleosome assembly protein 1 exchanges histone H2A-H2B dimers and assists nucleosome sliding. The Journal of biological chemistry *280*, 1817-1825.

Park, Y.J., Dyer, P.N., Tremethick, D.J., and Luger, K. (2004). A new fluorescence resonance energy transfer approach demonstrates that the histone variant H2AZ stabilizes the histone octamer within the nucleosome. The Journal of biological chemistry *279*, 24274-24282.

Park, Y.J., and Luger, K. (2006a). Structure and function of nucleosome assembly proteins. Biochemistry and cell biology = Biochimie et biologie cellulaire *84*, 549-558.

Park, Y.J., and Luger, K. (2006b). The structure of nucleosome assembly protein 1. Proceedings of the National Academy of Sciences of the United States of America *103*, 1248-1253.

Park, Y.J., and Luger, K. (2008). Histone chaperones in nucleosome eviction and histone exchange. Current opinion in structural biology *18*, 282-289.

Park, Y.J., McBryant, S.J., and Luger, K. (2008a). A beta-hairpin comprising the nuclear localization sequence sustains the self-associated states of nucleosome assembly protein 1. Journal of molecular biology *375*, 1076-1085.

Park, Y.J., Sudhoff, K.B., Andrews, A.J., Stargell, L.A., and Luger, K. (2008b). Histone chaperone specificity in Rtt109 activation. Nature structural & molecular biology.

Paull, T.T., Rogakou, E.P., Yamazaki, V., Kirchgessner, C.U., Gellert, M., and Bonner, W.M. (2000). A critical role for histone H2AX in recruitment of repair factors to nuclear foci after DNA damage. Curr Biol *10*, 886-895.

Paweletz, N. (2001). Walther Flemming: pioneer of mitosis research. Nat Rev Mol Cell Biol *2*, 72-75.

Paz, A., Zeev-Ben-Mordehai, T., Lundqvist, M., Sherman, E., Mylonas, E., Weiner, L., Haran, G., Svergun, D.I., Mulder, F.A., Sussman, J.L.*, et al.* (2008). Biophysical

characterization of the unstructured cytoplasmic domain of the human neuronal adhesion protein neuroligin 3. Biophysical journal *95*, 1928-1944.

Peltomaki, P. (2001). DNA mismatch repair and cancer. Mutation research *488*, 77-85.

Pflugrath, J.W. (1999). The finer things in X-ray diffraction data collection. Acta crystallographica *55*, 1718-1725.

Prilusky, J., Felder, C.E., Zeev-Ben-Mordehai, T., Rydberg, E.H., Man, O., Beckmann, J.S., Silman, I., and Sussman, J.L. (2005). FoldIndex: a simple tool to predict whether a given protein sequence is intrinsically unfolded. Bioinformatics *21*, 3435-3438.

Putnam, C.D., Hammel, M., Hura, G.L., and Tainer, J.A. (2007). X-ray solution scattering (SAXS) combined with crystallography and computation: defining accurate macromolecular structures, conformations and assemblies in solution. Q Rev Biophys *40*, 191-285.

Raisner, R.M., Hartley, P.D., Meneghini, M.D., Bao, M.Z., Liu, C.L., Schreiber, S.L., Rando, O.J., and Madhani, H.D. (2005). Histone variant H2A.Z marks the 5' ends of both active and inactive genes in euchromatin. Cell *123*, 233-248.

Rajasekar, K., Muntaha, S.T., Tame, J.R., Kommareddy, S., Morris, G., Wharton, C.W., Thomas, C.M., White, S.A., Hyde, E.I., and Scott, D.J. (2010). Order and disorder in the domain organization of the plasmid partition protein KorB. The Journal of biological chemistry *285*, 15440-15449.

Ramakrishnan, V. (1997). Histone H1 and chromatin higher-order structure. Critical reviews in eukaryotic gene expression *7*, 215-230.

Ransom, M., Dennehey, B.K., and Tyler, J.K. (2010). Chaperoning histones during DNA replication and repair. Cell *140*, 183-195.

Redon, C., Pilch, D., Rogakou, E., Sedelnikova, O., Newrock, K., and Bonner, W. (2002). Histone H2A variants H2AX and H2AZ. Curr Opin Genet Dev *12*, 162-169.

Redon, C., Pilch, D.R., Rogakou, E.P., Orr, A.H., Lowndes, N.F., and Bonner, W.M. (2003). Yeast histone 2A serine 129 is essential for the efficient repair of checkpoint-blind DNA damage. EMBO Rep *4*, 678-684.

Richmond, T.J., and Davey, C.A. (2003). The structure of DNA in the nucleosome core. Nature *423*, 145-150.

Ridgway, P., Brown, K.D., Rangasamy, D., Svensson, U., and Tremethick, D.J. (2004). Unique residues on the H2A.Z containing nucleosome surface are important for Xenopus laevis development. The Journal of biological chemistry *279*, 43815-43820.

Romero, P., Obradovic, Z., Li, X., Garner, E.C., Brown, C.J., and Dunker, A.K. (2001). Sequence complexity of disordered protein. Proteins *42*, 38-48.

Ruhl, D.D., Jin, J., Cai, Y., Swanson, S., Florens, L., Washburn, M.P., Conaway, R.C., Conaway, J.W., and Chrivia, J.C. (2006). Purification of a human SRCAP complex that remodels chromatin by incorporating the histone variant H2A.Z into nucleosomes. Biochemistry *45*, 5671-5677.

Schneider, J., Bajwa, P., Johnson, F.C., Bhaumik, S.R., and Shilatifard, A. (2006). Rtt109 is required for proper H3K56 acetylation: a chromatin mark associated with the elongating RNA polymerase II. The Journal of biological chemistry *281*, 37270-37274.

Schwarz, P.M., and Hansen, J.C. (1994). Formation and stability of higher order chromatin structures. Contributions of the histone octamer. The Journal of biological chemistry *269*, 16284-16289.

Selth, L., and Svejstrup, J.Q. (2007). Vps75, a new yeast member of the NAP histone chaperone family. J Biol Chem *282*, 12358-12362.

Seo, S.B., McNamara, P., Heo, S., Turner, A., Lane, W.S., and Chakravarti, D. (2001). Regulation of histone acetylation and transcription by INHAT, a human cellular complex containing the set oncoprotein. Cell *104*, 119-130.

Shechter, D., Dormann, H.L., Allis, C.D., and Hake, S.B. (2007). Extraction, purification and analysis of histones. Nature protocols *2*, 1445-1457.

Shen, X., Mizuguchi, G., Hamiche, A., and Wu, C. (2000). A chromatin remodelling complex involved in transcription and DNA processing. Nature *406*, 541-544.

Shikama, N., Chan, H.M., Krstic-Demonacos, M., Smith, L., Lee, C.W., Cairns, W., and La Thangue, N.B. (2000). Functional interaction between nucleosome assembly proteins and p300/CREB-binding protein family coactivators. Molecular and cellular biology *20*, 8933-8943.

Simpson, R.T., and Stafford, D.W. (1983). Structural features of a phased nucleosome core particle. Proceedings of the National Academy of Sciences of the United States of America *80*, 51-55.

Smith, K.C. (2004). Recombinational DNA repair: the ignored repair systems. Bioessays *26*, 1322-1326.

Suto, R.K., Clarkson, M.J., Tremethick, D.J., and Luger, K. (2000). Crystal structure of a nucleosome core particle containing the variant histone H2A.Z. Nat Struct Biol *7*, 1121-1124.

Svergun, D.I. (1992). Determination of the regularization parameter in indirect-transform methods using perceptual criteria. J Appl Cryst *25*, 495-503.

Svergun, D.I. (2003a). PRIMUS: A Windows PC-based system for small-angle scattering data analysis. J Appl Cryst *36*, 1277-1282.

Svergun, D.I., Barberato, C. and Koch, M.H.J. (1995). CRYSOL – a Program to Evaluate X-ray Solution Scattering of Biological Macromolecules from Atomic Coordinates. J Appl Cryst *28*, 768-773.

Svergun, D.I., Petoukhov, M.V., and Koch, M.H. (2001). Determination of domain structure of proteins from X-ray solution scattering. Biophysical journal *80*, 2946-2953.

Svergun, V.V.V.a.D.I. (2003b). Uniqueness of ab intio shape determination in small angle scattering. J Appl Cryst *36*, 860-864.

Tompa, P. (2002). Intrinsically unstructured proteins. Trends in biochemical sciences *27*, 527-533.

Tompa, P. (2005). The interplay between structure and function in intrinsically unstructured proteins. FEBS letters *579*, 3346-3354.

Tsubota, T., Berndsen, C.E., Erkmann, J.A., Smith, C.L., Yang, L., Freitas, M.A., Denu, J.M., and Kaufman, P.D. (2007). Histone H3-K56 acetylation is catalyzed by histone chaperone-dependent complexes. Molecular cell *25*, 703-712.

Tsutakawa, S.E., Hura, G.L., Frankel, K.A., Cooper, P.K., and Tainer, J.A. (2007). Structural analysis of flexible proteins in solution by small angle X-ray scattering combined with crystallography. Journal of structural biology *158*, 214-223.

van Attikum, H., Fritsch, O., and Gasser, S.M. (2007). Distinct roles for SWR1 and INO80 chromatin remodeling complexes at chromosomal double-strand breaks. The EMBO journal *26*, 4113-4125.

van Attikum, H., Fritsch, O., Hohn, B., and Gasser, S.M. (2004). Recruitment of the INO80 complex by H2A phosphorylation links ATP-dependent chromatin remodeling with DNA double-strand break repair. Cell *119*, 777-788.

Van Holde, K.E. (1988). Chromatin. New York: Springer Verlag.

Vucetic, S., Xie, H., Iakoucheva, L.M., Oldfield, C.J., Dunker, A.K., Obradovic, Z., and Uversky, V.N. (2007). Functional anthology of intrinsic disorder. 2. Cellular components, domains, technical terms, developmental processes, and coding sequence diversities correlated with long disordered regions. Journal of proteome research *6*, 1899-1916.

Walker, J.R., Corpina, R.A., and Goldberg, J. (2001). Structure of the Ku heterodimer bound to DNA and its implications for double-strand break repair. Nature *412*, 607-614.

Walter, P.P., Owen-Hughes, T.A., Cote, J., and Workman, J.L. (1995). Stimulation of transcription factor binding and histone displacement by nucleosome assembly protein 1 and nucleoplasmin requires disruption of the histone octamer. Molecular and cellular biology *15*, 6178-6187.

Wan, Y., Chiang, J.H., Lin, C.H., Arens, C.E., Saleem, R.A., Smith, J.J., and Aitchison, J.D. (2009). Histone chaperone Chz1p regulates H2B ubiquitination and subtelomeric anti-silencing. Nucleic Acids Res *38*, 1431-1440.

Ward, J.J., Sodhi, J.S., McGuffin, L.J., Buxton, B.F., and Jones, D.T. (2004). Prediction and functional analysis of native disorder in proteins from the three kingdoms of life. Journal of molecular biology *337*, 635-645.

Wriggers, W. (2010). Using Situs for the integration of multi-resolution structures. Biophysical reviews *2*, 21-27.

Wriggers, W., Milligan, R.A., and McCammon, J.A. (1999). Situs: A package for docking crystal structures into low-resolution maps from electron microscopy. Journal of structural biology *125*, 185-195.

Wu, W.H., Alami, S., Luk, E., Wu, C.H., Sen, S., Mizuguchi, G., Wei, D., and Wu, C. (2005). Swc2 is a widely conserved H2AZ-binding module essential for ATP-dependent histone exchange. Nature structural & molecular biology *12*, 1064-1071.

Xie, H., Vucetic, S., Iakoucheva, L.M., Oldfield, C.J., Dunker, A.K., Obradovic, Z., and Uversky, V.N. (2007a). Functional anthology of intrinsic disorder. 3. Ligands, post-translational modifications, and diseases associated with intrinsically disordered proteins. Journal of proteome research *6*, 1917-1932.

Xie, H., Vucetic, S., Iakoucheva, L.M., Oldfield, C.J., Dunker, A.K., Uversky, V.N., and Obradovic, Z. (2007b). Functional anthology of intrinsic disorder. 1. Biological processes and functions of proteins with long disordered regions. Journal of proteome research *6*, 1882-1898.

Yodh, J.G., Woodbury, N., Shlyakhtenko, L.S., Lyubchenko, Y.L., and Lohr, D. (2002). Mapping nucleosome locations on the 208-12 by AFM provides clear evidence for cooperativity in array occupation. Biochemistry *41*, 3565-3574.

Zhang, H., Roberts, D.N., and Cairns, B.R. (2005). Genome-wide dynamics of Htz1, a histone H2A variant that poises repressed/basal promoters for activation through histone loss. Cell *123*, 219-231.

Zhou, Z., Feng, H., Hansen, D.F., Kato, H., Luk, E., Freedberg, D.I., Kay, L.E., Wu, C., and Bai, Y. (2008). NMR structure of chaperone Chz1 complexed with histones H2A.Z-H2B. Nature structural & molecular biology *15*, 868-869.

Zlatanova, J., Seebart, C., and Tomschik, M. (2007). Nap1: taking a closer look at a juggler protein of extraordinary skills. Faseb J *21*, 1294-1310.